

Air Force Institute of Technology

AFIT Scholar

Theses and Dissertations

Student Graduate Works

9-2022

Additive Manufacturing of Molybdenum for High Temperature Structural Applications

Megan L. Bustin

Follow this and additional works at: <https://scholar.afit.edu/etd>



Part of the [Aerospace Engineering Commons](#), and the [Manufacturing Commons](#)

Recommended Citation

Bustin, Megan L., "Additive Manufacturing of Molybdenum for High Temperature Structural Applications" (2022). *Theses and Dissertations*. 5531.

<https://scholar.afit.edu/etd/5531>

This Thesis is brought to you for free and open access by the Student Graduate Works at AFIT Scholar. It has been accepted for inclusion in Theses and Dissertations by an authorized administrator of AFIT Scholar. For more information, please contact AFIT.ENWL.Repository@us.af.mil.



**ADDITIVE MANUFACTURING OF MOLYBDENUM FOR HIGH
TEMPERATURE STRUCTURAL APPLICATIONS**

THESIS

Megan L. Bustin, Major, USMC

AFIT-ENY-MS-22-S-111

AIR UNIVERSITY

AIR FORCE INSTITUTE OF TECHNOLOGY

Wright-Patterson Air Force Base, Ohio

DISTRIBUTION STATEMENT A.

APPROVED FOR PUBLIC RELEASE; DISTRIBUTION UNLIMITED.

The views expressed in this thesis are those of the author and do not reflect the official policy or position of the United States Air Force, Department of Defense, or the United States Government. This material is declared a work of the U.S. Government and is not subject to copyright protection in the United States.

AFIT-ENY-MS-22-S-111

ADDITIVE MANUFACTURING OF MOLYBDENUM FOR HIGH TEMPERATURE
STRUCTURAL APPLICATIONS

THESIS

Presented to the Faculty

Department of Aeronautics and Astronautics

Graduate School of Engineering and Management

Air Force Institute of Technology

Air University

Air Education and Training Command

In Partial Fulfillment of the Requirements for the
Degree of Master of Science in Aeronautical Engineering

Megan L. Bustin, MS

Major, USMC

September 2022

DISTRIBUTION STATEMENT A.
APPROVED FOR PUBLIC RELEASE; DISTRIBUTION UNLIMITED.

AFIT-ENY-MS-22-S-111

ADDITIVE MANUFACTURING OF MOLYBDENUM FOR HIGH TEMPERATURE
STRUCTURAL APPLICATIONS

Megan L. Bustin, MS

Major, USMC

Committee Membership:

Maj R. A. Kemnitz, PhD
Chair

Maj J. S. Brewer, PhD
Member

Dr. Carl R. Hartsfield, PhD
Member

Abstract

This research considered additive manufactured (AM) molybdenum (Mo) and the effect of three variables on microstructure, mechanical properties, and the relationship between the two. Test temperature, laser speed, and build atmosphere were varied, and samples tested and analyzed using a three-point bending test, chemical composition, and optical and scanning electron microscopy. The relationship among variables and results using Design of Experiments was limited compared to the inclusion of every tested sample. Most effects were expected. Samples tested at room temperature were brittle without statistical significance. Increasing laser speed resulted in decreased ductility and strain, smaller grain sizes, and increased quantity of grains. Percentage of hydrogen in the build atmosphere had very little effect compared to the other variables. Nitrogen was preferable to an argon build atmosphere, results showing both higher stresses and strains under the same conditions. Stress followed expectations given oxygen content, keyhole porosity, and un-sintered materials. Maximum stress occurred at an intermediate laser speed and volumetric energy density (VED). Despite resulting porosity, nitrogen as a build atmosphere shows promise in AM fully dense Mo. Heat treatments and adjusting VED contribute to producing fully dense Mo and should be considered in future work.

Acknowledgments

I would like to express my sincere appreciation to my faculty advisor for his guidance and support throughout the course of this thesis effort. The insight and experience were certainly appreciated. I would like to also thank my family, friends, and partner for all their support throughout the last two years.

Megan L. Bustin

Table of Contents

	Page
Abstract	1
Table of Contents	3
List of Figures	5
List of Tables	9
I. Introduction	10
1.1 General Issue	10
1.2 Problem Statement.....	10
1.3 Research Focus and Objectives	11
1.4 Investigative Questions	12
1.5 Methodology.....	12
1.6 Assumptions/Limitations.....	12
1.7 Implications	13
1.8 Preview	13
II. Literature Review	15
2.1 Chapter Overview.....	15
2.2 High Temperature Materials.....	15
2.3 Metallurgy/Processing of Molybdenum	28
2.4 Additive Manufacturing of Molybdenum	35
2.5 Summary.....	47
III. Methodology	48
3.1 Chapter Overview.....	48

3.2 Design of Experiments	48
3.3 Preparation of Metal Powders	51
3.4 AM of Samples.....	51
3.5 Procedures and Processes for Mechanical Testing.....	53
3.5.1 Polishing and Drying.....	53
3.5.2 Mechanical Tests	54
3.6 Microstructure and Fracture Surface Analysis	59
3.7 Summary.....	63
IV. Analysis and Results.....	64
4.1 Chapter Overview.....	64
4.2 Experimental Results.....	64
4.3 ANOVA Results.....	75
4.4 Investigative Questions Answered	121
4.5 Summary.....	122
V. Conclusions and Recommendations	124
5.1 Conclusions of Research	124
5.2 Recommendations for Future Work	126
5.3 Summary.....	128
Bibliography	129

List of Figures

	Page
Figure 1. "Tensile strength of pure metals at elevated temperature." Reproduced from Campbell [7].....	17
Figure 2. "Tensile strength-density ratios for pure metals at elevated temperatures." Reproduced from Campbell [7]	18
Figure 3. "Principal commercial forms and end uses of molybdenum"[9, p.29]. Republished with permission of Taylor & Francis Group LLC - Books from Extractive metallurgy of molybdenum, Gupta, C. K., 1992; permission conveyed through Copyright Clearance Center, Inc.	19
Figure 4. "Elevated-Temperature Tensile Strength According to Alloy System". Reproduced from Campbell [7]	24
Figure 5. Tensile strength of swaged, carbide-strengthened molybdenum alloys at 2400° F" [8]. Republished with permission of Elsevier Science & Technology Journals, from A review of chromium, molybdenum, and tungsten alloys, Klopp, William D., Vol. 42 Issue 3, 1975; permission conveyed through Copyright Clearance Center, Inc.....	25
Figure 6. "Effect of temperature on the oxidation of unalloyed molybdenum"[9, p. 16]. Republished with permission of Taylor & Francis Group LLC - Books from Extractive metallurgy of molybdenum, Gupta, C. K., 1992; permission conveyed through Copyright Clearance Center, Inc.	27
Figure 7. "Optically determined average porosity as a function of volumetric energy density (VED) for different process parameters" [32]. This figure was published in Materials and Design, Vol 191, Higashi, M. and Ozaki, T., Selective Laser Melting	

of Pure Molybdenum: Evolution of Defect and Crystallographic Texture with Process Parameters, 1-11, Copyright Elsevier (2020). Used with permission.....	42
Figure 8. Effect of Argon Atmosphere on Stress and Strain	46
Figure 9. Illustration of additively manufactured sample	52
Figure 10. Concept Laser MLab Cusing 200R 3D metal printer.....	53
Figure 11. (a) Buehler EcoMet 300 Pro Grinder Polisher (Lake Bluff, IL, USA) and (b) Omegalux LMF-3500 furnace (Stamford, CT)	55
Figure 12. the Material Testing System (MTS) Model 810 (MTS Systems Corporation, Eden Prairie, MN, USA)	56
Figure 13. 810 Material Test System with the MTS 653 Furnace and 647 Hydraulic Wedge Grip	57
Figure 14. TESCAN MAIA3 scanning electron microscope	60
Figure 15. Example fracture surface images from a variety of sample conditions.....	61
Figure 16. MetLab Metpress A and carbon puck	62
Figure 17. Zeiss Axio Observer Z1m Optical Microscope.....	62
Figure 18. Room Temperature and High Temperature three-point bending tests results comparing scan speed to stress and break angle.	69
Figure 19. Flexural Stress vs. Strain Curves for the room temperature three-point bending tests.....	73
Figure 20. Flexural Stress vs. Strain Curves for the high temperature three-point bending test	74
Figure 21. Ultimate Tensile Strain Response to Significant Factor Variance for the DOE design space.	79

Figure 22. Optical microscopic pictures of each representative sample at 2.5 magnification.....	81
Figure 23. Ultimate Tensile Stress Response to Significant Factor Variance for the DOE design space.	82
Figure 24. Optical microscopic pictures of each etched representative sample at 2.5 magnification.....	83
Figure 25. Yield Stress relationship between laser speed and test temperature for all test data.	87
Figure 26. Ultimate Tensile Stress relationship between laser speed and test temperature for all test data.	90
Figure 27. Ultimate Tensile Strain relationship between laser speed and test temperature for all test data.	91
Figure 28. Final Strain relationship between laser speed and test temperature for all test data.	92
Figure 29. Young's Modulus relationship between test temperature and laser speed for all test data.....	93
Figure 30. ANOVA results by factor for Young's Modulus for all data points	98
Figure 31. Yield Stress ANOVA model graph for N ₂ samples	102
Figure 32. Yield Stress result of temperature and laser speed for 2.5% H ₂ samples.....	104
Figure 33. Ultimate Tensile Stress result of temperature and laser speed for N ₂ samples	105
Figure 34. Ultimate Tensile Stress relationship between test temperature and laser speed for 2.5% H ₂ samples.....	106

Figure 35. Strain at maximum stress data from unpublished Mo in Ar and Ar-3% H ₂ and three N ₂ and H ₂ environments at room temperature	107
Figure 36. Strain at maximum stress data from unpublished Mo in Ar and Ar-3% H ₂ and three N ₂ and H ₂ environments at room temperature and 600°C	108
Figure 37. Maximum Stress data from unpublished Mo in Ar and Ar-3% H ₂ and three N ₂ and H ₂ environments at room temperature and 600°C.....	109
Figure 38. Yield Stress result for high temperature test samples.	112
Figure 39. Ultimate Tensile Strength result for high temperature test samples.....	113
Figure 40 Fracture surfaces from high temperature three-point bending test. Top to bottom: 0% H ₂ , 2.5% H ₂ , 5% H ₂ . From left to right, 100, 200, 400, 600 mm/s laser speed.....	114
Figure 41. Fracture surface of representative samples from room temperature three-point bending test. Top to bottom: 0% H ₂ , 2.5% H ₂ , 5% H ₂ . From left to right, 100, 200, 400, 600 mm/s laser speed.	115
Figure 42. Notional fracture path around grain boundaries for 100 and 600 mm/s samples at 0% H ₂	117
Figure 43. Ultimate Tensile Strain result for high temperature test samples.....	119
Figure 44. Final Strain result for high temperature test samples.	120
Figure 45. Young's Modulus result for high temperature test samples.....	121

List of Tables

	Page
Table 1. Design space per Design of Experiments (DOE).	50
Table 2. Statistically significant ANOVA results by factor and analyzed sample groups.	78
Table 3. Chemical analysis of samples, providing weight percent of oxygen, nitrogen and hydrogen for each representative sample and pure powder Mo.	84
Table 4. ANOVA for Quadratic Model of Yield Stress for all data points	88

ADDITIVE MANUFACTURING OF MOLYBDENUM FOR HIGH TEMPERATURE STRUCTURAL APPLICATIONS

I. Introduction

1.1 General Issue

Improving performance and survivability of aeronautical parts and machines involves use of new or previously unused materials with desired mechanical properties, such as high strength and some strain at high or super high temperatures. Molybdenum (Mo) does not occur as a free element but was discovered in the 1700s, eventually refined and used extensively during both World Wars, and its properties are now well-known [1]. Refractory metals are those metallic elements resistant to heat and wear, including tungsten, molybdenum, niobium, tantalum, and rhenium. As a refractory metal, Mo and its alloys have desirable characteristics for high temperature applications to include retaining strength at high temperatures, high thermal conductivity, and ductility at high temperature [2], but it is brittle at room temperature and pure Mo oxidizes readily in an oxidizing atmosphere. Additive manufacturing (AM) is a means to create parts of such dimensions difficult or impossible to replicate using traditional manufacturing methods, to include use in high temperature or aeronautical purposes. The drawback of AM is the likelihood of introducing impurities like oxides and manufacturing structures with cracks or porosity, weakening the part and diminishing desired characteristics.

1.2 Problem Statement

Crack free Mo has been AM'd under specific conditions [3,4], but some part designs may necessitate changing certain conditions previously used, such as supports or alloyed materials. The processing parameters, like laser speed, affect the microstructure

of the material thus the resulting mechanical properties. Rapid oxidation of Mo at the higher temperatures [5] required for AM also requires methods to limit or eliminate the presence of oxygen, as well as other impurities before and during manufacturing. The use of Argon (Ar) as a shield gas is one means to limit the oxidation during AM, but the use of other gases, possibly nitrogen with H₂, may improve the resulting mechanical properties of samples. (In this paper, the terms shield gas and build atmosphere will be used interchangeably.) The Mo ductile to brittle transition temperature (DBTT) has been measured anywhere from -120° [6] to above 100°C depending on purity, density, heat treatments of the AM samples [4], so test results for mechanical properties of Mo below and above the DBTT will differ accordingly.

1.3 Research Focus and Objectives

The focus of this research is to determine to what extent testing temperature, laser speed, and shield gas affect mechanical properties, the stress and strain, of AM Mo. The interaction of oxygen and hydrogen at high temperatures suggests an increased hydrogen content in the shield gas would react with and thus reduce the oxygen content in samples. Nitrogen is itself reactive to a greater extent than Ar and may improve properties if such a reaction reduces the oxide presence at grain boundaries. Laser speed is directly related to the volumetric energy density (VED), and studies have shown VED as a major contributor to identified trends in test data.

The objectives are: to qualitatively and quantitatively characterize the mechanical properties of AM Mo under the three different variables, to characterize the microstructure of AM Mo under the three different variables, and to relate the microstructure to the mechanical properties of AM Mo.

1.4 Investigative Questions

The effect of the build atmosphere in AM is one question not answered in literature. Does the chosen shield gas make a difference in stress, strain, or ductility? To what extent does the percentage of hydrogen in that atmosphere impact said properties? How would the microstructure be affected by the changing build atmosphere?

1.5 Methodology

As outlined in Chapter III, 12 Mo test samples were AM in three different build atmospheres (100% N₂, 97.5% N₂ with 2.5% H₂, and 95% N₂ with 5% H₂) and four laser speeds (100, 200, 400, and 600 mm/s) for a total of 144 samples. Design of Experiments was used to limit the number of samples necessary for a complete analysis, though each sample tested was included in later analysis. A three-point bending test at one of three temperatures was conducted: high temperature at 600°C, 'room temperature' at 25°C, and an 'intermediate' temperature of 288°C. Analysis included chemical composition, use of a scanning electron microscope (SEM) for the fracture surfaces, and optical microscopy of porosity and grain structure.

1.6 Assumptions/Limitations

Random variation in the processing of samples is assumed. Random sampling, or selection of each sample for each individual test was conducted randomly to account for any uncontrolled or nuisance variable. The powder used for AM is uniform for all builds. Any variation is a result of the three variables of this study: laser speed, test temperature and build atmosphere.

1.7 Implications

The reduced cost of AM Mo parts requiring little to no post-processing but retaining similar mechanical properties when compared to traditional methods can increase parts availability and high-temperature applications. Understanding the exact AM process parameters required, especially in conjunction with lower cost materials, can increase overall preparedness and ultimately survivability in the aeronautics field and reduce the need for certain newer alloys that may be expensive financially and environmentally in byproducts produced.

1.8 Preview

Chapter II. Literature Review discusses high temperature applications of materials, processing and extraction of Mo, and AM of Mo. Traditional methods developed to extract and process Mo controlled the chemical and physical interactions of Mo and alloys to reduce impurities and achieve fully dense, pure Mo for high temperature applications. AM builds upon these methods by fabricating designs not achievable by traditional methods using Mo powder and various design parameters. Understanding fully how such factors as a build atmosphere and energy density per volume affect Mo during AM could impact future work and high temperature applications of Mo.

Chapter III. Methodology reviews processes conducted to build specimens with AM, test specimens using three-point bending tests at various temperatures, and analyze data and samples post-process with scanning electron microscopes, optical microscopes, and statistical analysis software.

Chapter IV. Analysis presents the results of Section III. Data is analyzed using Stat-Ease and MATLAB software and Design of Experiments (DOE). After initial analysis using DOE, results from further comparison of various groups of samples is presented, along with analysis of the microstructure to explain the statistical results. Comparison to expected results and past experiments are included in this section.

Chapter V. Conclusions summarizes the findings as it relates to the initial question of utilizing AM to develop Mo metallic structures for applications with desirable chemical and/or physical properties. Explanation for the results is put into context with the qualitative and quantitative analysis utilizing software and microscopic tools. Any difficulties with the research encountered is stated, as well as the future path forward.

II. Literature Review

2.1 Chapter Overview

The purpose of this chapter is to review literature related to high temperature materials and applications, traditional metallurgy, and AM of Mo. The purpose of discussing high temperature materials is the direct correlation to pursuing Mo as a subject of interest, the pros of using Mo as well as the limitations as a material or alloy in such materials. Those utilizing traditional metallurgy methods recognized limitations in Mo as it related to impurities and corrosion, thus developed methods to avoid oxygenation and benefit from the high-temperature properties of Mo. Traditional methods, however, do not allow for more refined or unique shapes that could benefit future high-temperature applications. AM has the benefit of creating nearly any design desired, but must respect the reasoning behind and results of processing Mo in traditional methods for AM to be useful. Impurities and density of materials must be considered throughout processing in order to achieve desired end-product properties. Fully understanding the effects of design parameters on end-product AM Mo could result in better design methods, improving desirable properties, and increased high-temperature applications of Mo.

2.2 High Temperature Materials

High temperature materials are those that possess specific combinations of mechanical properties, oxidation or corrosion resistance, physical properties, and fabricability that enable a high service temperature [7]. Refractory metals including Mo have some of the highest melting points of any element, but are susceptible to oxidation at high temperature, which must be considered in design and application of materials [7].

The high melting point, high-temperature strength, and high electrical conductivity have led to uses as electrical components in light bulbs and radios such as heaters in electric furnaces, and thermocouples in the early 1900s [2,7,8]. Producing larger ingots of Mo, over 1000 kg, has led to uses of the metal in larger scale applications, such as turbine blades and parts of jet engines and rockets [8]. The exact properties required of a material depend on the desired use, such as low density and high-temperature strength for aerodynamic applications or electrical conductivity at high temperatures in electrical components [7].

Figure 1 [7] shows the plot the tensile strength of annealed pure metals versus temperature. Refractory metals have not only the highest melting points (except carbon), but also maintain high tensile strength at elevated temperatures. Near room-temperature, Mo has the third highest tensile strength. Vanadium has higher strength when measured from just above room temperature to around 500°C (932°F), but the only pure metals stronger than Mo are tungsten (W) and rhenium (Re) from 500°C through about 1400°C (2552°F). Mo maintains some strength through 1900°C (3452°F) whereas most other metals fail below about 900°C (1652°F).

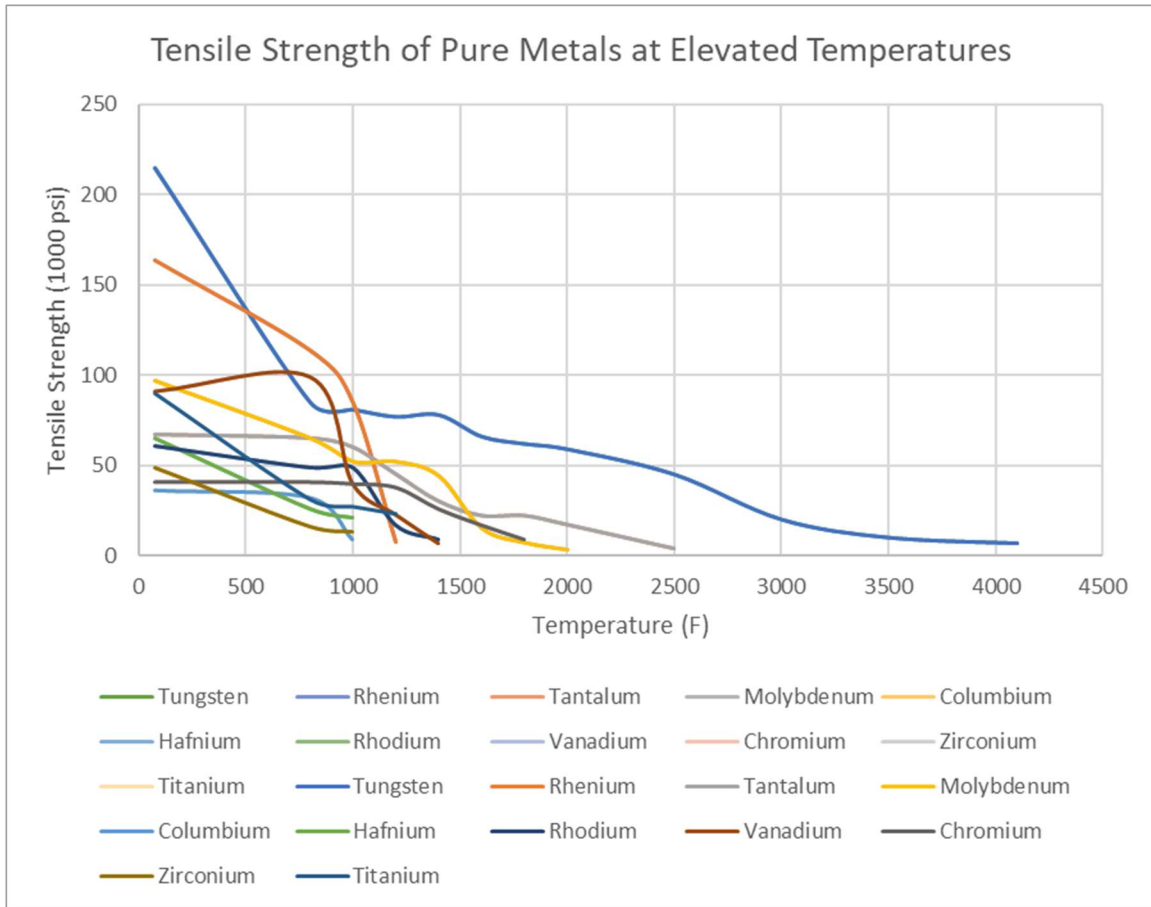


Figure 1. "Tensile strength of pure metals at elevated temperature." Reproduced from Campbell [7]

Figure 2 [7] plots tensile strength per density versus temperatures. Ideally, the strongest material at the lightest density would be used in applications where weight mattered, such as in air frames or engine parts for airplanes, rockets, missiles, etc. As seen in Figure 2, that ideal cannot be reached with pure metals. The materials with the highest strength to density ratios cannot withstand elevated temperatures above about 800°C (1472°F). The best materials at elevated temperatures when looking at a strength to density ratio also tend to be the ones with the highest melting point: Mo, W, and Re. Both the high melting point and modulus of elasticity of Mo [9] offset a higher cost in

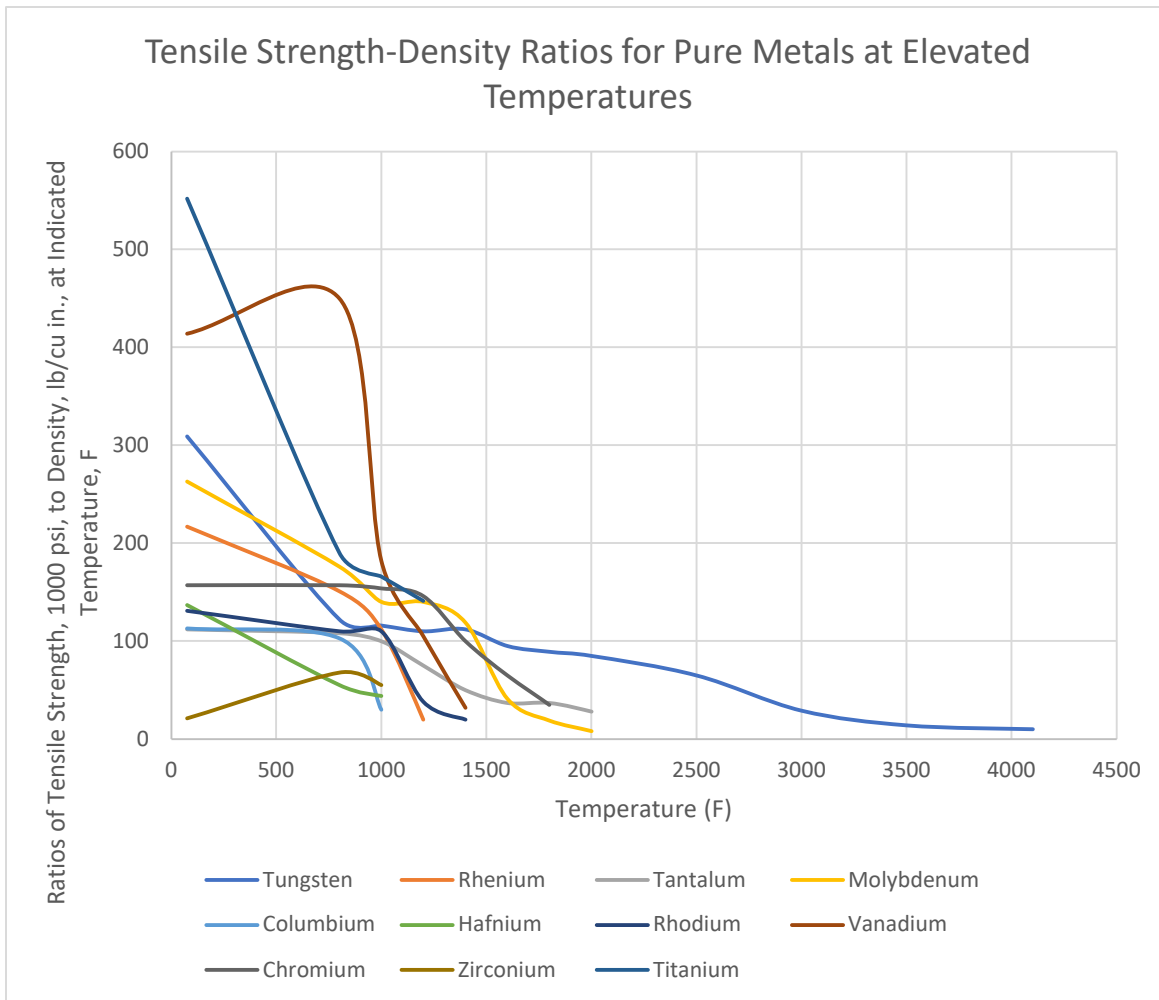


Figure 2. "Tensile strength-density ratios for pure metals at elevated temperatures."
Reproduced from Campbell [7]

weight of using a material with a high density. These mechanical properties of maintaining strength at high temperature, and of sufficient density for structural applications, is what makes Mo a good candidate for a wide spectrum of uses at high temperatures.

Mechanical properties of Mo naturally led to adoption in a variety of fields, see Figure 3. For example, the Mo modulus of elasticity measured at an 800°C (1472°F) working temperature is higher than steel at room temperature [10], and the useful strength

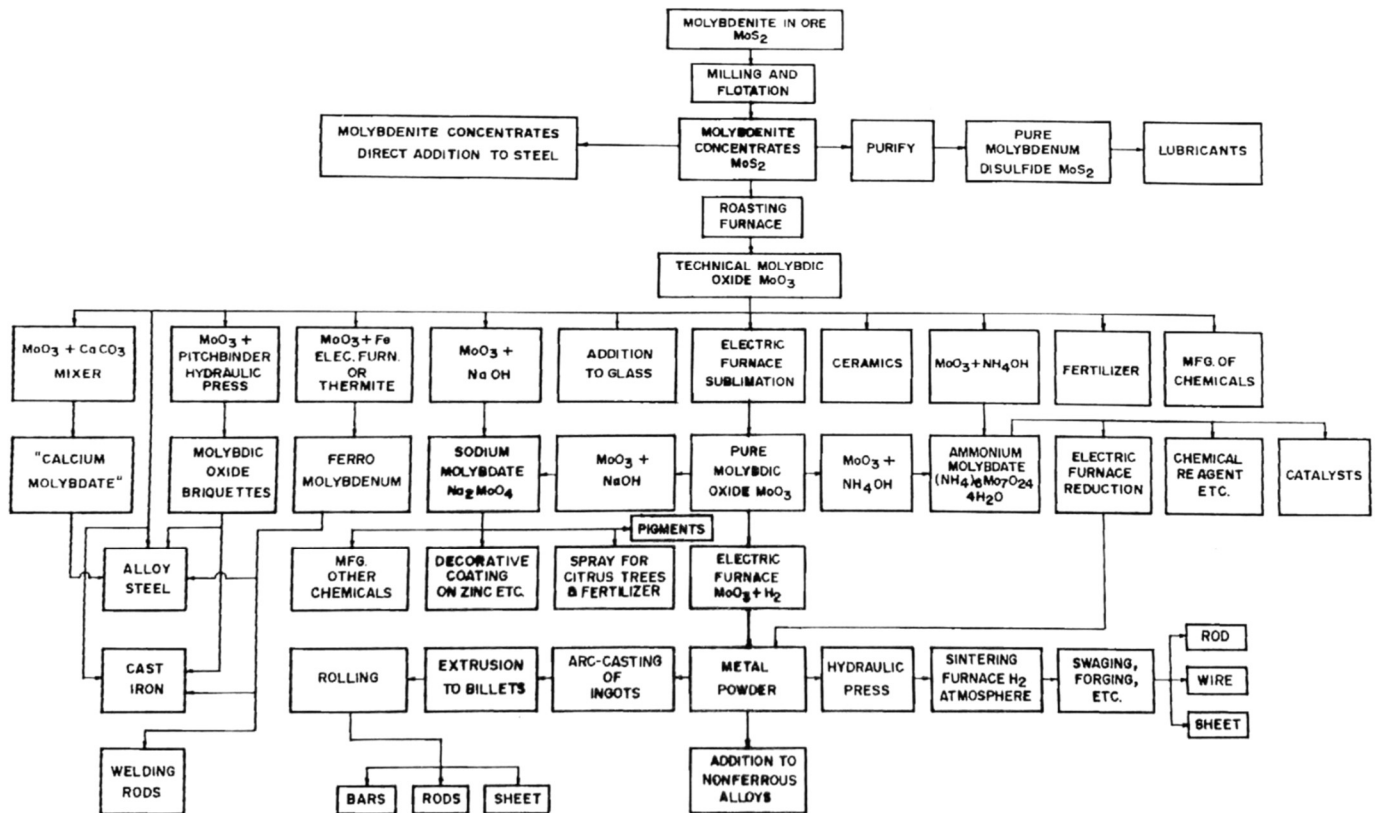


Figure 3. "Principal commercial forms and end uses of molybdenum"[9, p.29].
 Republished with permission of Taylor & Francis Group LLC - Books from Extractive metallurgy of molybdenum, Gupta, C. K., 1992; permission conveyed through Copyright Clearance Center, Inc.

of Mo exceeds superalloys above 850°C (1562°F). The coefficient of thermal expansion for Mo is ½ or less that of steels, limiting the threat of cracks [10]. Mo bars, rods or sheets may be preferred over other pure metals for those reasons. Similarly, alloying in various steels, or alloys added to a base Mo, generates yet more materials with unique properties.

One such application is in jet engine parts. Jet engine performance as measured by the power produced is a function of engine temperature [11]. Current limits on engine temperature derive from the melting temperature of the materials that comprise the engine parts, specifically near the turbine rotor inlet as the hottest part of the engine [11]. Refractory metal alloys can withstand higher temperatures than the nickel alloys common in engines, but must also meet other specifications such as ductility, oxidation resistance, strength, and creep resistance at high temperatures [11]. In a jet engine environment, all parts must resist oxidation or corrosion at high temperatures in a corrosive atmosphere.

The low oxidation resistance of pure Mo can be mitigated when used in alloys, like silicon alloys, possibly by forming more complex, stable ions [7]. Research into designing and fabricating an alloyed microstructure with increased strength that would not need to be forged or conventionally worked, thus not changing the microstructure after fabrication, is a burgeoning area of study [11]. If such a method could be mass produced, engine temperatures and efficiency could be increased as the current infrastructure for cooling turbine blades, necessary as engines become hotter and more powerful, requires energy and extra weight [11].

Another high temperature property of Mo, creep resistance [12], coupled with the low thermal neutron capture property, lends itself to structural use in atomic reactors [8].

However, the poor oxidation resistance of Mo at high temperatures [1], embrittlement due to radiation at low temperatures, and joining issues [12] hinders its use in the latest Generation IV reactors. The induced radioactivity due to neutron radiation in simulations suggests reactor walls made of specific Mo isotopes also would remain radioactive significantly longer after decommissioning than W or iron (Fe) [13]. Further research and development would be needed to ascertain the cost-benefit of fabricating reactor walls using specific isotopes of Mo, the longevity and waste disposal requirements based on reactivity of materials actually used [13].

Mentioned earlier, Mo is used in the electrical industry. Mo thermal conductivity decreases with increasing temperature, but is higher than many high-temperature alloys [10]. The thermal conductivity and low specific heat allow Mo to be heated and cooled rapidly, which is especially useful in electrical applications, like the mandrels that support W filaments in lightbulbs [10]. The coefficient of thermal expansion nearly matches borosilicate glass, making Mo an ideal metal for welding joints or use in electronic tubes [10]. Heating elements with Mo used in furnaces rarely wear out before other parts of high temperature furnaces, as long as a non-oxidizing atmosphere such as hydrogen is used [10]. Electrical switches involving mercury are often made of Mo due to the resistance of Mo to react with liquid mercury [10].

The benefit of alloys is the ability to design a material or process the alloy in such a way as to achieve a particular combination of properties that may not exist in a pure metal, not just increasing oxidation resistance as mentioned previously. For example, if an application once used W, but requires a lower working temperature such that Mo suffices, a Mo-W alloy may be designed that has a higher strength than pure Mo and

maintains or improves high-temperature properties. Beneficially, that alloy is easier to process than W due to its decreased hardness.

By the mid-1950s, more than 75% of industrially produced Mo was used in Fe-based alloys, or steels, to improve or maintain the high temperature properties of the alloy [14]. The addition of Mo to steels increases hardenability, lowers temper brittleness by allowing a slower cooling during tempering, enables better machinability, and increases the high temperature strength of steels [8,10]. For example, exhaust valves for internal combustion engines rely on added Mo to reduce the temper brittleness of the alloy, but requires each of the aforementioned properties for proper performance in the engine [10].

The amount of Mo added to each alloy varies from 0.1 to 10% by weight [10], thus accounting for some of the changes in the mechanical properties and applications of steel.

Low-alloy normalized steels may have up to 1% of Mo, and are intended for use at a service temperature of 1000°F (537 °C) for longer periods of time [7]. Uses include pipes for boilers or high-pressure steam lines and are only modestly corrosion resistant in the absence of chromium or silicon [7,10]. Alloyed parts with 1-9% chromium and Mo are used in steam plants and oil refineries and have increased corrosion resistance, but not as much as highly alloyed steels [10]. Five percent chromium-Mo-vanadium steels were once used as tools to work other metals but now are used in structural applications such as airplanes given their high-strength properties [7]. Nearly all steam turbine rotors are alloys with 0.4%-0.6% Mo, where the Mo is required for high temperature and high strength for the expected high loads [10].

An entire group of steels are designed specifically for high temperatures. Nickel based alloys containing Mo, and no carbon (C), have better corrosion resistance at high temperature applications than stainless steels [10]. Low-alloyed heat-treatable steels may have small amounts of Mo, and are heat treated to withstand short-duration rapid-onset loads like in rocket components at a working temperature around 650°C [7]. These steels are not corrosion resistant but either develop an oxide coating at high temperatures [7], or else require additional alloying elements such as nickel and chromium for oxidation resistance [10].

For corrosion resistant stainless steels, those having 12-13% chromium to improve corrosion resistance, the addition of Mo has an analogous effect [10]. Austenitic stainless steel is used in industrial and maritime corrosive environments because they possess a greater resistance to pitting and crevice corrosion due to the addition of Mo [10]. Ferritic steels have a greater resistance to stress corrosion, and these steels are used in solar heating applications when one additionally considers the low coefficient of thermal expansion and high coefficient of thermal conductivity imbued by Mo [10]. Martensitic stainless steels rely on the Mo to improve corrosion resistance, and is best used in cutting blades and surgical tools [10].

Improving properties occurs by alloying or substructural control with processing, both of which change the microstructure from what naturally occurs in a pure metal [9]. Often, zirconium, hafnium, and titanium are alloyed with Mo to limit recrystallization so that desired properties are maintained at higher working temperatures rather than removed by processing [7]. It should not be a surprise that Mo alloyed with titanium, W,

or zirconium have better strength and creep resistance than pure Mo and maintain high-temperature properties [7].

Figure 4 [7] shows the elevated temperature tensile strength of various alloys. Looking at the figure, one can see that between a temperature of 950°C and 1500°C (1742°F - 2732°F), Mo alloys have the highest strength, which is noticeably higher than pure Mo seen in Figure 1. Preparation of these Mo alloys can often be similar to methods of preparing pure Mo: arc-casting or powder metallurgy followed by extrusion [7]. Alternatively, Mo as an alloying element rather than the base tends to increase strength and high-temperature properties of the alloy compared to the base metal. Many nickel- and chromium-based alloys have up to 10% Mo in the alloy [7].

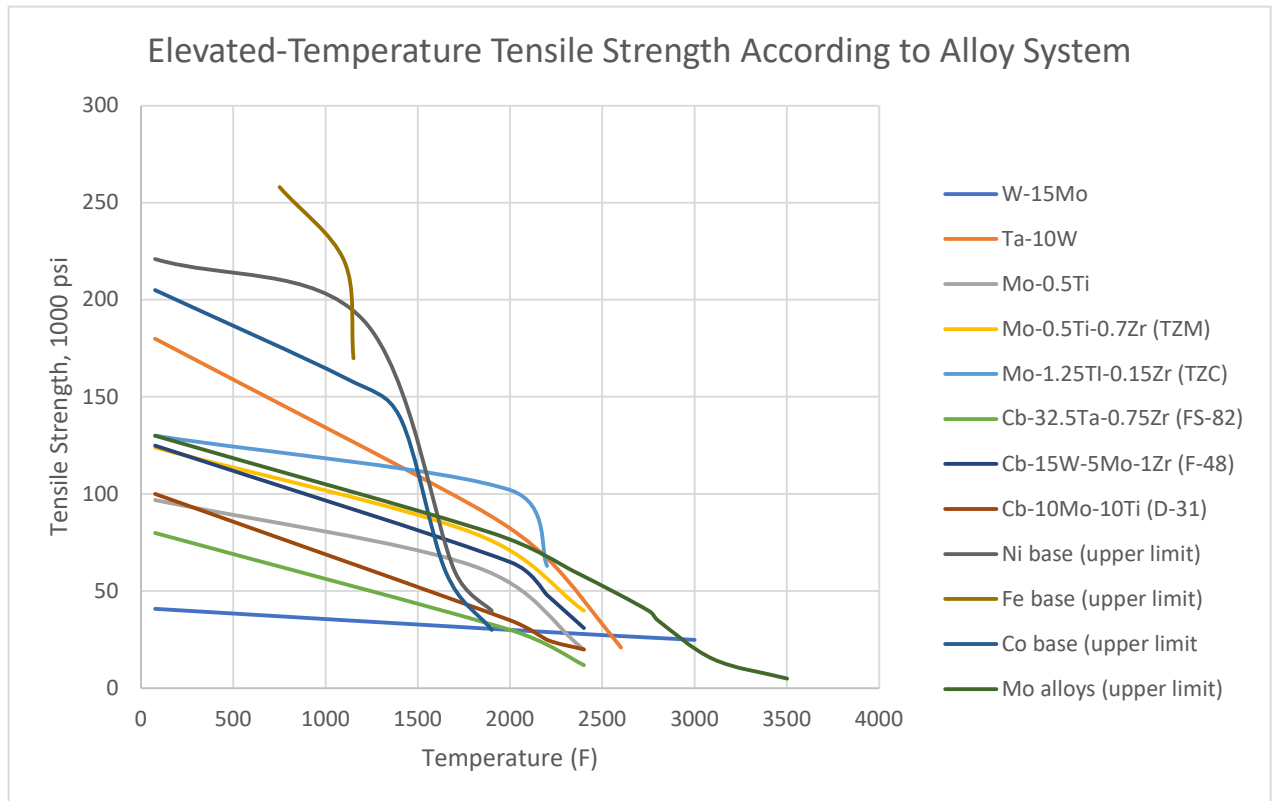


Figure 4. "Elevated-Temperature Tensile Strength According to Alloy System". Reproduced from Campbell [7]

By the 1970s, metallurgists determined that an optimal alloy of Mo, 2.5% Re, and hafnium carbide (Mo-2Re-Hf-C) has high strength above the synergistic effects found in alloying titanium carbide or zirconium carbide, the commercial products TZM or TZC [9] (see Figure 5). To achieve the strength-hardening results, Mo-2Re-Hf-C was extruded at 4000°F and swaged at 2500°F, but samples were less ductile than Mo-Hf-C alloys extruded at 3500°F [9]. A trade-off exists between ductility and strength properties [9].

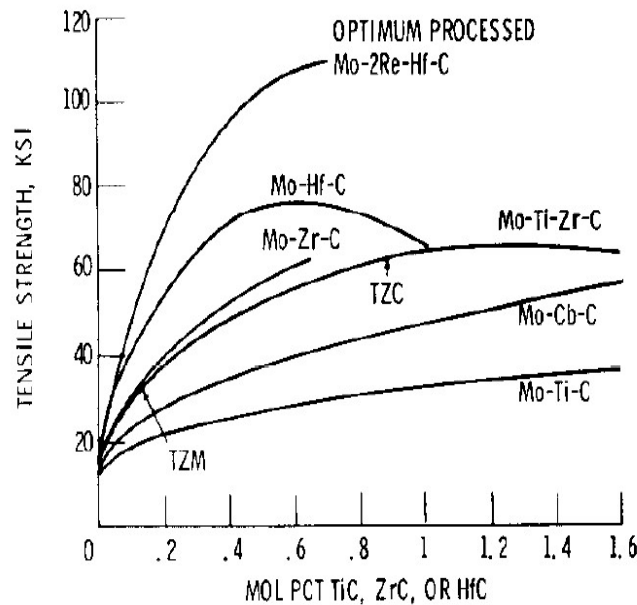


Figure 5. Tensile strength of swaged, carbide-strengthened molybdenum alloys at 2400° F" [8]. Republished with permission of Elsevier Science & Technology Journals, from A review of chromium, molybdenum, and tungsten alloys, Klopp, William D., Vol. 42 Issue 3, 1975; permission conveyed through Copyright Clearance Center, Inc.

Looking at improving its use at lower temperatures combined with high temperature strength in order to expand the overall uses of Mo, multiple studies involve Mo alloyed with Re to take advantage of the rhenium ductilizing effect [9]. Alloys with Re are shown to possess increased ductility, creep resistance, and strength at room

temperature compared to pure Mo [15] or other refractory metals, and some of those improvements are retained above the recrystallization temperature [7]. Specific processing of a Mo alloy with 26.4at.% - 31.8at.% Re had greater strength at high temperatures as well as greater ductility at lower temperatures [16] (the solubility limit for Re in Mo depends on temperature, with a maximum solubility of 43at.% at 2440°C [17]).

Other elements besides Re increase the DBTT of Mo, which may need to be countered by a third alloying element when designing the alloy [9]. Results from testing showed a ternary Mo alloy with 26.5% Re by atomic weight possesses a lower DBTT than pure Mo, while the addition of 1.5% hafnium by atomic weight, increased the strength of the alloy to that on par with pure Re at about 1430°C [16].

That increased ductility allows for better fabrication, but so would softening of a material [9]. Solution softening is a process that reduces the hardness of a material by means of alloying, but only reduces the DBTT in the case of Re [9]. Osmium, iridium, and platinum all demonstrate solution softening with Mo to some degree, depending on the percentage of the solute, and with trends noticeably related to the percentage of the element in the alloy, in the solute, and as the number of electrons in the outer shell, the electron configuration, changes [9].

A better understanding of the processing pure metals translates to better processing of alloys, making alloys easier with which to work. As noted, many alloys possess improved properties over pure metals, and powder metallurgy may lead to the creation of desired shapes not otherwise manufactured by simply AM desired parts in a single step without additional processing. Depending on the alloys used, cost of

fabrication and processing may be less than that of pure metals, with improved properties [16].

Mo is stable at room temperature and inert in Ar, helium, and hydrogen atmospheres, thus useful in vacuum furnaces [10]. At elevated temperatures, as low as 400° and especially above 600°C, use of Mo would be impractical as a pure metal in an oxidizing atmosphere [10]. Oxidation of Mo is repeatedly mentioned as a limiting factor in some applications, or at least a consideration, because mass loss due to oxidation in Mo and its alloys reduces strength compared to an intact specimen (see Figure 6). High oxidation resistance and high-temperature properties do not exist in the same natural elements. Since Mo oxidizes at high temperatures, the solutions to this problem are to remain in a non-oxidizing atmosphere, apply an oxidation resistant coating to Mo, alloy

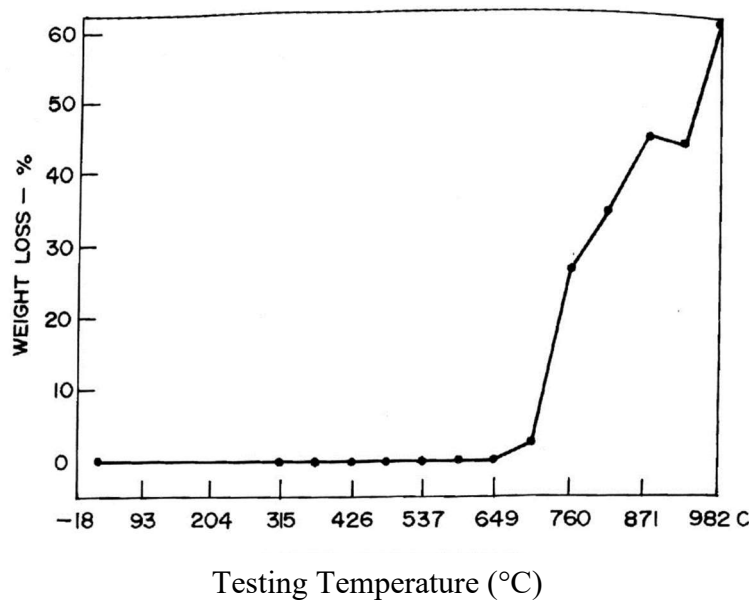


Figure 6. "Effect of temperature on the oxidation of unalloyed molybdenum"[9, p. 16]. Republished with permission of Taylor & Francis Group LLC - Books from Extractive metallurgy of molybdenum, Gupta, C. K., 1992; permission conveyed through Copyright Clearance Center, Inc.

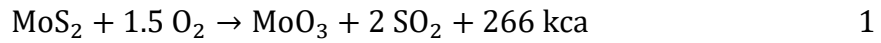
Mo to prevent oxidation, or use in a short duration mission (like missiles) such that oxidation does not matter [10]. In some cases, catastrophic oxidation may take place, which is the term for rapid oxidation at lower temperatures as liquid oxide forms, which disrupts any protective oxide scale, thus further oxidation continues to occur [5].

Molybdenum trioxide, MoO_3 , melts around 795°C [5] and oxide formation is observed in Mo alloys in the presence of oxygen at temperatures from 760°C - 815°C , with the rate of formation increasing with time and in stagnant atmospheres [18]. In some alloys that experience catastrophic oxidation, adjoining samples not otherwise as susceptible to catastrophic oxidation were made more susceptible to the same catastrophic oxidation with the increased amounts of MoO_3 in the atmosphere [18]. This vapor transport also led to catastrophic oxidation in systems without other sources of oxygen [18]. Analysis showed that the progression of oxidation was not intragranular [18] and tends to be porous at the interface.

2.3 Metallurgy/Processing of Molybdenum

Like virtually all metals, Mo does not exist naturally in its pure state, but must be processed before commercial use. Mo commonly exists as MoS_2 but is found in smaller concentrations within ores that contain other commercially useful elements in larger quantities, such as copper. Extracting large amounts of copper often leads to the extraction of Mo from the same veins. MoS_2 can be separated from copper sulfides and other sulfides by flotation using the differences in densities of the compounds [8]. Two common methods exist for processing Mo, a metallurgical and a chemical process. The main steps of each process are detailed in the following discussion.

Molybdenite, MoS_2 , is the primary bearing ore found in nature. The first steps for both processes involve separating molybdenite concentrates and roasting them to elicit, most commonly, impure MoO_3 [8]. Possible reactions when processing molybdenite are represented by the following two chemical formulas:

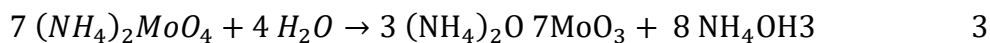


Controlling the temperature range of roasting is essential. If roasting takes place in an overheated oven, above 600°C - 700°C , reaction 2 occurs producing MoO_2 [8]. The insolubility of MoO_2 in ammonia water means sintering then occurs [8], which is not favorable for extracting Mo. Depending on the presence of other impurities, molybdates with zinc, calcium, lead, and copper may also form if the oven temperature is too low, 500°C - 600°C [8]. The ovens may be flame furnaces with manual raking of the materials [8], multiple-hearth furnaces with mechanical raking, or fluidized-bed furnaces. The result of roasting is called a calcine.

After roasting, MoO_3 is still impure in calcine form, so it is distilled through a furnace. The furnace temperature is kept around 900°C – 1100°C , leading to higher vapor pressures of MoO_3 and collection of the gas through the exhaust hood [8]. If lead remains a contaminate after roasting, the temperature in the furnace is usually lowered, between 900°C - 1000°C , so that lead molybdate does not volatilize (1050°C) and contaminate the MoO_3 gas [8]. Other common contaminants are stable at 900°C - 1000°C , such as copper and Fe, so there is no risk to those gases forming [8]. While not all the MoO_3 is volatilized, the gas that is volatilized is 99.95% MoO_3 [8].

Rather than using furnaces to convert MoO_3 to a gas, chemically a calcine can be treated by leaching MoO_3 into an ammonia solution. Some impurities are first removed by water, leaving MoO_3 and some molybdates in the remaining solid. Not every calcine has the same chemical makeup, and Mo can exist in the calcine as various metal molybdates, MoO_2 , MoO_3 , and molybdenite [8]. Calcium molybdate, molybdenite and MoO_2 are insoluble in ammonia and become part of the tailings, but the other compounds will pass into solution upon leaching with ammonia [8]. The leached solution contains copper and Fe, removed with the addition of ammonium sulfide.

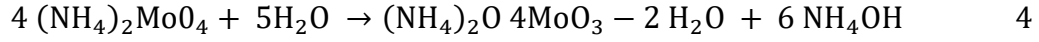
At this point in the chemical process, one of two methods will take place to isolate MoO_3 . Ammonium molybdate is stable with excess ammonia, so evaporation of some of the ammonia leads to an ammonium paramolybdate (Eq. 3) [8]. Keeping an excess of free ammonia prevents lower ammonia content molybdates (more acidic) from forming [8].



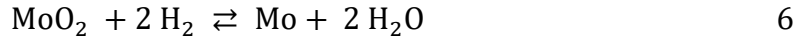
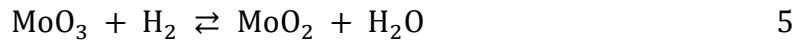
The evaporated solution is then crystallized, and the molybdate is separated by centrifuge. Multiple crystallization steps are required, with low purity after the first stage. To raise the percentage of isolated MoO_3 , some steps are repeated more than once, adding to the processing time [8].

The second method after removing the sulfides, is neutralization by adding hydrochloric acid to reduce the solution pH to 2-3 and form molybdate precipitates, primarily tetramolybdate dihydrate (Eq. 4) [8]. Centrifuging, filtration, and washing with water eliminate most contaminants except chloride, which is removed upon recrystallization [8]. Further leaching may occur for the residue after initial leaching, as

well as other chemical processes such as soda-ash fusion are conducted for, low-grade Mo concentrates.



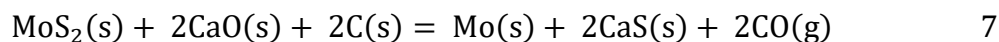
Molybdenum trioxide is further reduced to pure Mo by reducing agents such as hydrogen [8], and often in two stages [8,14] (see Eqs. 5-6). The two stages are designed to eliminate any water vapor causing a coarse powder product [14]. Since the reaction is reversible, the water vapor in the hydrogen gas, or wet hydrogen, must be removed to keep the reduction reaction going to completion and further purifying the Mo [1]. The pure Mo metal powders are used in further metallurgical processes when an impure form does not have the desired physical properties.



For both the metallurgical and chemical processes, steps are often repeated multiple times to elicit higher yields and eliminate impurities. Impurities, even slight traces, “may drastically change the ultimate properties of the consolidated metal” [1, p.48]. The processes mentioned above also work best for Mo concentrations greater than 54% [19]. For the lower concentrated molybdenite samples, an alternative process is required for fiscal reasons, a greater return during the process, and environmental reasons.

Equation (1) produces sulphur dioxide, a toxin. Soda ash roasting and lime enhanced carbothermic reductions [19] take the sulphide of molybdenite to sodium sulphate and calcium sulphide, not SO_2 (see Eq. 7). MoO_3 and Mo metal are further refined by C adsorption desorption and electrorefining respectively [19]. The benefit

over other chemical leaching is that the byproducts of Na_2SO_4 and CaS/CaSO_4 are useful chemicals in industry rather than toxic [19].



Many metals are melted and cast into a desired shape. Arc melting involves melting a powder to eliminate voids of a closely packed powder. This method is fast, but requires high temperatures and leads to large grains. Arc melting is not feasible on a large scale with Mo due to the high melting point [14]. Powder metallurgy is instead the preferred method for mass producing pure Mo items.

Powder metallurgy is a similar method to arc melting in that it takes a powder and uses pressure and heat below the melting point to decrease voids in the powder. Often, further processing, either with heat treatments or hot isostatic pressing [20] is necessary to increase the density. For smaller bars, around 18 inches by 1.5 inches or smaller, Mo powder is pressed into steel dies, possibly presintered in a hydrogen atmosphere at 1000°C [14], then high-temperature sintered at 2200°C - 2400°C [8]. Larger bars (around 30-100 kg) are made with hydrostatic pressing in elastic shells and sintered with indirect radiation heating [8].

The purity of the metal powder greatly affects the properties of the Mo metal. Unfortunately, exposure to air contaminates Mo powder at room temperature [21]. With low melting temperatures of oxides, catastrophic oxidation diffuses rapidly, and negatively affects material properties of any specimen fabricated in the presence of heat and oxygen. Measures must be taken to reduce or eliminate sources of oxygen in materials and/or the atmosphere during processing since in most instances, fabrication requires high temperatures. This is again why deoxidization matters to such a great

extent, and why the use of Mo metals began after the development of methods to produce such deoxidized metals. High temperature extrusion as well as arc-melting are the two traditional means used to take Mo powder and produce a desired sized item for final product shaping [1].

Arc-melting in a vacuum occurs when the Mo electrode and molten Mo arc with an 8,000 Amp or more current, and the flame of the arc further melts the Mo into a desired-shaped mold. Ductile Mo is desirable since brittle Mo cannot be forged or worked into other shapes without cracking, so deoxidizing while melting the Mo into the mould is imperative [8]. Oxygen readily reacts with Mo powders to form MoO_2 , so that reaction must either be prevented, which is difficult, or deoxidized. Adding C to the Mo electrode in its processing is one method for deoxidation. More than one melting ensures uniform distribution of C or other alloys for deoxidation as desired [8]. The arc-melting process can be used for ingots, and from those, fabricate wires, sheets, and tubes for commercial use.

Previous experiments varied the method of deoxidation during arc-melting to find the best means of deoxidation to include H_2 gas in a vacuum, addition of powdered C in a vacuum, and using an aluminum solid in an Ar environment. In a vacuum during arc-melting of Mo powder, H_2 , O_2 and carbon monoxide (CO) gases form, and the amount increased over time as measured by the increased pressure over time [14]. The decreased porosity in the ingots resulted from greater deoxidation [14]. H_2 gas was considered as an alternative deoxidizer, but the problem with using H_2 gas was the limited time Mo existed as a liquid due to the high melting temperature, thus limited time for H_2 to react in a balanced reaction [14].

Since only some of the metals used as electrodes could be alloyed, another method of introducing C or deoxidation agents was via powder while melting the metal [14]. Carbon was preferred as a deoxidizer in a vacuum environment because the high melting temperatures and turbulence during the melt led to high diffusion of C, thus the reaction produced more CO gas. It is believed that some partial pressure of CO remained despite the vacuum pumps operating during melting. Interestingly, this partial pressure of CO on the surface of the melted Mo is the believed reason for “microporosity found in all deoxidized ingots” [10, p.44]. When placed in an Ar environment, a C deoxidizer is not preferred due to excessive porosity in ingots [14]. Without the vacuum pumps continually reducing the partial pressure of CO, a larger partial pressure of CO on the surface results in more CO in the solution, the ingot.

An Ar environment with a solid aluminum deoxidizer was considered instead of a vacuum with a C powder deoxidizer. The reaction with aluminum elicited solid products (Al_2O_3) with high melting points (2072°C) [14,22]. Since the losses of aluminum deoxidizer was not as great compared to the C in a vacuum, the aluminum was preferred deoxidizer in Ar environments [14].

By the late-1950s, further primary working of Mo on large-scale ingots occurred often by means of extrusion before rolling or forging to generate mill products [23]. Mill products would then be fabricated to the desired final shapes such as sheets, bars, wires. Hot working occurs at a temperature which recrystallization takes place during the deformation and reheating processes. In the 1950s, the equipment to extrude Mo could not handle the high temperature required for Mo recrystallization, usually above 1650°C [23], nor would the higher temperature be ideal for limiting contamination. Thus,

extrusion was the primary means that was economically feasible for working Mo, but it occurred at lower temperatures, around 1260°C [23]. Annealing can reduce stresses, but recrystallization will result in embrittlement [14].

2.4 Additive Manufacturing of Molybdenum

AM can be classified by the base material used: solids, powders, or liquids [24]. Using powders as a base material is a process that builds a part or specimen by melting metal powder one thin layer at a time in a specific shape, and building up vertically with respect to the build plate upon which the part is attached. There are four main types of powder AM: laser metal deposition (LMD), direct metal laser sintering (DMLS), selective laser melting (SLM), and electron beam melting (EBM) [24]. The last three are all types of powder bed fusion. DMLS does not fully melt the metal during the manufacture process and often applies to microscale objects [24]. EBM uses more energy and higher temperatures than a laser that sinters metal powders, meant for high-temperature superalloys, and operates in a vacuum rather than an inert gas like SLM [24]. SLM melts the metals and is the manufacturing method examined in this thesis.

Metallurgical processing methods, such as heating or deforming, change the microstructure and mechanical properties of metals. Because properties are impacted by microstructure, properties are inherent to processing routes. Some common examples to manipulate metallic shapes include forging, extrusion, and rolling. Forging breaks down grain structure with physical deformation by compression, such as a striking hammer, while extrusion can change both shape and orientation of grains [10]. Extremely elongated grains in rolled parts increase the hardness of a material [10]. Any type of

mechanical work imparted to a metal tends to reduce the grain size [7], resulting in higher strengths, decreased tensile elongation, and in Mo, low bend and impact properties [10]. Heating a metal can have multiple effects, the primary ones of importance being recovery, recrystallization, and grain growth.

AM has the potential to create or build final or near final state components in need of little further processing. Mo parts would not need to be extruded or forged into desired shapes because the initial build is the final designed size and shape. Yet, AM still introduces unique microstructural and material features, which must be considered. Density of AM materials and its effect on properties, existence of transgranular or intergranular cracks or fractures, and molybdenum oxides embedded in materials all must be countered in achieving a desirable end product with favorable properties without further processing. This chapter will seek to elucidate the effects of AM on the properties of printed Mo.

The earliest or first group to process Mo was Faidel et al. in 2015 [25], who found that despite the high melting point, Mo could be manufactured by SLM but it was susceptible to cracking. With a high DBTT, as the Mo layer cools, tensile stress can lead to cracking [4]. Faidel et al. investigated the specific parameters of SLM with Mo using a 200 W laser to increase the density of manufactured parts changing one variable at a time: spot velocity, layer thickness, and overlap [25].

Keeping the spot velocity at 556 mm/s and layer thickness of 45 μm , an overlap of 10 μm led to a smooth surface while the 30 μm overlap had a rough surface and higher porosity due to doubling of the heat load, greater thermal strains, and larger deformations [25]. Changing the layer thickness to 25 μm , the same two overlaps were compared. The

10 μm overlap showed regular defects but the 30 μm was so porous that a lack of fusion of parts resulted in no visible continuous layers [25].

In Faidel's experiment, spot velocity remained at 556 mm/s with an overlap of 10 μm while the layer thickness was reduced from 45 μm to 25 μm [25]. Porosity was reduced in the samples with smaller layer thicknesses [25]. A density of only 82.5% was achieved with these parameters [25]. That low density was readily observed in AM parts with an abundance of cracks despite spherical atomized, 99.95wt% pure Mo powder [25]. Some studies found that spherical powders tend to attain higher densities than angular ones because of superior packing [26], but other factors negatively affected the density as reported in this article.

A primary benefit of Mo is the high strength at high temperatures. Yet all the cracks inherent to the AM process mean that those existing flaws in the material introduce stress concentrations and greatly diminish the ultimate strength of that AM material [27]. There could be no practical application of such a material. If Mo could be additively manufactured without cracks, however, the uses of Mo could exceed the developments made in the 1940s, the heyday of metallurgical developments of Mo [14]. The physical settings or laser power, hatch spacing, layer thicknesses, etc. of AM were only one area of study. Understanding the underlying chemistry allowed for further investigations.

The most important aspect, historically, of chemistry to processing Mo has been the effect of impurity elements on the ductility and brittleness of the material. In 1963, NASA doped W powder with oxygen and assessed the strength with a three-point bending test. Increasing oxygen content resulted in increased DBTT and lowered

ultimate tensile and yield strengths due to segregation of oxygen at grain boundaries and interaction of oxygen with impurities in the lattice [28]. Similarities occur with Mo [29], where increased oxygen content resulted in increased hardness and a change from intergranular to transgranular fracture modes, and affected density and grain size. These and similar findings lead to a need to control the impurities of any AM Mo product.

The oxygen impurity of the manufactured Mo comes from both oxidation of Mo powder when exposed to air during general handling and high temperature oxidation from the AM printer atmosphere during processing [1,30]. A typical Mo powder will have 0.05-0.15% oxygen, 0.002-0.003% nitrogen, and a trace amount of hydrogen impurities [2]. Controlling the oxidation occurs by either preventing oxidation from occurring throughout the lifetime of the powder, or alloying to prevent oxygen from reacting with Mo and reducing the detrimental effects [30]. If oxygen remains in the powder and subsequent parts without any means to remove the oxygen during a build, molybdenum oxide forms and is segregated to the grain boundaries because of the low solubility of oxygen in Mo [30]. The molybdenum oxide weakens grain boundaries and leads to cracking and porosity in build parts [30].

To overcome these issues, several groups proposed tweaks or changes to the process to improve the properties of printed Mo. Leitner and Braun both found success using C as an alloying addition [31,32]. Alloys were produced from powders that were mixed, pressed, sintered, forged, and recrystallized and annealed [31,33]. Leitner et al. [31] recognized in Mo-Hf alloys that C and boron can increase the strength at grain boundaries while oxygen decreases grain boundary strength and increased the likelihood of fracture at a grain boundary. Braun et al. [32] manufactured a 99.5% density sample

of Mo -0.45wt% C using laser powder bed fusion with little to no cracking. The oxygen was soluble at the interface of alpha Mo and gamma Mo₂C increasing the strength between the two formations and preventing cracks [32]. Gamma Mo₂C also traps oxygen, “increasing the grain boundary strength of alpha-Mo / alpha-Mo grains by preventing oxygen from being segregated at these boundaries” [25, p.6].

Kaserer et al. produced crack-free, fully dense Mo through AM without the necessary steps of pressing, sintering, forging, and recrystallizing by alloying with C [3]. The team used spherical powders mixed together for a Mo-0.45wt% C, used Ar gas to shield the material from oxygen during SLM, heated substrate plates at 800°C, and used a zig-zag pattern during the build with a 67° rotation between layers [3]. Without C, Mo under the same parameters still possessed visible cracks, high porosity, and exhibited intergranular fracture patterns [3]. With the addition of C, however, the Mo alloy displayed a transgranular fracture mode, half the oxygen and 12% of the C was outgassed during processing, mean bending strength was on par with recrystallized pure Mo AM parts, and the density measured 99.7% [3].

The addition of the C caused a cellular vice planar solidification, leading to increased grain boundary area with reduced segregated oxygen [3]. The outgassing of CO and reaction with residual oxygen in the build chamber may be the reason for the reduced C and oxygen contents of the final material [3]. Finally, the build plate temperature reduces the thermal gradient and thermal stresses to suppress crack growth [3].

While the addition of C can help achieve low porosity, and can improve properties in alloyed material compared to pure Mo, further studies investigated means to

AM a pure, near 100% dense, Mo part. In 2017 Wang et al. utilized skinny supports, not the addition of C or alloying elements, which resulted in a slower heat transfer and less cracking of AM parts [4]. Crack-free Mo at 99.1% theoretical density was manufactured by processing the Mo powder prior to fabrication in combination with the use of a support structure [4]. Dry granulation and plasma spheroidization powder led to larger diameter, spherical powder Mo which increased the packing density [4].

Faidel et al. found that even with a high calculated energy input per unit volume above 1000 J/mm^3 , cracks still formed when using a 200 W laser power [25]. When conducting their experiments, Wang et al. [4] used a 400 W laser power instead of a 200 W to create 99% dense samples. The resulting standardized laser absorption from a 400 W laser resulted in fine grain boundaries [4]. Longitudinal and transverse cracks still formed without additional changes to the build, but by rotating the scanning direction 67° , crack growth deviated rather than continuing unabated through the entire structure [4].

The crack-free Mo formed when utilizing a supporting structure for the build, which reduced the rate that the heat dissipated. Reducing the heat loss resulted in reducing the residual stresses generated during the build, and thus cracking [4]. The supports enabled the printed parts to remain at high temperatures longer during heating by ensuring low conductivity powder rather than a large conductive, solid metal path surrounded the build [4].

Zhou et al. [34] investigated W and balling phenomena and its relation to SLM sample density. Balling phenomena occurs during SLM when melted droplets solidify in a globular formation rather than wetting the substrate and spreading sufficiently due to

thermal gradients between the droplets and substrate [34]. The droplets then create cavities which subsequent layers of powder and melting do not fill, resulting in porous material during AM.

Multiple ways were found to improve the wetting process, thus decrease pores and increase density. Remelting the surface prior to adding the next powder layer resulted in denser W samples [34]. Körner [26] recognized more densely packed powders improve the wetting process with regards to simulation of selective beam melting. Plasma spheroidization of the powder being melted increased both density of the powder and laser absorption, thus improving the wetting of the substrate [35]. It is reasonable to presume that similar findings would apply to SLM and Mo in the interest of gaining the densest samples possible.

Higashi [36] expanded upon earlier studies by looking at the effect of process parameters on defect formation, specifically looking at porosity, crystallographic texture, and melt pool characteristics of AM Mo. Laser power, scan speed, and layer thickness were varied, but trends could almost all be explained by comparing overall VED, Figure 7. "Optically determined average porosity as a function of volumetric energy density (VED) for different process parameters" [32]. This figure was published in Materials and Design, Vol 191, Higashi, M. and Ozaki, T., Selective Laser Melting of Pure Molybdenum: Evolution of Defect and Crystallographic Texture with Process

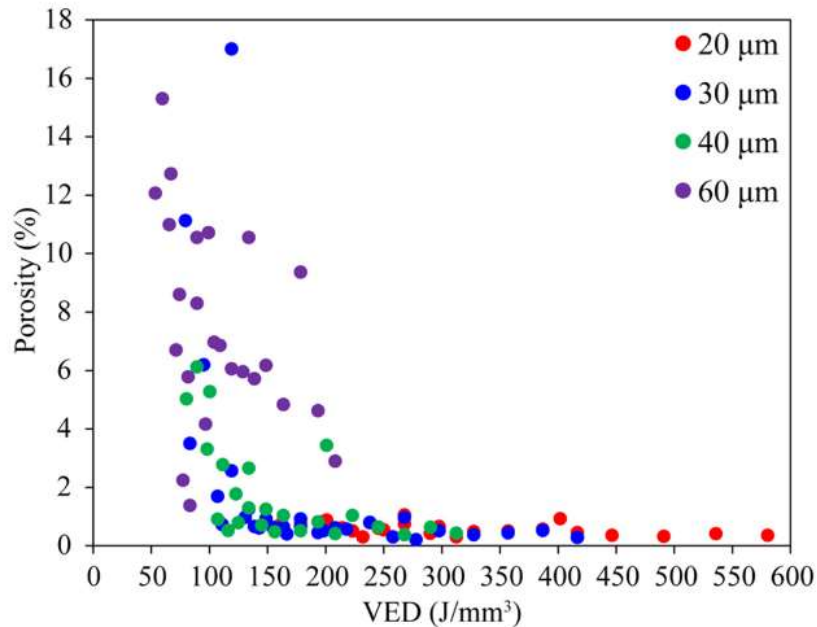


Figure 7. "Optically determined average porosity as a function of volumetric energy density (VED) for different process parameters" [32]. This figure was published in Materials and Design, Vol 191, Higashi, M. and Ozaki, T., Selective Laser Melting of Pure Molybdenum: Evolution of Defect and Crystallographic Texture with Process Parameters, 1-11, Copyright Elsevier (2020). Used with permission.

Parameters, 1-11, Copyright Elsevier (2020). Used with permission. see Figure 7.

"Optically determined average porosity as a function of volumetric energy density (VED) for different process parameters" [32]. This figure was published in Materials and Design, Vol 191, Higashi, M. and Ozaki, T., Selective Laser Melting of Pure Molybdenum: Evolution of Defect and Crystallographic Texture with Process Parameters, 1-11, Copyright Elsevier (2020). Used with permission. [36]. Samples with less than 1% porosity were formed only if the volumetric energy density, VED, exceeded 150 J/mm³ [36]. Higashi used different combinations of laser powers (100-350 W) and laser speeds (400-4,000 mm/s) to achieve these results [36]. At the lower power end, 100 W, and slowest speed, 400 mm/s, samples had at least 15% porosity [36]. Only with a

higher power of 200 W could a sample of <1% porosity be manufactured using the slowest laser speed of 400 mm/s [36].

Samples showed one or two types of pores. Lack of fusion pores could be eliminated with increased VED, but keyhole pores, “spherical pores generally attributed to the entrapment of metal vapors within melt pools”, always remained, possibly due to oxidation behavior of Mo [28, p3].

MoO₃ melts at 805°C and volatilizes at 1155°C, while Mo melts above 2600°C during AM. This logic regarding metal vapors is a reasonable assumption if the Mo powder is no longer pure but was oxidized, as is likely the case if the Mo powder was ever in an air environment. This presence of keyhole pores at every VED highlights another reason for the necessity to eliminate impurities in the Mo powder and prevent oxidation.

In analyzing the microstructure of SLM samples, Higashi et al. noted that the VED derived from contributing factors as well as the scan speed independently influenced crystal structure [36]. A <001> structure formed at nearly every lower VED value, below 250 J/mm³, and <110> formed at higher VED values [36]. When the microstructure did not fit the pattern explained by VED, it was found that the <001> structure only formed at scan speeds above 800 mm/s and the <110> structure only formed at 400 and 600 mm/s [36]. A <111> structure only formed at 400 mm/s with VED below 400 J/mm³ [36].

The reason for the variation in microstructure along the build direction is directly tied to the shape of molten pool, which is tied to scan speed and temperature gradient [36]. Grains in the melt pool form <001> structures when solidifying, but the average

angle of these orientations varied with scan speed. At higher scan speeds, all else being the same, a shallower, narrower pool developed, and the $\langle 001 \rangle$ orientation of crystals that formed towards the center vertical had higher angles [36]. The higher angles meant that on average, with respect to the top surface, $\langle 001 \rangle$ orientation was measured, while lower angles at slower scan speeds and lower temperature gradients had a $\langle 110 \rangle$ orientation along the build direction [36].

Kinkade assessed the effect of energy density, scan strategies, and atmospheres on the mechanical properties of SLM Mo alloyed with Re [37]. Like other studies, Kinkade recognized that higher VED led to higher densities and better mechanical properties in his materials, and increasing Re up to 25% near the solubility limit improved the mechanical properties the most [37]. Improved ductility corresponded to the addition of increasing amounts of Re compared to pure Mo in any environment [37].

Kinkade proposed multiple reasons for the better bending strength and reduced strain in samples built in the hydrogen environment compared to the Ar environment [37]. First, reduced grain size and fewer impurities at grain boundaries might be the reason for strengthened boundaries [37]. Second, hydrogen reacting with the oxygen or preventing oxygen from segregating at grain boundaries may lead to nucleation sites and transgranular fractures [37]. Samples in the Ar environment lacked the nucleation [37] sites. Third, the hydrogen atmosphere may result in reducing the trioxide present to dioxide, which refined the microstructure or removed oxygen from powder [37].

While many researchers conducted studies on the parameters of SLM, and on SLM of Mo, little has been done on the effect of atmospheres under which SLM occurs. Besides Kinkade, one notable exception is the work by Jing Dong, et, al, and their study

of microstructure and properties of AM W under nitrogen and Ar [38]. Keeping all other parameters the same, Dong et al. found that nitrogen was more helpful in additively manufacturing W than Ar [38]. Samples under both atmospheres were manufactured at 400 and 450 W, achieved above 95% density compared to theoretical density, and oxygen content of the processed W was below 0.080%, much less than the 0.056wt% of the pre-processed powder [38].

Each of the properties studied followed what was to be expected from the respective densities, besides similar microstructures [38]. The specimens from a 450 W laser power were denser than 400 W, and those under nitrogen were denser than Ar [38]. The surfaces of the denser specimens were smoother with less globular islands, had fewer pores when viewed under microscopes, had a higher microhardness and compressive strength, and possessed higher bending strength [38].

The rapid quenching, smaller crystallite sizes, and higher density translated to improved properties of W under nitrogen compared to Ar [38]. Manufacturing under nitrogen caused lower surface roughness due to lower dynamic viscosity of the molten pool [38]. There were no oxide peaks when analyzed with x-ray diffraction, but crystalline size was distinctly different. The rapid cooling during SLM under nitrogen gas quenched the materials to inhibit fast growth of crystallites, and the resulting W specimen had a higher nitrogen content [38]. It is likely that similar results to those of W under Ar and nitrogen atmospheres would be found when testing Mo powders and AM specimens.

In unpublished experiments, Kemnitz et al. found that an Ar-3%H₂ environment improved the max stress before breaking or bending for W, see Figure 8. Because of

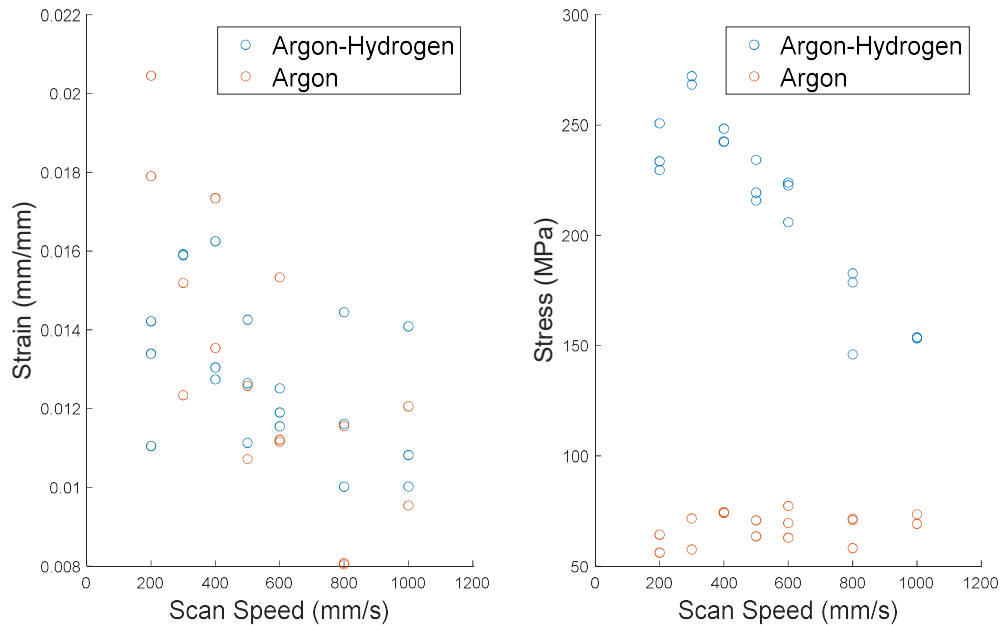


Figure 8. Effect of Argon Atmosphere on Stress and Strain

similarities between W and Mo, a change in build atmosphere may prove helpful for printing Mo, too. The effect on strain is not as apparent as the effect of the atmosphere on stress when conducting a three-point bending test on AM samples.

These investigations have shown that Mo may be processed by SLM, and tweaks to the process appear to help building pure, fully dense Mo, including variations on the substrate plate shape and temperature, process parameters like VED, and shield gas or build atmosphere. Minimal reporting has been done on strength or bulk material properties and further work is needed.

2.5 Summary

This chapter presented discussions on high temperature materials, processing and extraction of Mo, and AM of Mo. As a refractory metal, Mo possesses desirable properties for high temperature applications but can be limited due to low oxidation resistance of the material, low DBTT, and shapes of the material for use in specific parts requiring additional processing. Traditional processing methods, arc-melting, powder metallurgy, and various extraction methods take precautions to manufacture fully dense, pure Mo. These methods can be time consuming and limit the shapes that could be explored when compared to using AM. AM poses its own set of problems to reduce oxygen impurities and improve density, i.e., prevent cracking. Attempts thus far include alloying with C or other materials to reduce oxygen content, using spherical powders, increasing the build plate temperature, increasing VED, using support structures during the build, and to a limited degree adjusting the build atmosphere with similar refractory metals. The latter is an area of research explored in the next chapter.

III. Methodology

3.1 Chapter Overview

The purpose of this chapter is to discuss the means to characterize the additively manufactured Mo specimens and how the change in laser speed, atmospheric composition, and temperature for the tests affected the specimens. Each test or analytical method is described in sufficient detail for reproduction. Results of the testing according to these methods are presented in Chapter IV.

3.2 Design of Experiments

Design of Experiments (DOE) is a means to develop an experiment or set of experiments with multiple variables, and with high statistical accuracy determine the influence of each variable on the results of the experiment. Developed by Fisher in the 1920s, the superiority of DOE over one variable at a time (OVAT) is the ability to use a single experiment to test multiple variables at once and the interaction thereof, reducing the required resources and time while improving the ability to determine optimal parameters for desired results [39].

In this study, two processing parameters (laser speed and build atmosphere) and the three-point bending test temperature were varied. Laser speed indirectly relates to the change in VED (Eq. 8), and 100-600mm/s is an ideal laser speed range because the curve of the energy density vs. strength for specimens changes around these values. Build atmosphere is one parameter not thoroughly studied in literature and one of the primary focuses in this study. Since the process of AM may change the inherent properties of Mo specimens, changing the temperature for a three-point bending test could characterize the

DBTT, and was the initial test conducted. Strength, strain, and the angle of break of the specimen under a load were measured to analyze ductility given the low DBTT of Mo.

$$VED = \frac{\text{Laser power}}{(\text{laser speed} \cdot \text{spacing} \cdot \text{powder thickness})} \quad 8$$

A two-level factor in DOE means that a single factor or variable will either be one of two values for an input [39], i.e., a laser speed of 100 or 600 mm/s, an atmosphere with 100% N₂ or 95% N₂/5% H₂, and a testing temperature of 25°C or 600 °C. A full factorial design looks at all possible combinations of factors [39] and would predict the values of each of the three variables to elicit the best result within the boundaries set by the high and low input values. The goal for this statistical analysis with DOE is to then determine which variable influenced the ductility the greatest and lead to the most appropriate follow-on testing for tangible results.

A two-level, full factorial design requires 2^k samples, with k being the number of variables [39]. With a replicate of three for each of the eight necessary samples to improve statistical significance, plus four samples at the center point of each of the three variables, 28 samples would be needed for this DOE. Three to five center points are recommended in a full factorial design to provide some inherent variability and check for curvature. Without a sufficient number of center points, a valid lack of fit test cannot be run due to insufficient degrees of freedom, and no quadratic terms can be included in the model. Since the design parameters had laser speeds at 200 and 400 rather than any at 350 mm/s, four middle specimens were chosen rather than those exactly at the mid-point. Adding center points achieves a similar higher power as replication, without replicating all data points (see Table 1).

Factorial designs assume a linear relationship between the variables and results. Significant p-values of a center point means the relationship is not linear but a curvature, and response surface models would be needed for quadratic fits. Without enough data, the statistically significant mid-point values would likely go undetected.

The design space was used as stated with a couple small deviations. Energy density is a significant factor in results. A change in laser speed from 200 to 100 doubles the energy density but is still relatively low. Since VED only changes with laser speed for this experiment, more specimens were preferred at 400 and 600 mm/s instead of 350 mm/s, the center point as called for in DOE. In this experiment, 76 samples were tested by the three-point bending test: 36 at 25°C, four at a 288°C, and 36 at 600°C. For the purposes of simplicity, the ambient temperature of the lab in which the experiments were conducted was considered room temperature, approximately 25°C. The middle temperature of 288°C instead of 313°C was used due to a mistake in calculating the midpoint of 25°C and 600°C.

Table 1. Design space per Design of Experiments (DOE).

Run	Speed (mm/s)	Test Temperature (°C)	% H ₂	Run	Speed (mm/s)	Test Temperature (°C)	% H ₂
2	100	25	0	6	100	25	5
4	100	25	0	22	100	25	5
18	100	25	0	20	600	25	5
25	600	25	0	15	600	25	5
17	600	25	0	10	600	25	5
24	600	25	0	11	100	600	5
21	100	600	0	12	100	600	5
23	100	600	0	3	100	600	5
14	100	600	0	16	600	600	5
1	600	600	0	8	600	600	5

5	600	600	0	9	600	600	5
26	600	600	0	13	200	288	2.5
19	100	25	5	7	400	288	2.5
27	400	288	2.5	28	200	288	2.5

3.3 Preparation of Metal Powders

Pure Mo powder was purchased from Tekna (Sherbrouke, Quebec). The powder was plasma spheroidized and sieved to a -45 micron mesh. The pure powder was analyzed for oxygen and hydrogen content prior to AM because the oxygen content is an important parameter in the manufacturing of Mo.

3.4 AM of Samples

All specimens were produced with the Concept Laser MLab Cusing 200R 3D metal printer (Cincinnati, OH, USA). Twelve specimens were printed in three different atmospheres and at four separate laser speeds for a total of 144 specimens. The machine produces laser speeds between 50-2000 mm/s. The ideal laser speed in previous samples was found between 100 and 600 mm/s so those limits were used on this experiment per DOE, with actual laser speeds of 100 mm/s, 200 mm/s, 400 mm/s, and 600 mm/s. The machine shields in place prevent external influence, and the ambient atmosphere can be maintained as desired. The three atmospheres used were 100% N₂ (N₂ or 0% H₂), 97.5% N₂ with 2.5% H₂ (2.5 H₂), and 95% N₂ with 5% H₂ (5 H₂).

Other build parameters included the laser power, layer thickness, and hatch spacing, see Figure 9. The laser direction was rotated by 90 degrees from layer to layer. Previous research [36] has shown that laser power directly affects the melt pool size which impacts the depth of a weld by penetrating multiple layers deep. Laser power of 300-400W were found to be ideal for a good weld but corresponded to powder

thicknesses of 30-40 microns. The laser power on the Concept Laser MLab Cusing 200R 3D metal printer can be adjusted between 25-200 W. Since the higher power is necessary for sufficient quality

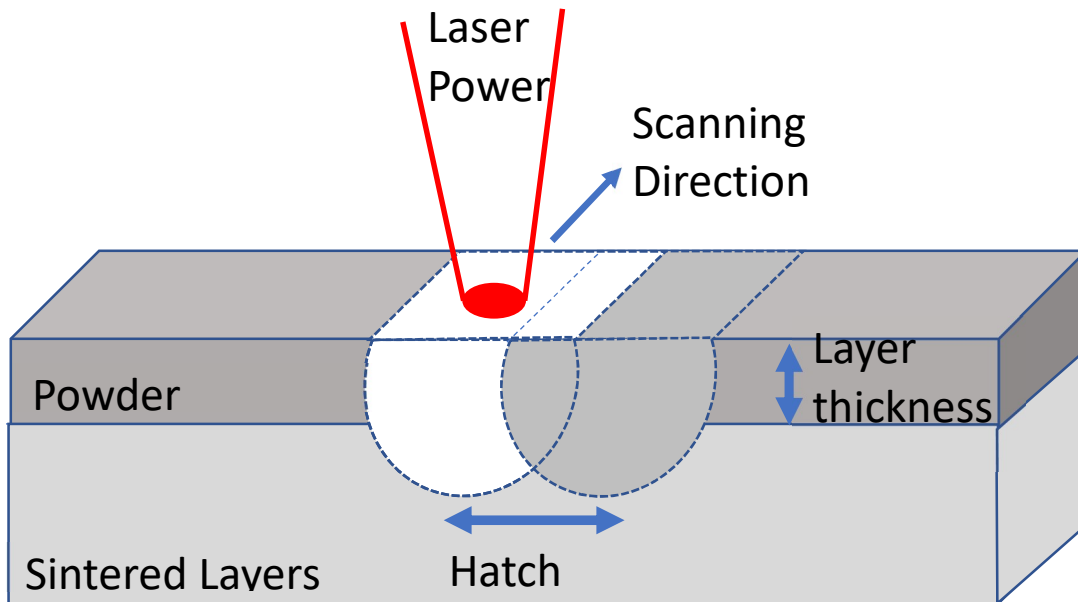


Figure 9. Illustration of additively manufactured sample

of welding, it was maintained at 200 W. The metal powder layer thickness can be set between 10-60 microns on the machine. Previous work with Kemnitz et al. used 20-40 microns layer thicknesses at 200 W and found 20 microns gave the best densification and welding, which was used in this experiment as well. The hatch spacing for 3D printed materials should allow 25-50% overlap for sufficient weld depth penetration. A spacing of 50 microns with a spot size of 50 microns was used for the Mo specimens.



Figure 10. Concept Laser MLab Cusing 200R 3D metal printer

3.5 Procedures and Processes for Mechanical Testing

3.5.1 Polishing and Drying

After the 144 specimens were manufacturing, each specimen was polished along the length vs. width sides to remove any particles stuck to the surfaces in preparation for testing. The intent in polishing was to remove the effects of surface finish on mechanical properties. A Buehler EcoMet 300 Pro Grinder Polisher (Lake Bluff, IL, USA) with 240 grit silicon carbide grinding disc papers was used, Figure 10 (a). Running water was used as the lubricant and coolant during the grinding process.

After grinding, all specimens were heated to 120°C for one hour to evaporate any water left on the samples or within surface connected porosity. Samples were heated in an Omegalux LMF-3500 furnace (Stamford, CT, USA), **Error! Reference source not found.** (b). The relatively low temperature was enough to dry the samples thoroughly, but not high enough to cause annealing. The annealing temperature for Mo is between 1950° and 2100°C [14]. Oxidation is not significant at 120°C. Length, width, and height measurements of each specimen were taken prior to conducting the three-point bending test.

3.5.2 Mechanical Tests

Prior to all mechanical tests, the length, width, and thickness of each sample was measured so that variations due to grinding or the AM process were mitigated.

3.5.2.1 Three-Point Bending Test at Room Temperature

The mechanical test conducted was a three point-bending test at room temperature for three specimens at each combination of atmosphere and laser speed (36 specimens) using the Material Testing System (MTS) Model 810 (MTS Systems Corporation, Eden Prairie, MN, USA), shown in Figure 11.

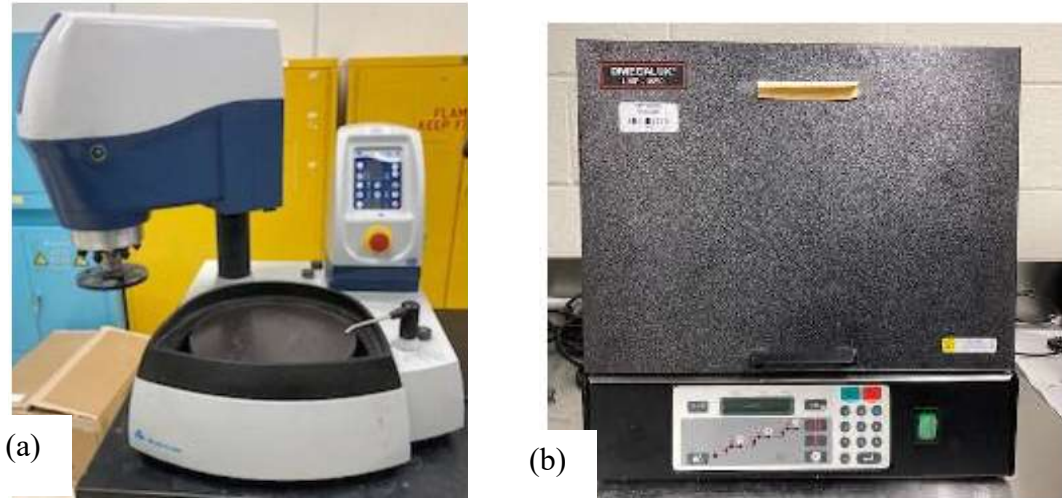


Figure 11. (a) Buehler EcoMet 300 Pro Grinder Polisher (Lake Bluff, IL, USA) and (b) Omegalux LMF-3500 furnace (Stamford, CT)

The testing procedure was conducted according to the following steps:

1. Each sample was placed in the machine on the lower two points of the bending fixture.
2. The distance between the lower points of the three-point bending test was re-measured and adjusted each test to ensure a distance of 14 mm from center to center of the pins.
3. The upper point was adjusted vertically until almost touching the specimen, with less than 0.2 mm of separation.
4. Force and displacement readings were zeroed.
5. Then the test procedure was initiated. A custom test procedure was developed using the MTS software. The test procedure included the following steps:
 - a. Data logging was initiated to record time, axial displacement, and force.

- b. A ramp function increased the displacement on the specimen at a rate of 0.01mm/s.
- c. The test was interrupted when a break was detected with a 50% change in axial force or a threshold of 0.2 kN was reached.
- d. After test interruption, data was exported and the test concluded.

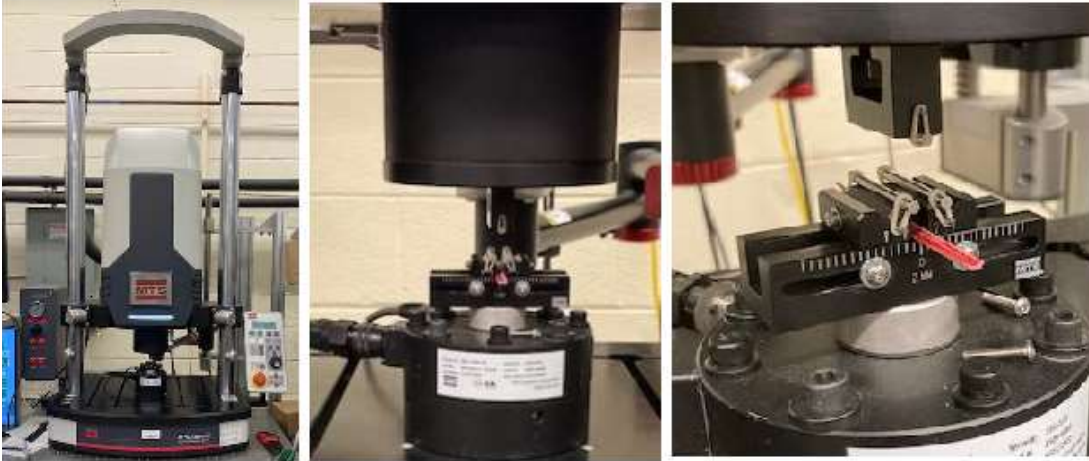


Figure 12. the Material Testing System (MTS) Model 810 (MTS Systems Corporation, Eden Prairie, MN, USA)

3.5.2.2 Three-Point Bending Test at Mid-Point Temperatures

The midpoint temperature test conducted for the four specimens used the MTS 810 Material Test System with the MTS 653 Furnace and 647 Hydraulic Wedge Grip (see Figure 13).

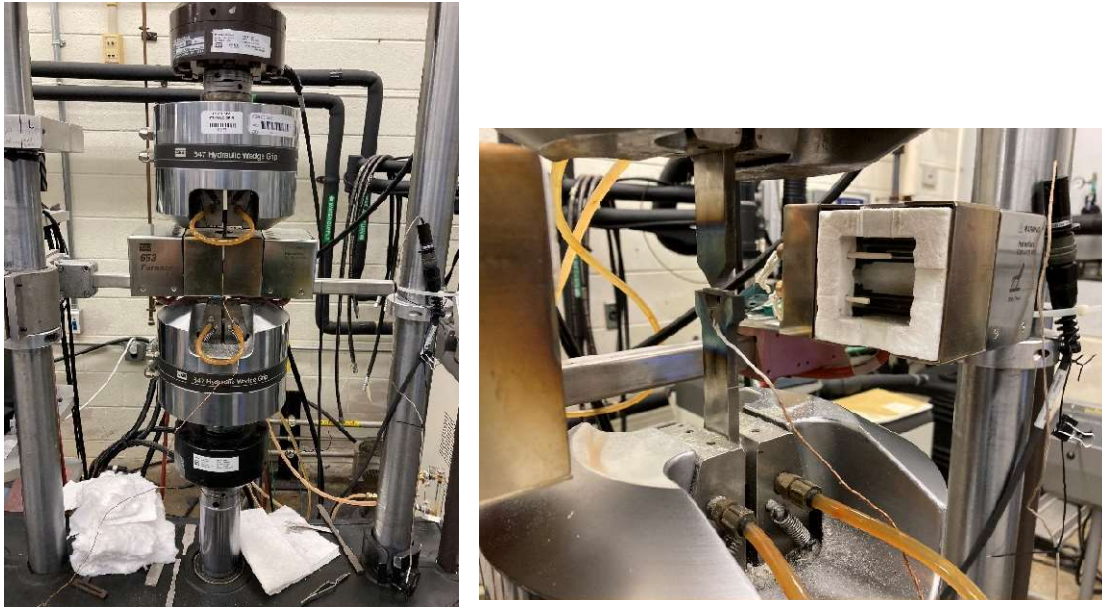


Figure 13. 810 Material Test System with the MTS 653 Furnace and 647 Hydraulic Wedge Grip

The testing procedure was conducted according to the following steps:

1. Each sample was placed in the machine on the lower two points of the bending fixture.
2. The distance between the lower points of the three-point bending test was re-measured and adjusted each test to ensure a distance of 14 mm from center to center of the pins.
3. The upper point was adjusted vertically until almost touching the specimen, with less than 0.2 mm of separation.
4. The left and right furnaces were placed around the sample to ensure proper heating.

5. The test procedure was initiated. A custom test procedure was developed using the MTS software. The test procedure included the following steps:
 - a. The temperature of the left and right furnaces was set to 288°C. The temperature was held for five minutes to ensure the specimens were also at 288°C.
 - b. Forces were zeroed after heating.
 - c. Contact between the specimen and upper hydraulic grip was established, confirmed by the applied force reaching -15 N (the compressive force read negative).
 - d. Data logging was initiated to record time, axial displacement, and force.
 - e. The displacement increased in magnitude at a rate of 0.01 mm/s, deforming the specimen.
 - f. The test concluded when the software read 0 N.

The left and right furnaces were turned off and separated. The lower hydraulic grip lowered, the specimen removed for further analysis, and data exported.

3.5.2.3 Three-Point Bending Test at High Temperature

The 600°C, high temperature three-point bending test for the 36 samples (same variation as the room-temperature test) was similar to the three-point bending test at mid-point temperature. The tests were conducted on the same machine as the mid-point test with only minor adjustments to efficiently conduct the test at 600°C versus 288°C.

3.5 Statistical Analysis Methods

MATLAB software was used to analyze the resultant mechanical test data. Time, displacement, and force data from each three-point test was collected, as well as

dimensions of the samples. Max stress, max strain, break stress, break strain, and break angles were calculated from the data using the code. These results were plotted for graphical analysis in MATLAB and the basis for the analysis of variance (ANOVA) computations using Stat-Ease software.

Stat-Ease Software was used to conduct ANOVA tests to determine any relationship between or among independent variables of the three-point test temperature, build atmosphere, and laser speed of the build when it came to results of the max stress, max strain, break stress, break strain, and break angle of the samples. ANOVA tests were conducted for the 24 samples from each atmosphere independently, the 26 samples from the DOE sample space, and the data from all 76 three-point tests conducted. Data was then split by test temperature for further ANOVA tests to determine if atmosphere, laser speed, or some interaction of those two variables impacted results independent of a changing test temperature. Depending on the data, the best model and transformation was applied in order to achieve significant models with no significant lack of fit.

3.6 Microstructure and Fracture Surface Analysis

Chemical Analysis

Chemical composition analysis was conducted by inert gas fusion by Miami Valley Materials Testing. Samples were run on a LECO (St. Joseph, MI) ONH 836 in accordance with ASTM E1409 for oxygen and nitrogen and ASTM E1447 for hydrogen. Testing was accomplished on pure powder prior to testing as well as AM samples after mechanical testing.

SEM and Optical Microscopy

Following the three-point bending tests, each sample was examined using a SEM and optical microscopes. The TESCAN MAIA3 scanning electron microscope (TESCAN, Brno, Czech Republic), shown in Figure 14, was used to examine the fracture



Figure 14. TESCAN MAIA3 scanning electron microscope surfaces and analyze differences in fracture patterns, oxidation present, and defining characteristics. Such characteristics include, but are not limited to: unmelted Mo powder, distinct river patterns in fracture surface, dendrites, and cracks due to fabrication (see Figure 15).

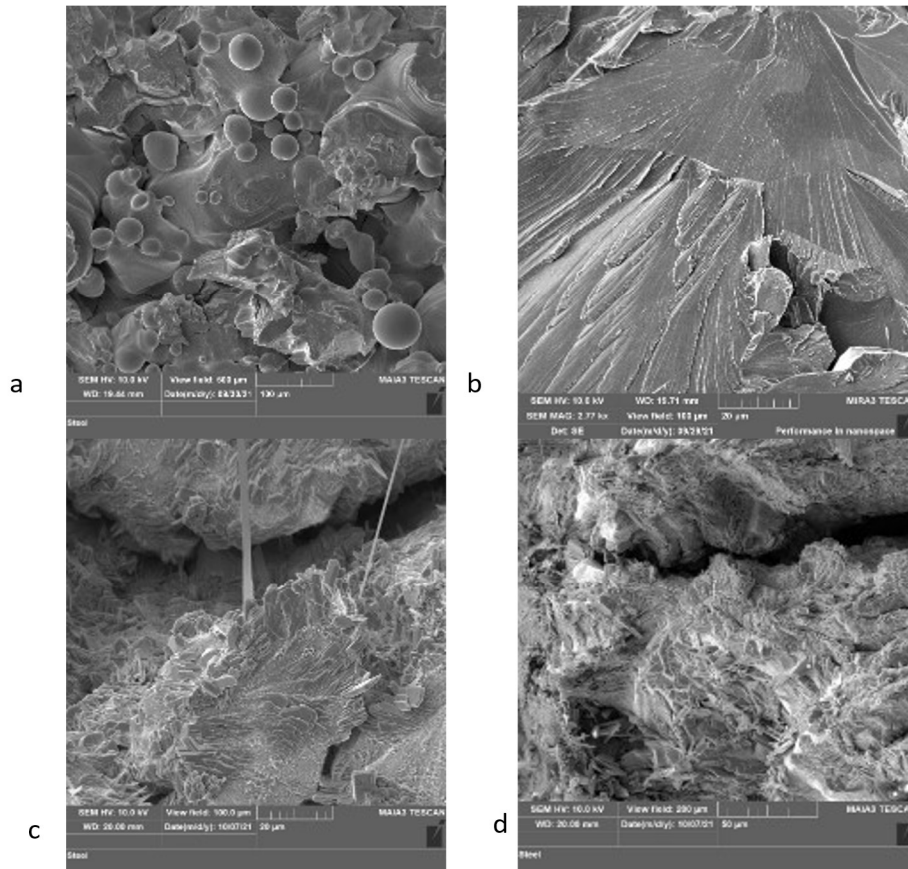


Figure 15. Example fracture surface images from a variety of sample conditions

Prior to optical microscope analysis, samples were separated by the atmosphere used during the build. A specimen from each of the four laser print speeds per build atmosphere were mounted together in a single carbon puck, with three pucks total. The MetLab Metpress A, see Figure 15, was used to create each puck, which was then polished using the Buehler EcoMet 300 Pro Grinder Polisher. Each puck was laid out with four samples side by side, one at each laser speed, with one puck for each build

atmosphere. Each puck was examined using the Zeiss Axio Observer Z1m optical microscope (Jena, Germany), see Figure 17.



Figure 16. MetLab Metpress A and carbon puck

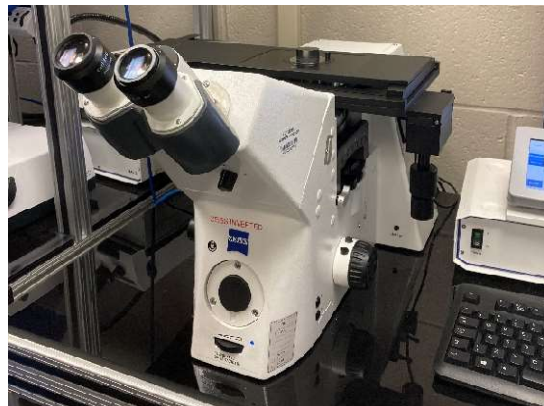


Figure 17. Zeiss Axio Observer Z1m Optical Microscope

The images taken with the optical microscope of each build speed and each atmosphere were used to compare qualitative porosity and grain size of the specimens. Various magnifications were used, including 2.5x, 5x, 10x, and 20x when analyzing porosity. Grinding of pucks took place with various grit paper, from 240-800 grit for one minute at a rotation speed of around 200 rotations/minute. Polishing occurred using

various diamond suspension solutions on a polishing pad. Etching took place with submitting the samples to two minutes of hydrogen peroxide before rinsing and cleaning the specimens with water and isopropyl alcohol.

3.7 Summary

DOE was used to define initial parameters of the experiment, totaling 28 samples needed for analysis: six samples at the N₂ and 5 H₂ atmospheres and 100 and 600 mm/s laser speeds to be tested at room temperature and 600°C, with four intermediate samples. Given some of the expected results, future tests, and analysis, 12 samples at each of the atmospheres and laser speeds were AM for a total of 144 samples.

AM samples built from plasma spheroidized powder in the three atmospheres were then polished and dried. The three-point bending tests at the three different test temperatures commenced. Quantitative analysis of the results took place with both MATLAB and Stat-Ease software.

Fracture surface of samples from the high and low temperature test were analyzed using SEM. Twelve sample were put into three carbon pucks according to atmosphere and analyzed under optical microscope for porosity, as well as another set of 12 samples analyzed by etching to assess the grain structure. Each of the 12 different samples and the Mo powder were analyzed for the chemical composition.

IV. Analysis and Results

4.1 Chapter Overview

This chapter presents the results and analysis from the experiments as outlined in Chapter III. The two main sections are the experimental results and the ANOVA quantitative analysis. The ANOVA analysis is further broken down into four subsections. The DOE results include optical microscopy analysis of porosity, etched micrographs, and chemical composition. The ANOVA from all data highlights the different trends and relationship between build parameters and physical properties not readily observed when just examining the 28 DOE samples. The third subsection provides analysis of samples that are grouped by atmosphere, and includes comparison to unpublished data of Mo samples built in Ar and Ar with 3% H₂ atmospheres. The final subsection is the ANOVA by mechanical test temperature. This subsection highlights the importance of utilizing high temperature testing to tease out the relationship of build parameters not otherwise seen in brittle, room temperature tested samples, and includes the SEM analysis.

4.2 Experimental Results

That data from the three-point tests was graphed in MATLAB according to the temperature of the test, comparing the scan speed vs. stress and the scan speed vs. break angle, see

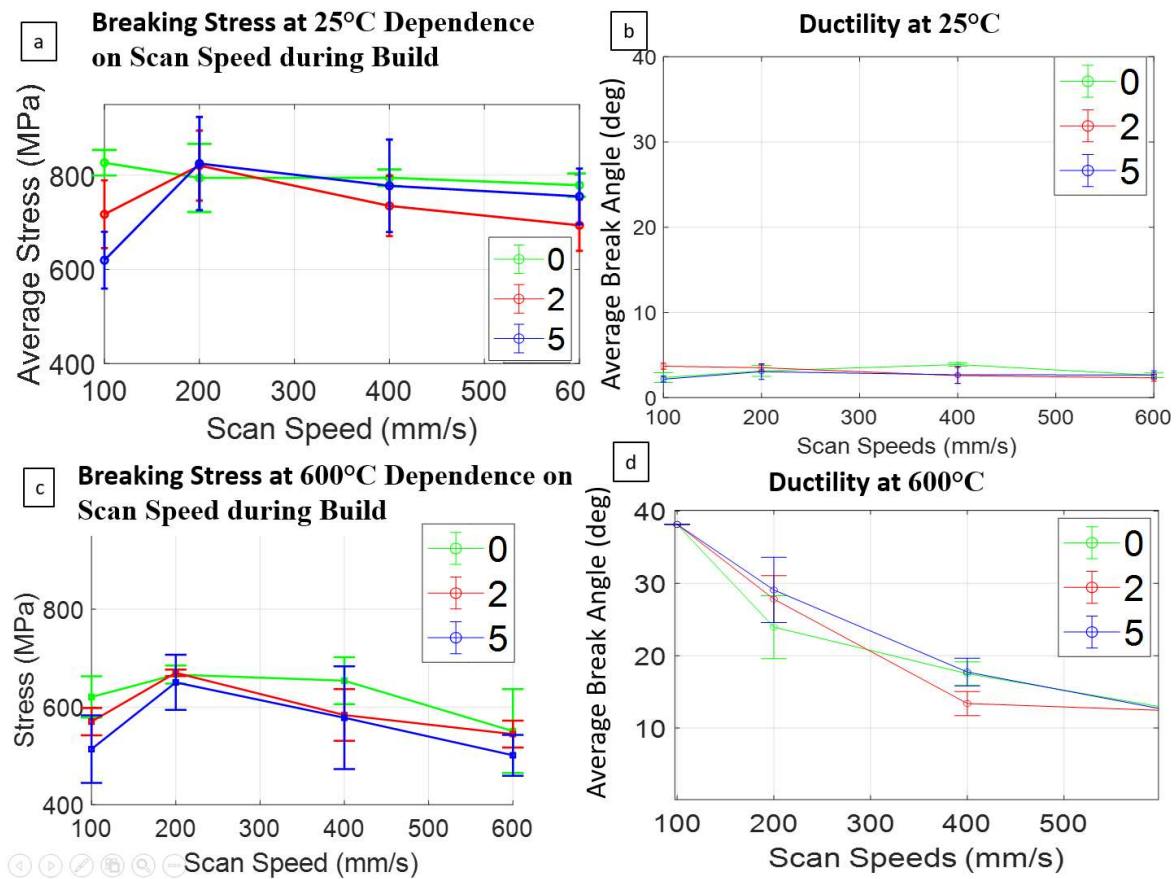


Figure 18. The different color lines in

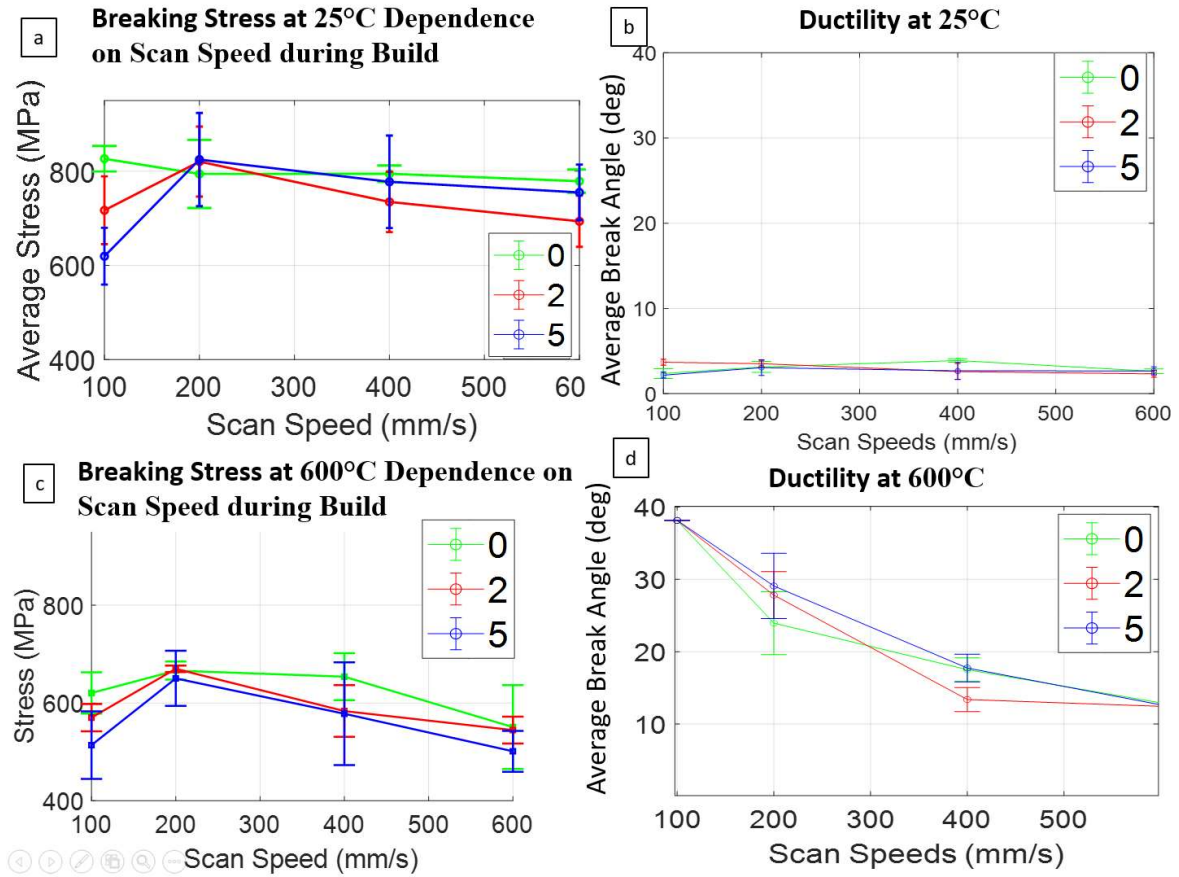


Figure 18 represent the different build atmospheres by the amount of H₂ present. In

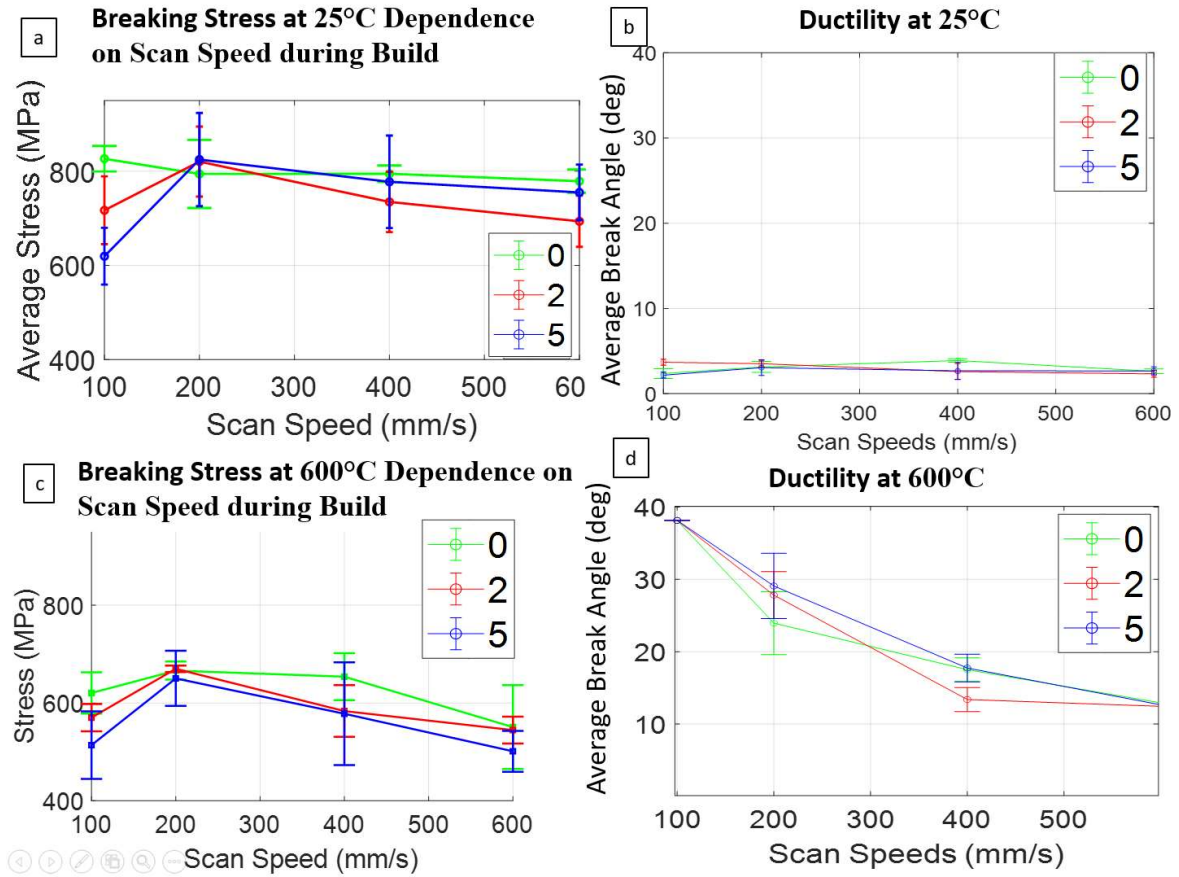


Figure 18b, there is no discernable pattern or trend for break angle with a spread of less than two degrees difference across the plotted averages. Room temperature samples exhibit very low ductility regardless of build atmosphere or scan speed. At elevated test temperature,

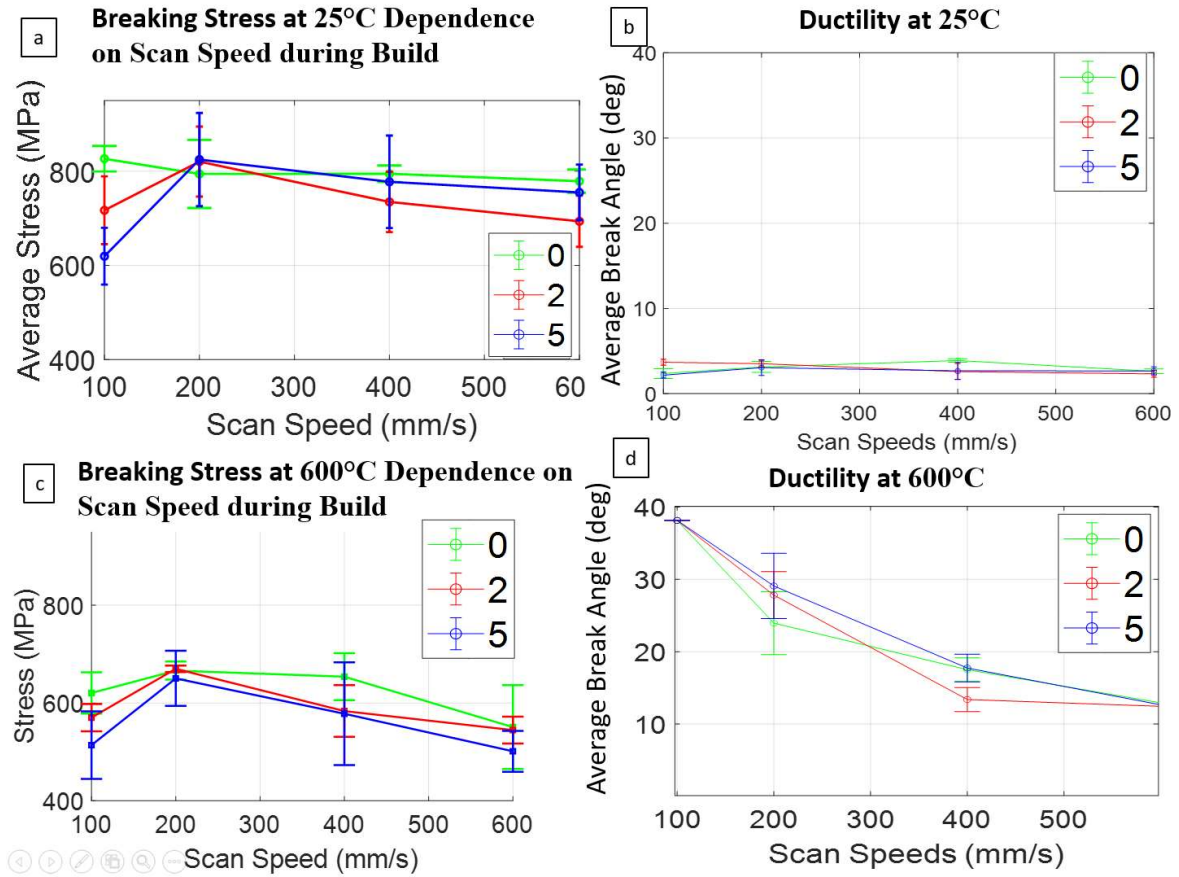


Figure 18d, there is a distinct trend across all build atmospheres in ductility where increasing scan speed results in a lower average break angle.

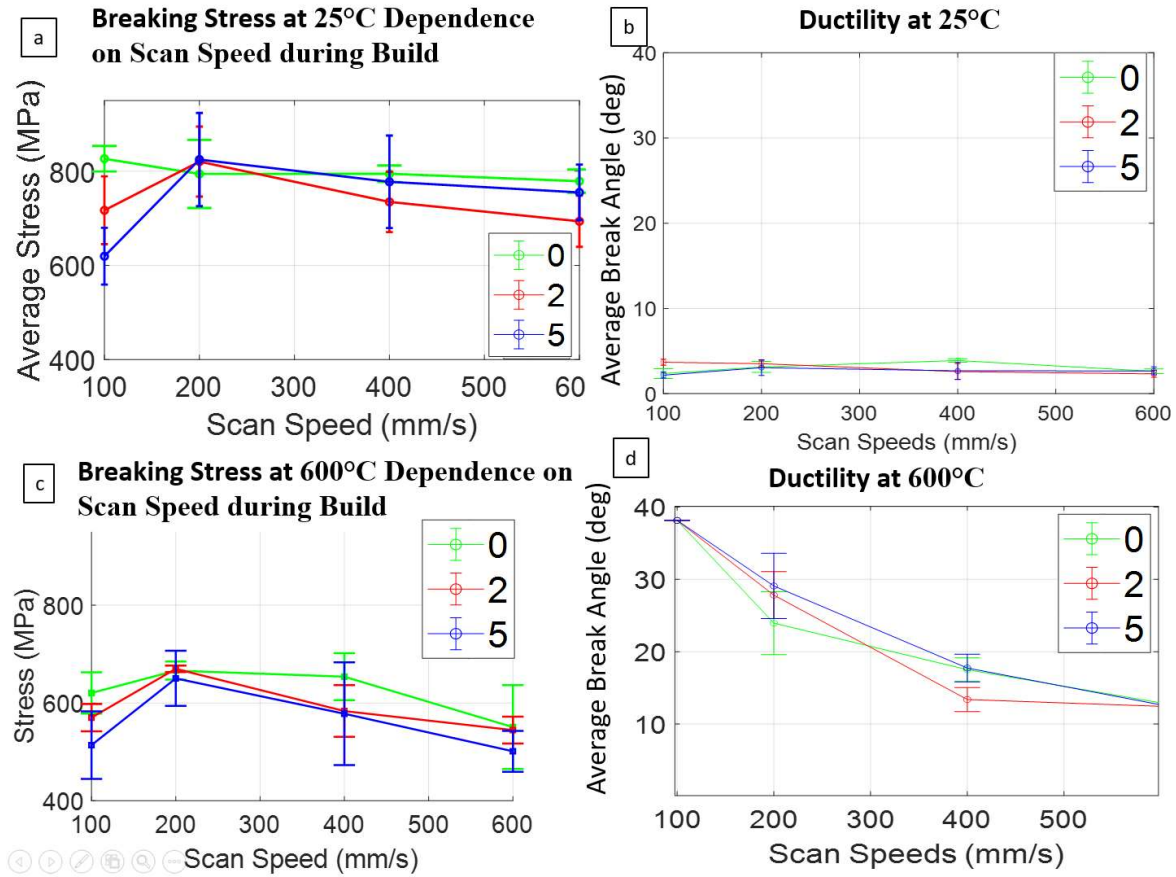


Figure 18. Room Temperature and High Temperature three-point bending tests results comparing scan speed to stress and break angle.

Both of these results are consistent with expectations. At room temperature, Mo is brittle [2] and a low break angle is expected for this type of material. At 600°C, above the DBTT [2], every break angle result is greater than that of the samples tested at room temperature. Mo samples exhibit higher ductility at lower laser speeds and a higher VED (Eq. 8). There does not appear to be a difference in the build atmosphere when comparing the break angles and scan speed at high test temperatures, but further discussion will be deferred to the quantitative analysis with DOE.

The stress vs. scan speed figure at room temperature, shown in

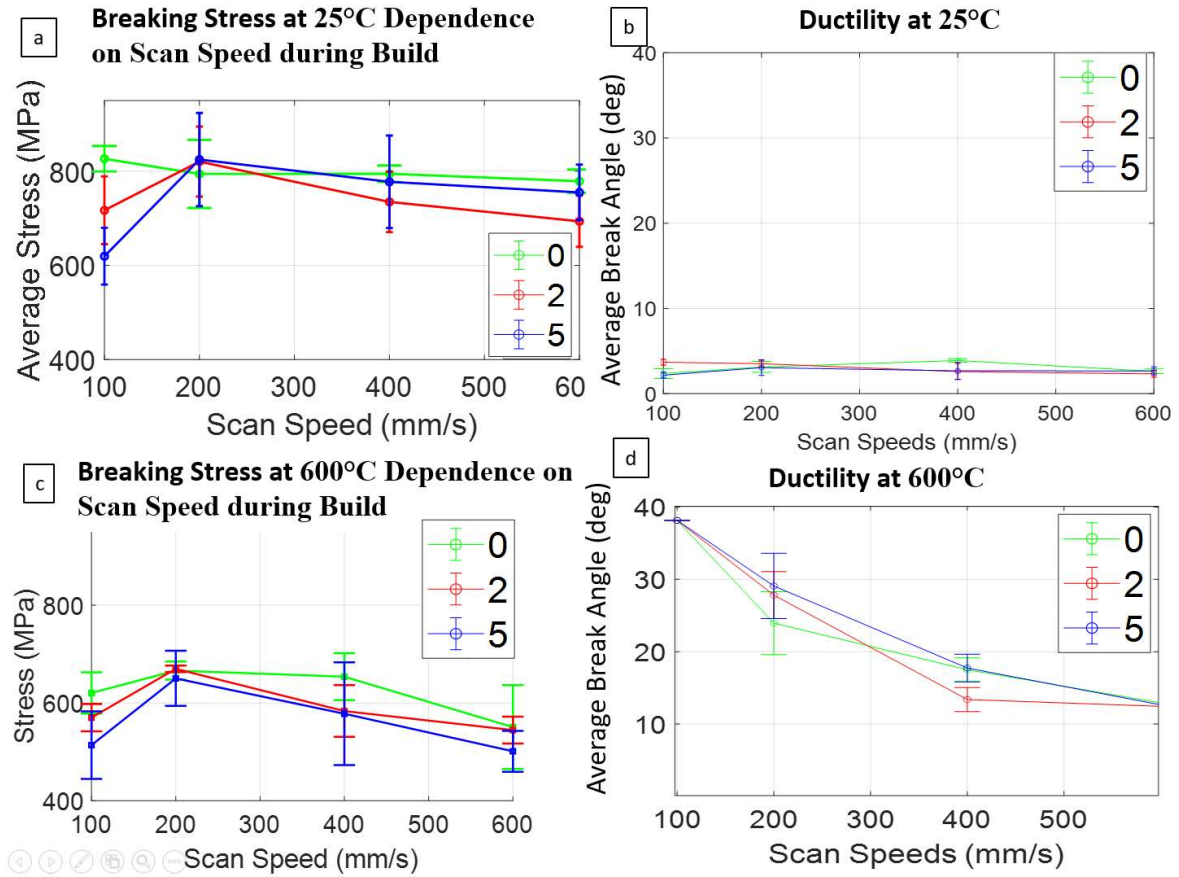


Figure 18a, again does not appear to have a discernible trend related to the build atmosphere. When the overlapping error bars are considered, any statistical significance is difficult to ascertain from this graph. Later discussion will further elaborate on quantitative analysis of tests.

The stresses, shown in

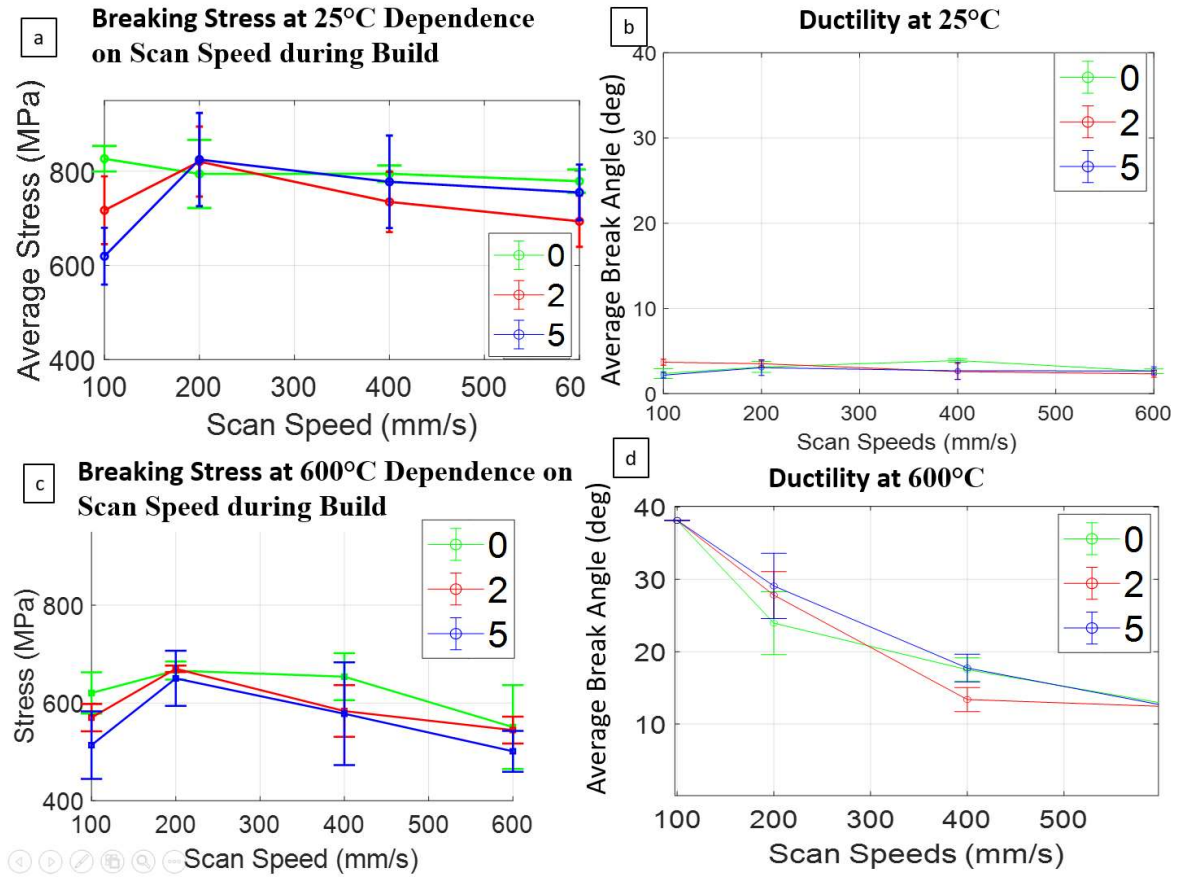


Figure 18c, show a similar small trend as the room temperature test with an increase of stress from 100 mm/s to 200 mm/s before decreasing across some samples, but with overlapping error bars, any statistical significance is difficult to ascertain. Comparing the results by temperature, every atmosphere shows an increase in stress from 100 mm/s to 200 mm/s in the high temperature test before decreasing instead of just the 2.5 H₂ and 5 H₂ samples in the room temperature test. Additionally, the relative stresses at each scan speed and atmosphere are lower for the high temperature specimens than the room temperature specimens. This is likely due to the increased ductility, and corresponding decreased strength at higher temperatures above the DBTT [9] as discussed in the preceding paragraphs.

Figure 19 depicts the stress vs. strain curves for the room temperature three-point bending tests, with each graph a separate build atmosphere and each set of colors a

Flexural Stress vs. Strain Curves for Room Temperature Test

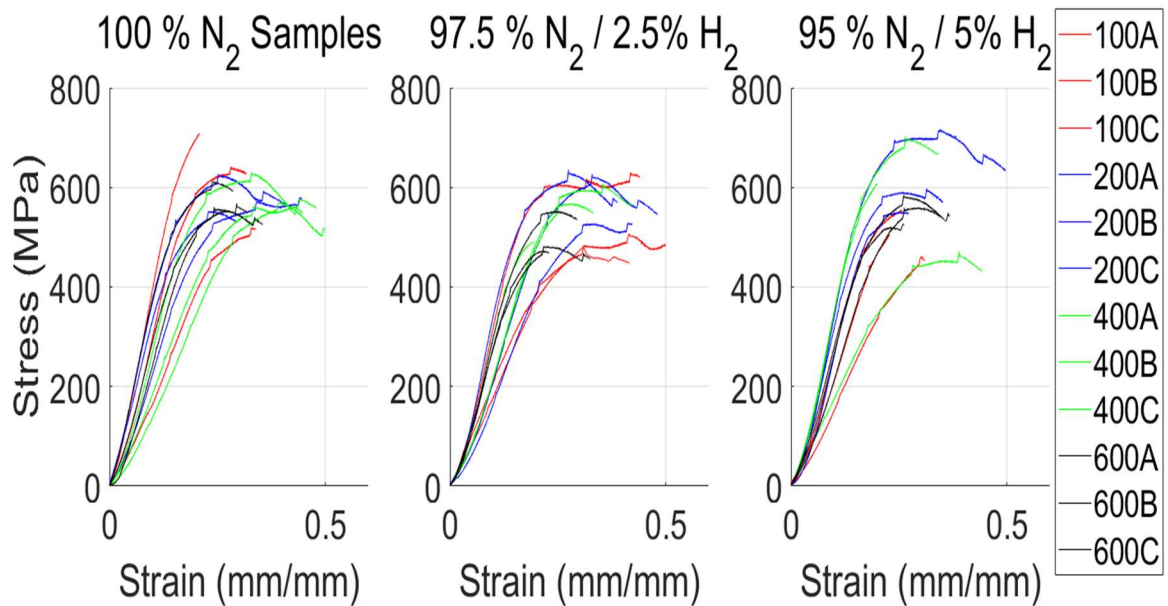


Figure 19. Flexural Stress vs. Strain Curves for the room temperature three-point bending tests

different scan speed. The displacement controlled bending test was continued after the maximum stress value was reached until the specimen carried less than 10 N.

Figure 20 depicts the same separation of build atmospheres and scan speeds but for the high-temperatures tests. In the room temperature samples, as the atmosphere increases in H₂, variability in the samples decreases and the Young's Modulus increases slightly. There is no further trend or distinct difference in any of the room temperature tests across build atmosphere or scan speed. All samples are relatively brittle, but much more ductile than at room-temperature.

Flexural Stress vs. Strain Curves for High Temperature Test

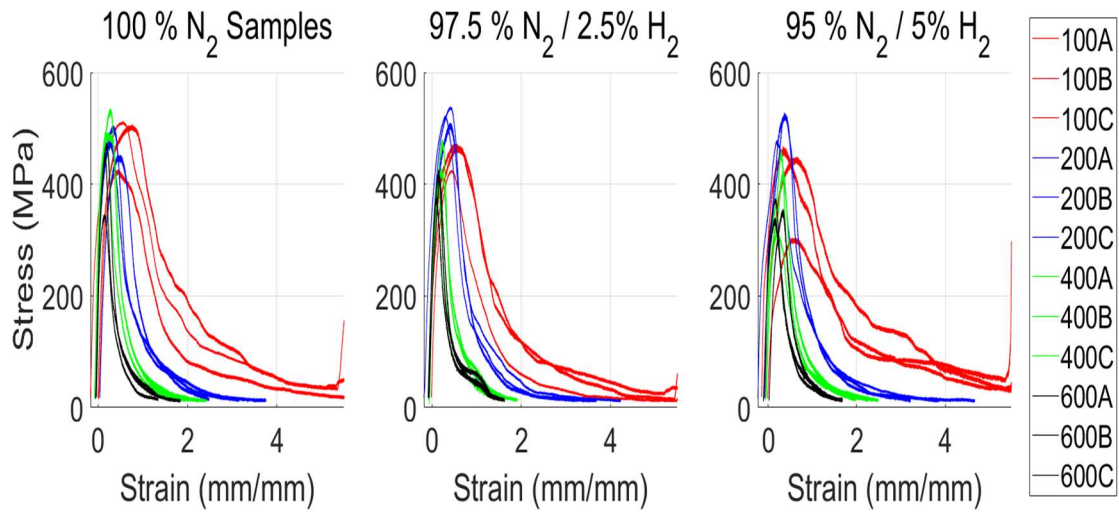


Figure 20. Flexural Stress vs. Strain Curves for the high temperature three-point bending test

The high-temperature test samples maintained some ductility, an order of magnitude improved over the room temperature samples, and many carried a load after initial fracture. The stresses of the high temperature samples are lower than those of the room temperature samples, which agrees with the earlier analysis. Looking just at the high temperature tests, there are two additional trends. First, lower laser speed samples exhibit the largest ductility, decreasing in strain as laser speed increases. Second, the 200 and 400 mm/s laser scan speeds tend to have higher ultimate stresses than other speeds. The ductility with lower scan speeds matches observations with the break angle results. The higher stresses at 200 mm/s corresponds to the weak trend in the stress vs. scan speed graphs.

4.3 ANOVA Results

Stat-ease software was used to quantitatively analyze the room temperature three-point bending test results, 600°C three-point bending test results, and the three-point bending test at 288°C results. An error resulted in using 288°C as the midpoint temperature instead of 312°C. For this analysis, the error of 25°C is unlikely to matter since the difference in temperature from 100°C and 600°C to 288°C is large enough in comparison to characterize a trend.

Per the DOE design space chosen, four control specimens were needed at the midpoint temperature of 288°C. Since the laser speeds to produce specimens were 200 and 400 mm/s instead of 350 mm/s (the midpoint), two specimens at 200 mm/s and two specimens at 400 mm/s were tested. A lack of center points reduces the statistical significance of the DOE design space. Instead of interpolating values from the 200 and 400 mm/s for two center point values (2.5 H₂ atmosphere, 288°C, and 350 mm/s laser speed), each of the results from the four control specimens were used in the statistical analysis.

The null hypothesis in an ANOVA is that there is no statistical difference among the group means. The Type III Sum of Squares ANOVA corresponded to each effect adjusted for every other effect in the model. The factors were A- scan speed from 100 to 600 mm/s, B- test temperature from 25°C to 600°C, and C- percent H₂ in the build atmosphere (N₂, 2.5 H₂, or 5 H₂). Any single factor or interaction of factors would be significant if the probability of occurrence, or p-value, was < 0.0001, and the null hypothesis rejected.

Residuals are the difference from an individual data point and the group mean. Data points, or transformation of data points as required for a best fit model, should fit the assumption of normally distributed residuals. While not shown in the following ANOVA tables, the predicted and adjusted R^2 values should be within 0.2, and the normal plot of residuals follow a line. For each ANOVA with a lack of fit p-value > 0.005 , as in not significant, the residuals and normal plot requirements were met and included for discussion.

The experimental results discussion focused on break angle as a measure of ductility, and stress and strain. The DOE quantitative analysis focused on other results to include yield stress, ultimate tensile stress, strain at ultimate tensile stress referred to as ultimate tensile strain in this paper, final strain, and Young's modulus. (Since this was a three-point bending test with compression, the ultimate tensile stress as calculated and referred to throughout this paper is often called flexural stress or strain.) ANOVA were conducted for the DOE design space, all specimens, as well as groups of samples at the same build atmosphere and at the same test temperature. Significant results are those which also had no significant lack of fit. Significant lack of fit means the error from those ANOVAs could not be determined to be due to the factors themselves versus from an ill-fitting model, thus the overall results could not be used. The summation of significant ANOVA results is listed in Table 2.

Significant ANOVA results were found in 25 of the 35 tests conducted. Laser scan speed and test temperature were the two primary factors. Of those ANOVA results where temperature could be a factor, temperature or the interaction of temperature and another factor is significant for all except the results of Young's Modulus. Similarly,

laser speed or its interaction with another factor is significant for all but three tests, highlighted in red in Table 2. Notably, atmosphere is only involved with nine results, and none of those are for ultimate tensile strain or final strain. There are no statistically significant results for the group of samples tested at room temperature.

The abbreviations for Table 2 are for the ANOVA test type and significant factors. Significant factors are: T, test temperature; A, build atmosphere; S, laser speed; TS, TA, SA are interaction of respective factors; and squared values are just that for quadratic models. Blank spaces in the table means that group had no statistically significant ANOVA results. ANOVA types are: SF, selective factorial; Q, quadratic; 2FI, two factor interaction; and L, linear.

The Stat-Ease software begins calculating the best fit model, or ANOVA type, by adding sequential sum of squares of linear terms to any intercept or blocks added in the design phase (none were added here). Then, the software considers adding the sum of squares of 2FI terms to the linear model and considers if the new terms improved the model. Similarly, the sum of squares of quadratic terms are added to the 2FI model and the best fit model overall is used in further analysis. The best model would meet several criteria: it is significant (p-value below 0.05), the addition of subsequent complex terms does not substantially improve the fit, a lack of fit test is not significant, it has a low standard deviation in comparison to other models, it has a high R-squared value and a low predicted residual sum of squares for the model.

The impact of varying laser speed or its interaction with another factor is significant for all but three tests. The significance of laser speed agrees with the findings

of Higashi et al. in that trends or values of VED, which is only varied by laser speed in the present study, explained nearly every trend [36].

Table 2. Statistically significant ANOVA results by factor and analyzed sample groups.

Select Samples	Yield Stress	Ultimate Tensile Stress	Ultimate Tensile Strain	Final Strain	Young's Modulus
DOE Design Space		SF: T, A	SF: T, S, TS		SF: S, A
All Samples	Q: T, S, A, TA, TS, SA, T ² , S ²	Q: T, A, S ²	2FI: T, S, TS	Q: T, S, TS, T ² , S ²	L: A
N ₂ (0% H ₂)	2FI: T	L: T, S	2FI: S, TS	2FI: T, S, TS	
2.5% H ₂	Q: T, TS, T ² , S ²	Q: T, S ⁵	2FI: T, S, TS	Q: T, S, TS, T ² , S ²	
5% H ₂			2FI: T, S, TS	2FI: T, S, TS	
600°C test	Q: S, A, S ²	Q: S, A, S ²	Q: S, S ²	Q: S, S ²	Q: A, S ²
25°C test					

ANOVA Analysis of DOE Design Space

Analysis of solely the DOE design space did not show statistically significant results in yield stress or final strain, but showed a strong relationship with two or three factors of test temperature, laser speed, and build atmosphere on the results of ultimate tensile stress, and ultimate tensile strain, and Young's modulus. Figure 21 shows the relationship between test temperature and laser speed to ultimate tensile strain. Build atmosphere is not significant, nor is the relationship of laser speed for the room

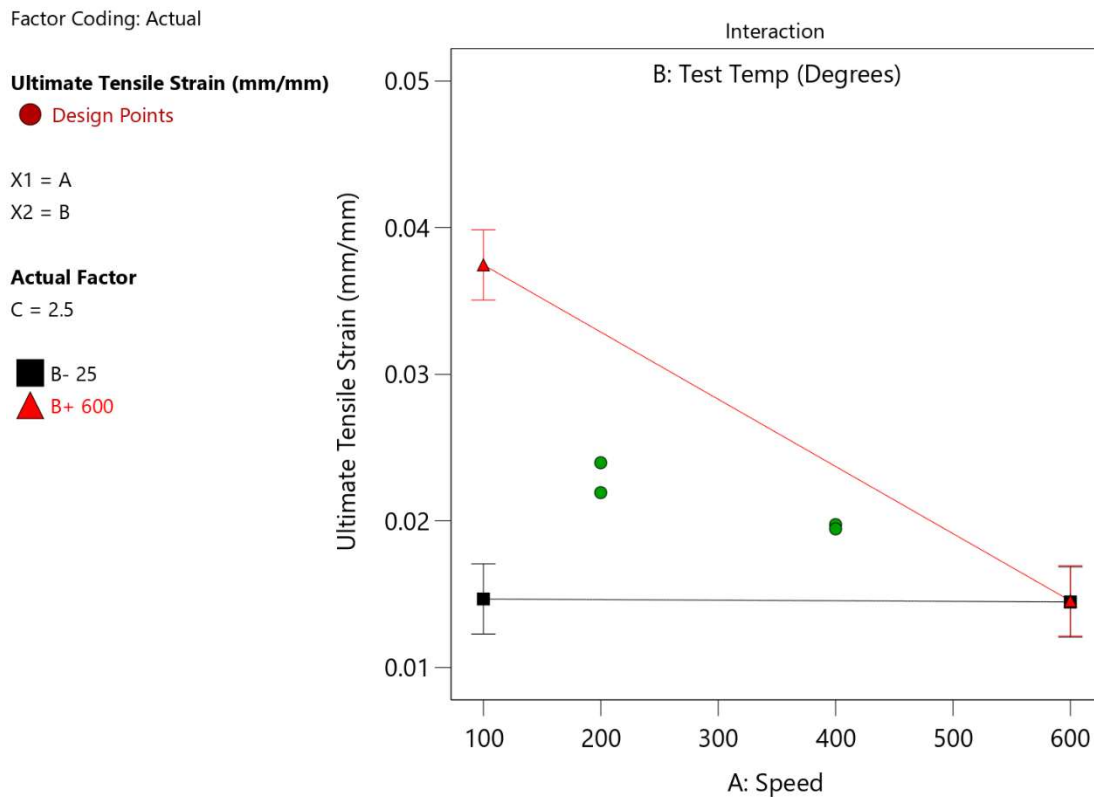


Figure 21. Ultimate Tensile Strain Response to Significant Factor Variance for the DOE design space.

temperature test. When testing at 600°C, the figure shows that lower laser speeds result in higher ultimate strains. This result makes sense in that lower laser speeds have a higher VED, are expected to have less porosity [38], larger grain size [7], a higher density [36], and therefore higher ductility.

Analysis of porosity did not lead to definitive conclusions regarding stress or strain results. Figure 22 depicts a representative sample of each build atmosphere by row and laser speed by column. The top row is N₂, the middle row is 2.5 H₂ and the bottom row is 5 H₂. From left to right, the columns represent the laser speeds of 100, 200, 400, and 600 mm/s. On sight, there is no significant difference or noticeable trends across build atmosphere or laser speed in porosity of samples. The snapshots in Figure 22 are not necessarily large enough or representative of the entire sample but selected for the largest or more interesting groupings of pores. To be used for statistical analysis would be misleading, so any small trends may not necessarily be trends across the samples. The pores as depicted do appear random in size, shape, and number, and unrelated to build direction or discernable grains. There is little further value in pursuing further analysis on porosity.

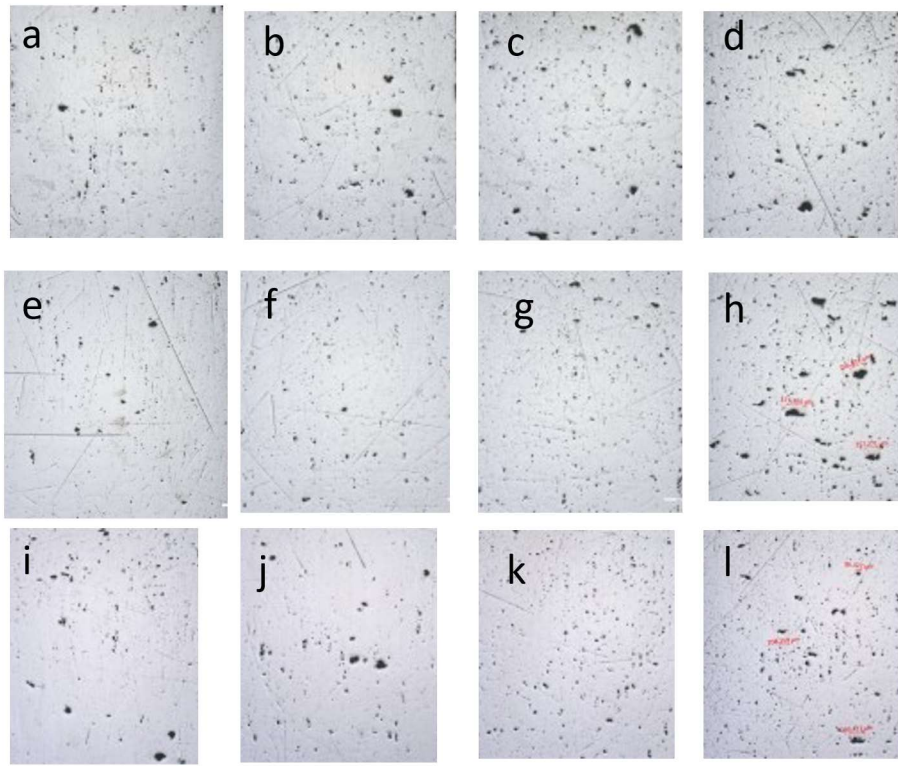


Figure 22. Optical microscopic pictures of each representative sample at 2.5 magnification.

Figure **23** show the relationship of test temperature and build atmosphere to ultimate tensile stress. This is one of the three tests in which the build speed is not a significant factor. Ultimate tensile stress increases with lower hydrogen content in the atmosphere and is higher in room temperature tests. The tradeoff in ductility and stress [9] remains prominent.

Factor Coding: Actual

Ultimate Tensile Stress (mm/mm)

● Design Points

X1 = B

X2 = C

Actual Factor

A = 400

■ C- 0

▲ C+ 5

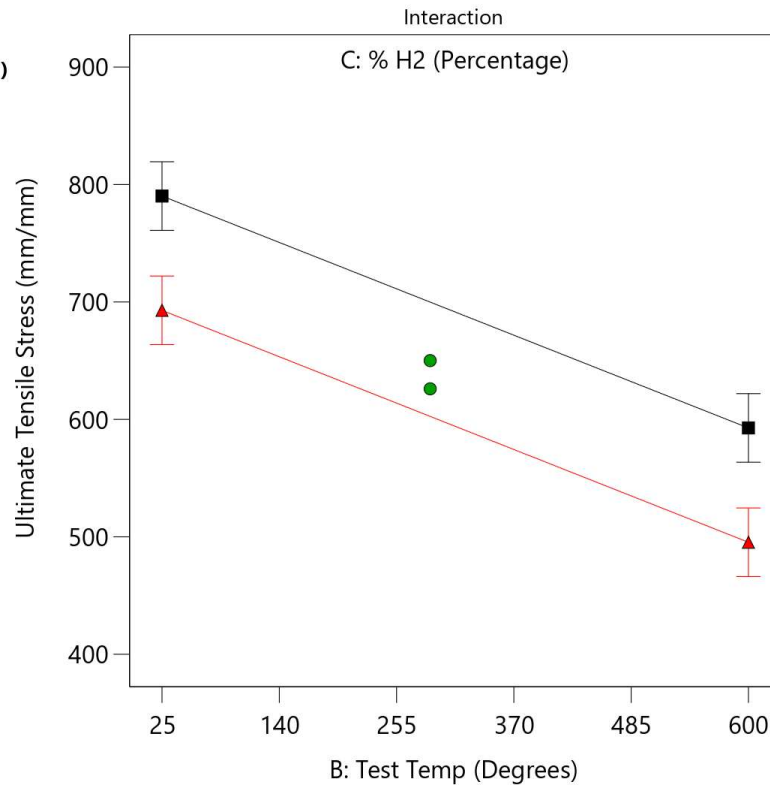


Figure 23. Ultimate Tensile Stress Response to Significant Factor Variance for the DOE design space.

Grain size can be compared using etched samples under an optical microscope.

Figure 24 shows representative etched samples to more readily identify trends in grain size. The rows from top to bottom are the different atmospheres, from N₂ to 5 H₂. The columns from left to right are the different laser speeds: 100, 200, 400, and 600 mm/s. Grain size noticeably decreases as you increase in laser speed. The larger grains appear

to be the N₂ and 5 H₂ samples, although this change is much less noticeable than the changes with laser speed. The increased

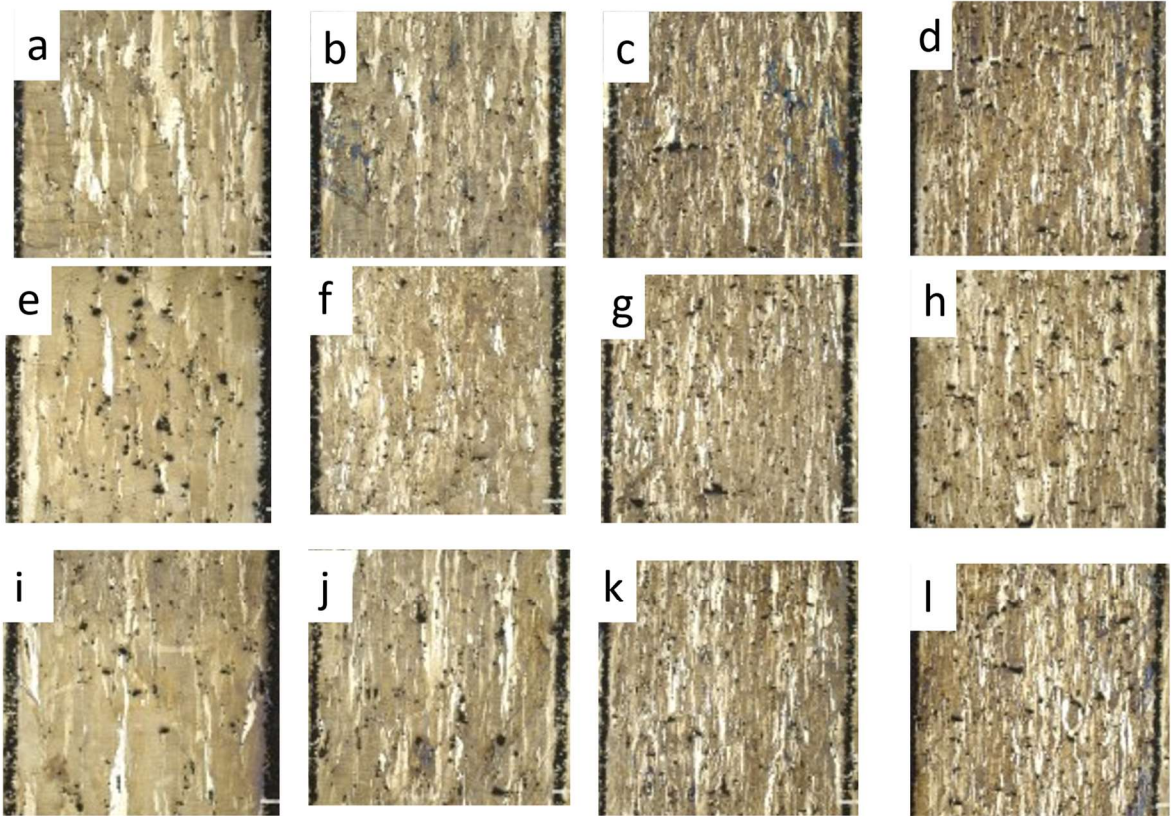


Figure 24. Optical microscopic pictures of each etched representative sample at 2.5 magnification.

quantity of grains and grain boundaries translates to a greater resistance to dislocation and less ductility [7]. If smaller grain size is the dominant factor in causing low strains and higher stresses in a high temperature test samples, then scan speed should be a

significant factor. That laser speed and to a lesser extent build atmosphere are significant factors for stress and strain exactly mirrors the ANOVA test results for DOE design space in tensile stress and strain.

Since impurities impact physical properties [1], a chemical analysis of samples could illuminate cause for changes in ductility, strains, and stresses. The analysis in Table 3 shows the Mo powder started with no detectable nitrogen and only 0.0006wt% of H₂. The chemical makeup for the sample built in 2.5 H₂ at 600 mm/s scan speed is an outlier (grayed out). That sample has nearly four times the amount of oxygen as any other sample, and corresponding anomalous low amounts of hydrogen and nitrogen. The rest of this analysis will ignore the anomalous result.

Table 3. Chemical analysis of samples, providing weight percent of oxygen, nitrogen and hydrogen for each representative sample and pure powder Mo.

Sample	Oxygen (wt%)	Nitrogen (wt%)	Hydrogen (wt%)
Powder Pure Mo	0.017	N/D	0.0006
Mo (100 mm/s)	0.027	0.074	0.0004
Mo (200 mm/s)	0.025	0.070	0.0010
Mo (400 mm/s)	0.022	0.058	0.0009
Mo (600 mm/s)	0.024	0.051	0.0004
Mo/2.5%H ₂ (100 mm/s)	0.039	0.063	0.0010
Mo/2.5% H ₂ (200 mm/s)	0.027	0.061	0.0006
Mo/2.5% H ₂ (400 mm/s)	0.026	0.054	0.0010
Mo/2.5% H ₂ (600 mm/s)	0.128	0.036	0.0005
Mo/5% H ₂ (100 mm/s)	0.017	0.062	0.0003
Mo/5% H ₂ (200 mm/s)	0.022	0.060	0.0009
Mo/5% H ₂ (400 mm/s)	0.014	0.054	0.0021
Mo/5% H ₂ (600 mm/s)	0.016	0.047	0.0005

General trends by elemental impurity vary. Collectively, every AM sample increased the nitrogen content, with the 400 and 600 mm/s speeds gaining less nitrogen than the 100 and 200 mm/s samples. Within each atmosphere, samples decreased in

nitrogen content as the laser speed increased. At each laser speed, the pure N₂ atmosphere samples had the most nitrogen, followed by the 2.5 H₂ and then 5 H₂ samples.

Looking at total impurities, neither scan speed nor atmosphere alone completely predicts the order of samples. The purest samples have either the lowest oxygen or hydrogen content, and the rest of the samples follow the trend of increasing impurities as laser speed decreases.

The lowest oxygen content was found in all four samples with a 5 H₂ build atmosphere. The low oxygen content is not just a result of increased hydrogen atmosphere reacting with the oxygen, because the next lowest oxygen content was found in the pure N₂ atmosphere samples. Only the four samples at the extremes of the design space, the N₂ and 5 H₂ build atmospheres at 100 and 600 mm/s, decreased in hydrogen content compared to the original powder.

Oxides formed at grain boundaries weaken the structure causing lower ultimate stresses [30], but the wt% of impurities do not specify what form or where the impurities exist within the sample and cannot be assumed. It was shown that the lower oxygen content samples (5 H₂) results in higher stresses. The oxygen content trend also fits with the grain size trend in atmospheres.

Since impurities can negatively affect properties like ductility, and both the 5 H₂ and N₂ build atmospheres have lower oxygen content, it seems confounding as to why the 2.5 H₂ build atmosphere samples have a higher max strain. There may be two answers. One, the answer is likely that stress and strain are not simply reliant on a single factor, chemical makeup and specifically oxygen content. Two, the actual values are very close

for N₂ and 2.5 H₂. The difference between the two could just be noise in the sample data whereas the chemical makeup of the 5 H₂ is distinct enough to be above any noise.

ANOVA analysis of all samples

The ANOVA of all samples resulted in quadratic relationships among three of the five factors and all ANOVA results being statistically significant. The increased number of samples provided enough data to support analysis with quadratic functions as opposed to 2FI or linear. Yield stress is shown in

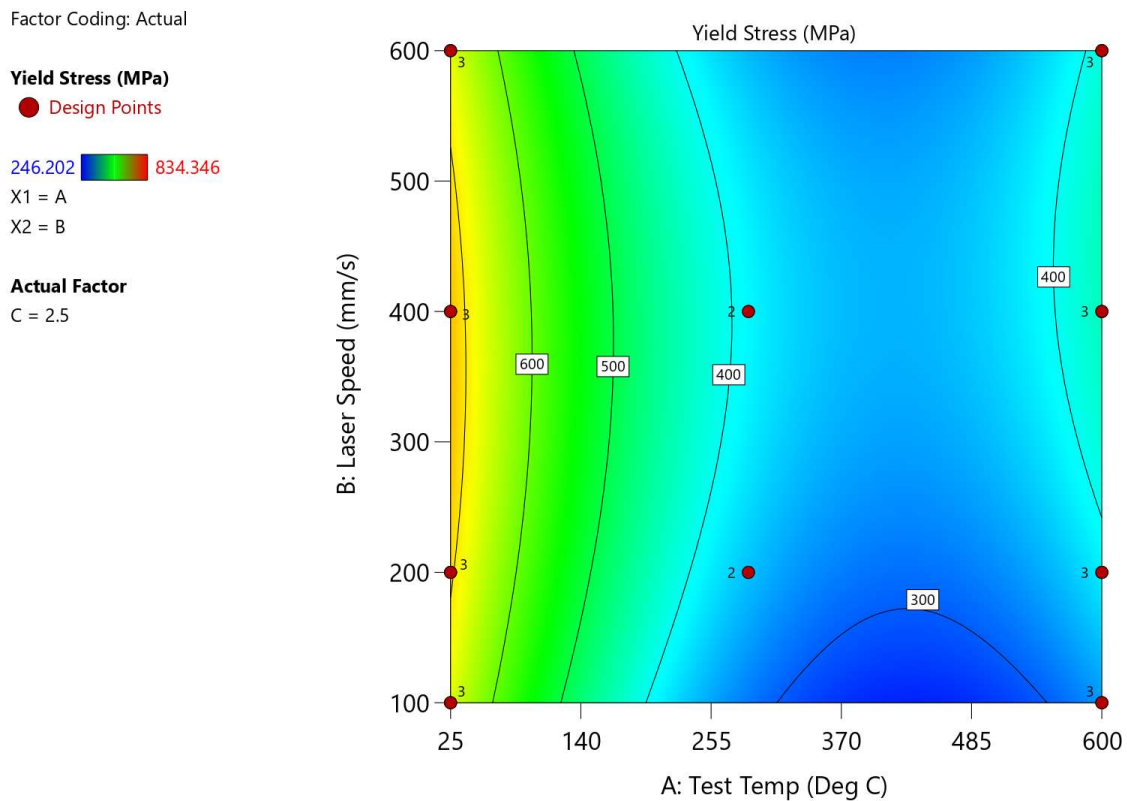


Figure 25 depicts the relationship between laser speed and test temperature at a 2.5 H₂

atmosphere. The figure shows a quadratic relationship, and both speed and test temperature being significant.

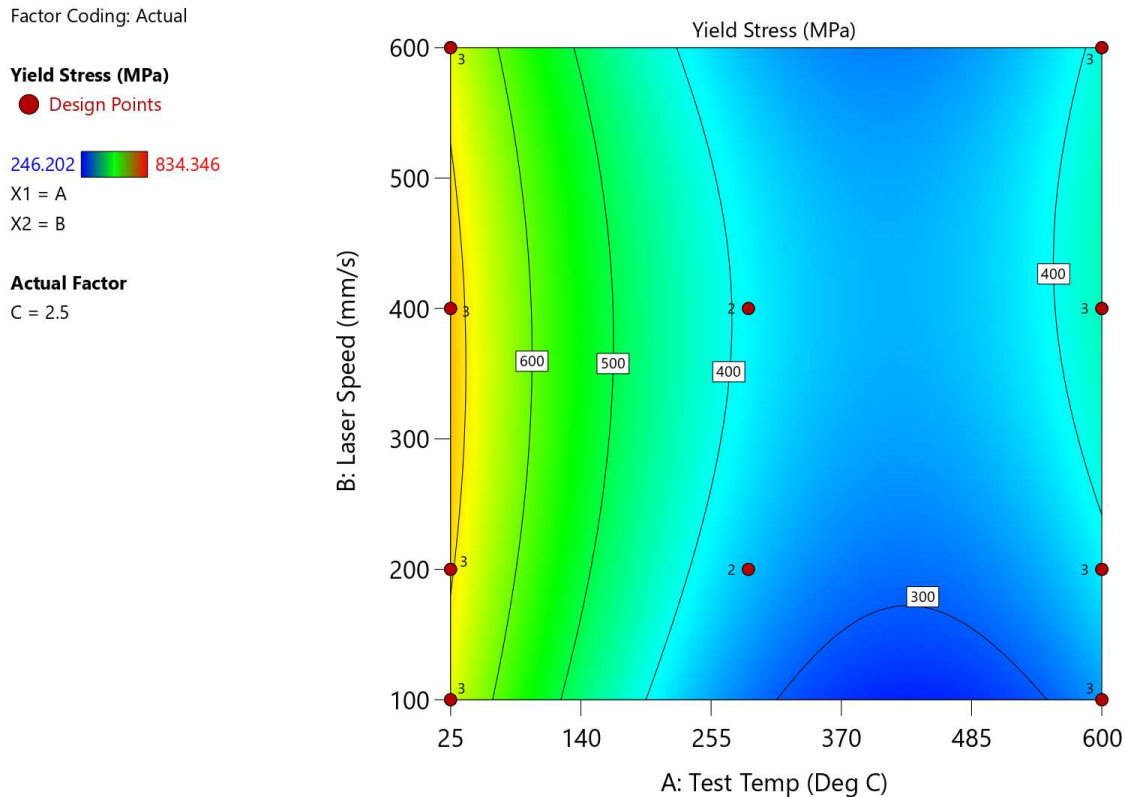


Figure 25. Yield Stress relationship between laser speed and test temperature for all test data.

Further analysis with Table 4 gives the relative significance of each factor by comparison of the F-factors. The larger the F-factor, the greater the variation between groupings compared to variation amongst all samples. In other words, larger F-values correspond to more significant factors. For yield stress, not only are speed and temperature significant, but so are atmosphere, the interaction of test temperature and speed, the interaction of test temperature and atmosphere, the interaction of speed and atmosphere, and squared values of temperature and laser speed. Test temperature is by far the most important factor, and its squared value, and then atmosphere. Comparison of

the yield stress graphs at each atmosphere, yield stress is highest at some middle laser speed at room temperature, and N₂ atmosphere.

These results are consistent with the DOE design space ultimate tensile stress relationship with temperature and atmosphere, but provides more information with more data. When AM, there is a relationship between power used and velocity or laser speed. At low velocities and high power, keyhole porosity occurs. Keyhole porosity occurs when AM metals get so hot that vapor forms during the manufacturing process multiple layers deep, and the metal solidifies over the pocket of vapor leaving pores in the final sample [36]. At low power and high velocity, a lack of fusion can occur because there is not enough heat to melt all the powder and get a fused layer throughout the surface [36].

Table 4. ANOVA for Quadratic Model of Yield Stress for all data points

Source	Sum of Squares	df	Mean Square	F-value	p-value
Model	1.923E+06	9	2.137E+05	77.34	< 0.0001
A-Test Temp	1.577E+06	1	1.577E+06	570.52	< 0.0001
B-Laser Speed	18007.62	1	18007.62	6.52	0.0130
C-% Atm	49015.04	1	49015.04	17.74	< 0.0001
AB	15475.18	1	15475.18	5.60	0.0209
AC	11629.54	1	11629.54	4.21	0.0442
BC	15632.69	1	15632.69	5.66	0.0203
A ²	1.317E+05	1	1.317E+05	47.68	< 0.0001
B ²	36149.85	1	36149.85	13.08	0.0006
C ²	4274.55	1	4274.55	1.55	0.2180
Residual	1.824E+05	66	2763.35		
Lack of Fit	59349.44	16	3709.34	1.51	0.1345
Pure Error	1.230E+05	50	2460.63		
Cor Total	2.106E+06	75			

Good welding occurs at some combination of power and velocity, and that is what the yield stress,

Factor Coding: Actual

Yield Stress (MPa)

● Design Points

246.202 834.346

X1 = A

X2 = B

Actual Factor

C = 2.5

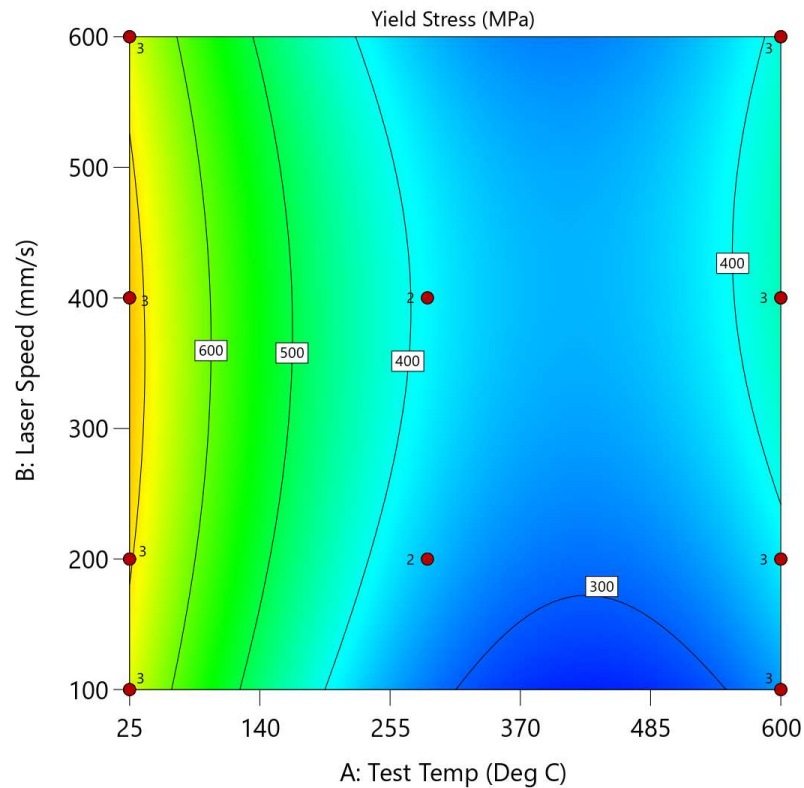


Figure 25, shows. Along a constant line of power, the best or highest yield stress occurs in between the high velocity/lack of diffusion area and the low velocity/keyhole porosity area. Test temperature is a factor because the high temperature test results in ductile materials and lower stresses. Atmosphere matters because of the impact on grain size and quantity and the effect on ductility.

Ultimate tensile stress shows a similar trend as yield stress, but not to the same degree. While still a quadratic relationship, only temperature, atmosphere, and the square of laser speed are significant factors. Figure 26 depicts the relationship between factors

and ultimate tensile stress. The same laser speed and test temperature combination for the highest yield stress also results in the strongest ultimate tensile stress. Understanding that relationship between laser speed and stress explains why Figure 20 depicts the larger stresses at each atmosphere for the 200 or 400 mm/s speeds instead of 100 mm/s and 600 mm/s.

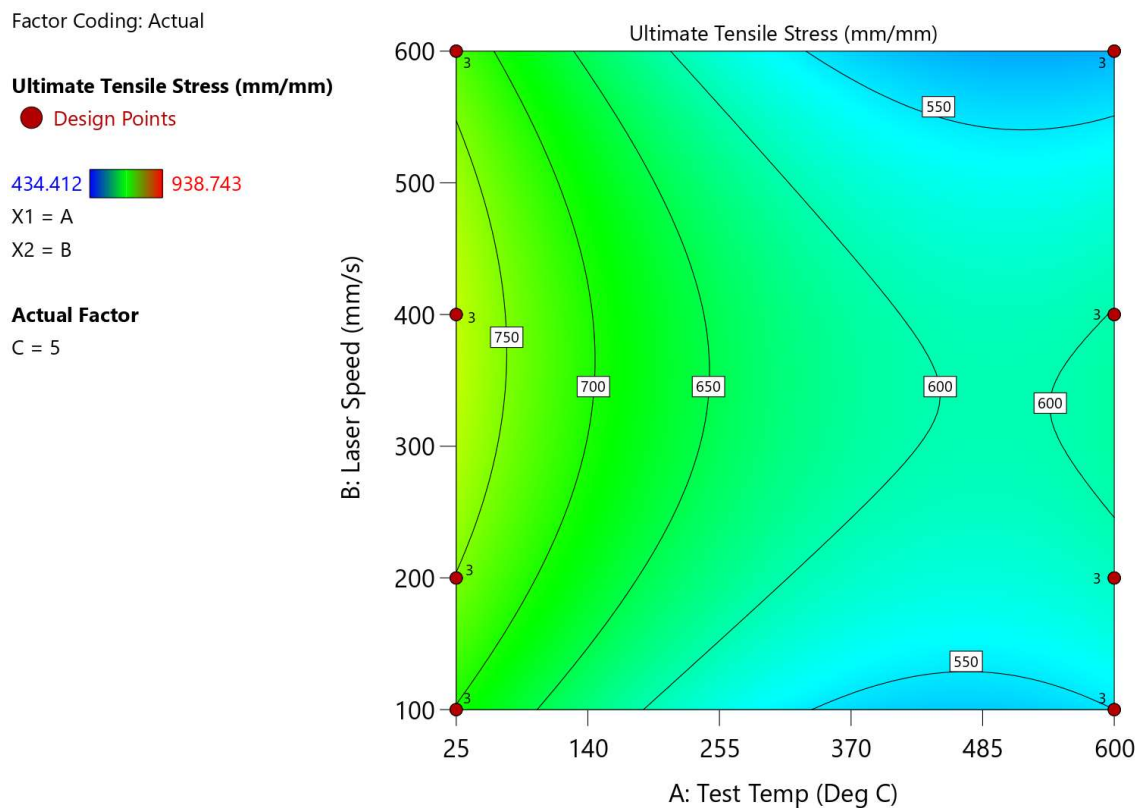


Figure 26. Ultimate Tensile Stress relationship between laser speed and test temperature for all test data.

Figure 27 and Figure 28 show the results of the ultimate tensile strain and final strain for all data points. Both relationships have significant factors of test temperature and speed and the interaction of the two. The final strain is a quadratic relationship with

the additional significant factors of the square of test temperature and speed. Ultimate tensile strain figure depicted is derived from a 2FI ANOVA. Atmosphere is not a significant factor in any strain result for any group of samples. The highest ultimate tensile strain and final strain are at high test temperatures and low speeds (which is expected for high VED and above the DBTT).

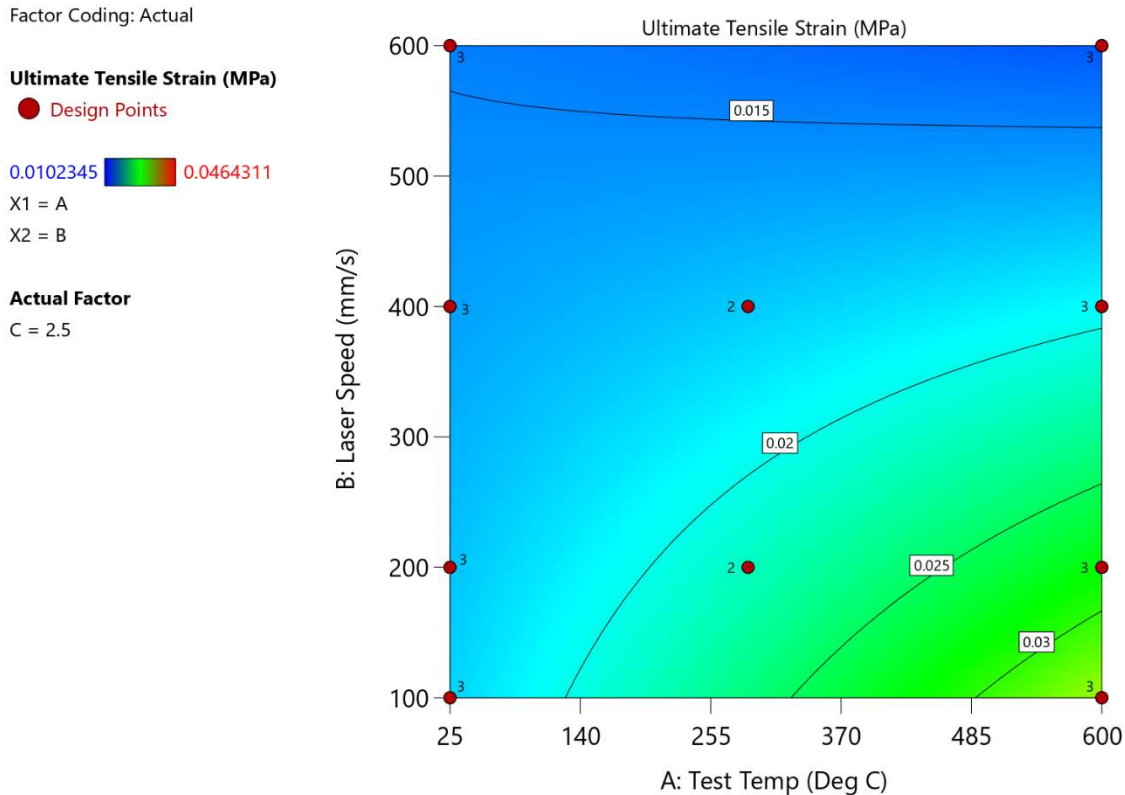


Figure 27. Ultimate Tensile Strain relationship between laser speed and test temperature for all test data.

As noted earlier, test temperature greatly affects ductility. There is no intermediate laser speed that maximizes strain. Results show that higher strains are achieved at lower speeds, and continues off the chart outside the design space. There would be a tradeoff in the usefulness of the material with such ductility and even lower stresses, but could be worth exploring.

Factor Coding: Actual

Final Strain (mm/mm)

● Design Points

0.0102345 0.352755

X1 = A

X2 = B

Actual Factor

C = 2.5

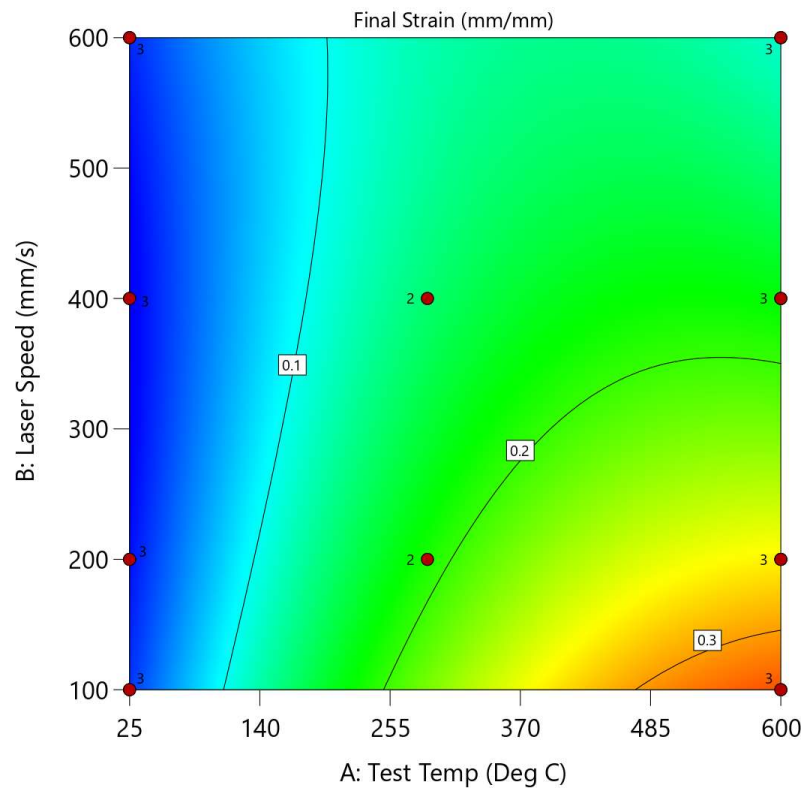


Figure 28. Final Strain relationship between laser speed and test temperature for all test data.

Factor Coding: Actual


3D Surface

Young's Modulus (N/m²)

Design Points:

● Above Surface

○ Below Surface

39988.7  111280

X1 = A

X2 = B

Actual Factor

C = 2.5

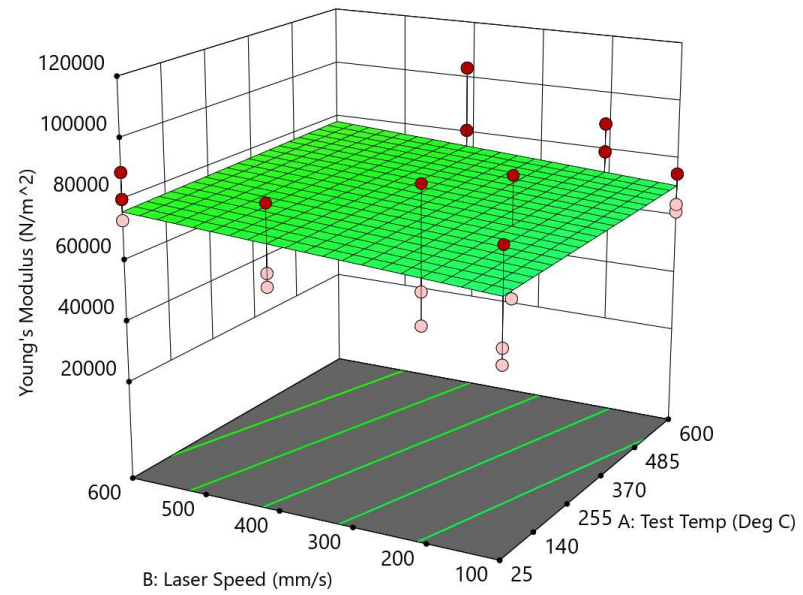


Figure 29. Young's Modulus relationship between test temperature and laser speed for all test data.

The results for Young's Modulus in

Factor Coding: Actual


3D Surface

Young's Modulus (N/m²)

Design Points:

● Above Surface

○ Below Surface

39988.7  111280

X1 = A

X2 = B

Actual Factor

C = 2.5

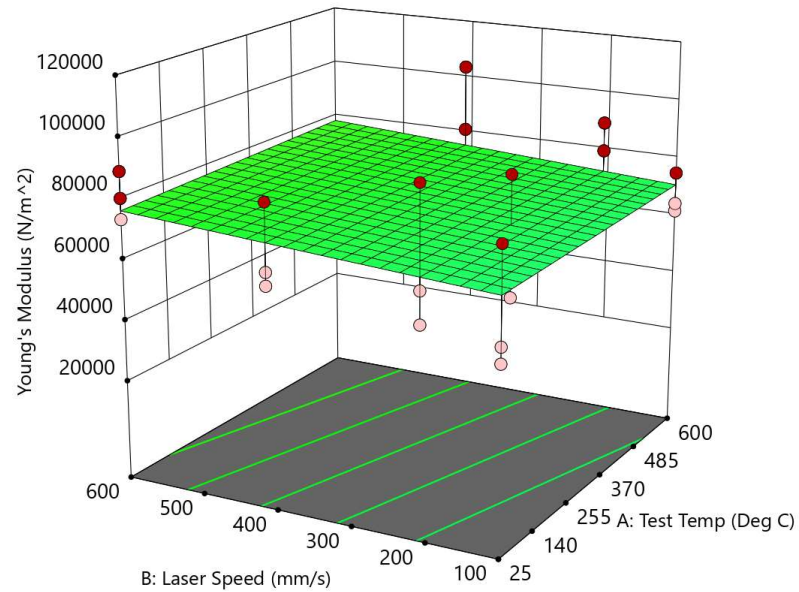


Figure 29 was interesting in that only atmosphere was a significant factor for all samples. (The DOE Design Space and the 600°C test also had speed or the square of speed as a significant factor, respectively.) The slope of the lines plotted in

Figure 19, the stress and strain curves for room temperature, are the Young's moduli and one can see only a very slight decreased slope from N₂ to 5 H₂.

While statistical significance can be taken from the ANOVA Figure 30 provides more information to explain the relationship among factors and Young's Modulus. The three factors of test temperature, laser speed, and atmosphere are plotted separately against Young's Modulus. Generally, the more vertical the line in each of the three subplots of Figure 30, the larger the impact or significance. The design points in red are plotted for 600°C, 600 mm/s, and N₂. Test temperature shows a near horizontal line and is insignificant. In aggregate, atmosphere is the only significant factor.

Factor Coding: Actual

3D Surface

Young's Modulus (N/m²)

Design Points:

● Above Surface

○ Below Surface

39988.7 111280

X1 = A

X2 = B

Actual Factor

C = 2.5

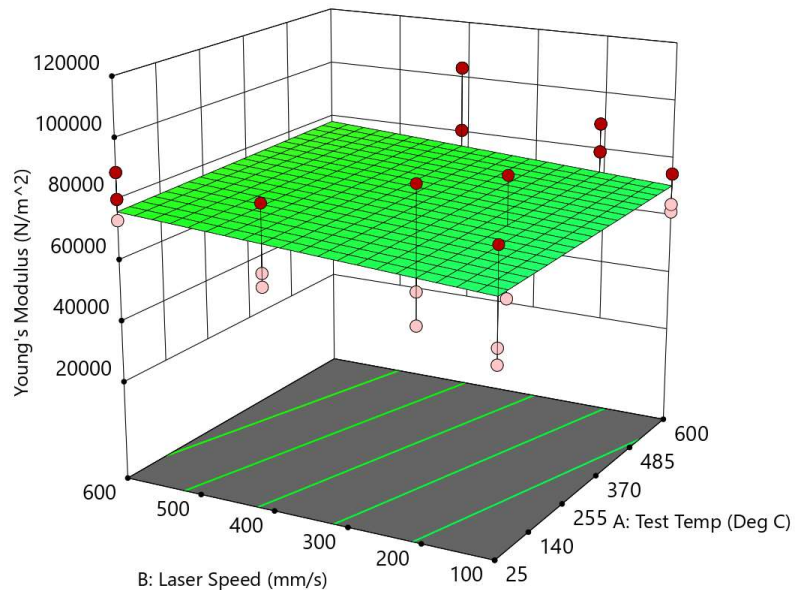


Figure 29 Figure 30 shows a trend in laser speed as it relates to Young's Modulus that is not apparent from

Factor Coding: Actual

3D Surface

Young's Modulus (N/m²)

Design Points:

● Above Surface

○ Below Surface

39988.7 111280

X1 = A

X2 = B

Actual Factor

C = 2.5

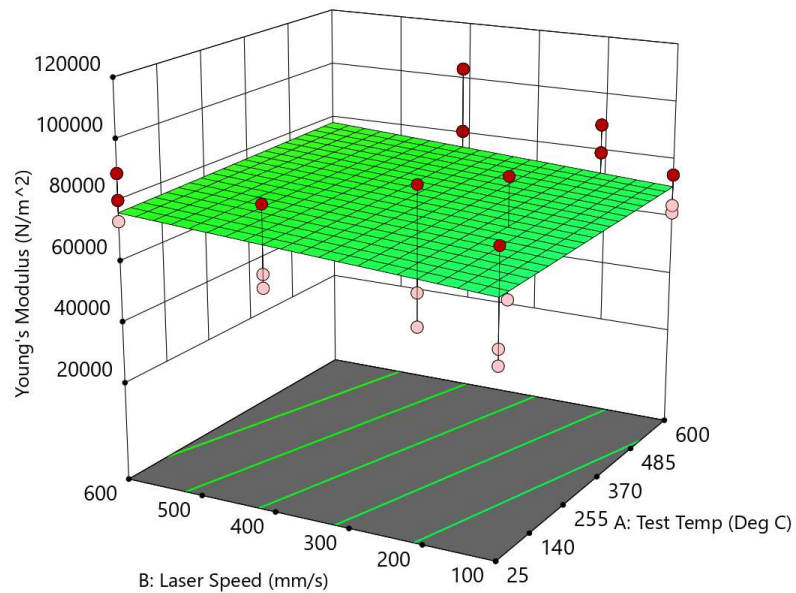


Figure 29. The data fit a linear model, but trends outside a purely linear relationship can be seen. The largest modulus occurs not with the highest laser speed, but peaks at 400 mm/s. Similarly, the lowest modulus for atmosphere occurs not at 5 H₂ but at the intermediate 2.5 H₂.

Young's Modulus is an inherent elastic property. Factors affecting stress or strain in the elastic region could have an impact on Young's Modulus, to include temperature, impurities, and grain size. As shown in Figure 30, even with the trend in laser speed or significance factor of atmosphere, the Young's Modulus of

Factor Coding: Actual

3D Surface

Young's Modulus (N/m²)

Design Points:

● Above Surface

○ Below Surface

39988.7  111280

X1 = A

X2 = B

Actual Factor

C = 2.5

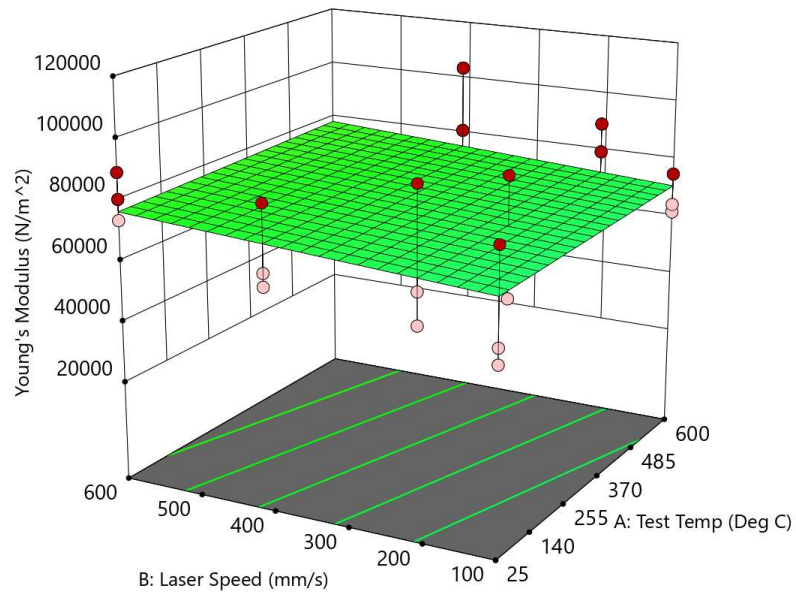


Figure 29 varies very little, which is true for the entire study. Increased strain that does occur at higher test temperatures is often outside the elastic region, seen more easily in Figure 20. Test temperature is not high enough or of significant duration to cause microstructural changes that could affect the Young's Modulus by a large amount, such as by annealing or recrystallization. Laser speed and atmosphere both affect the grain size, and proper welding of the material during the build depends on the overall VED controlled by laser speed in this study.

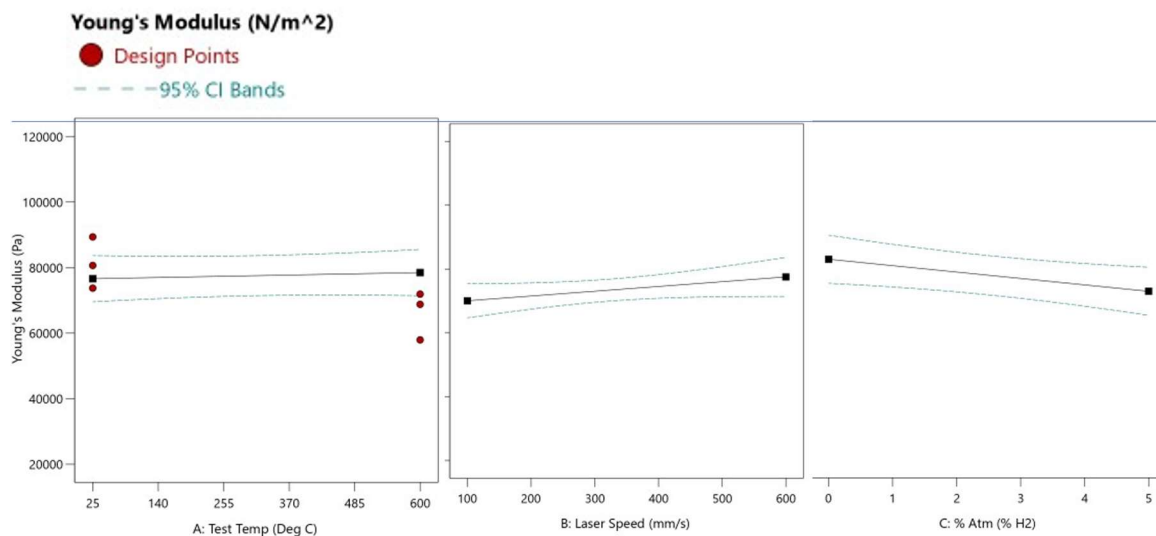


Figure 30. ANOVA results by factor for Young's Modulus for all data points

The interaction and the precedence of one factor over the other leads to difficulty in predicting a high or low Young's Modulus. Since larger grains occur with lower speeds and the N₂ or 5 H₂ build atmosphere, then one would predict those samples would have more strain and less stress, or a lower Young's Modulus. That trend holds for atmosphere even in the linear model ANOVA. For laser speed, however, the proper welding at the intermediate speeds is a larger factor than grain size when it comes to the modulus.

Factor Coding: Actual

Yield Stress (MPa)

● Design Points

246.202 834.346

X1 = A

X2 = B

Actual Factor

C = 2.5

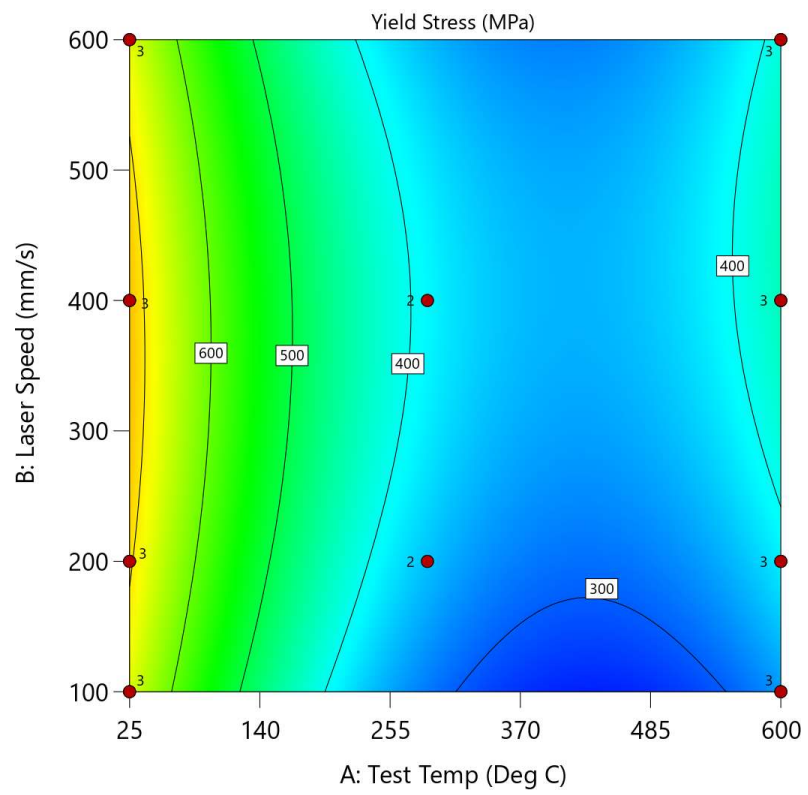


Figure 25 -

Factor Coding: Actual

3D Surface

Young's Modulus (N/m²)

Design Points:

● Above Surface

○ Below Surface

39988.7  111280

X1 = A

X2 = B

Actual Factor

C = 2.5

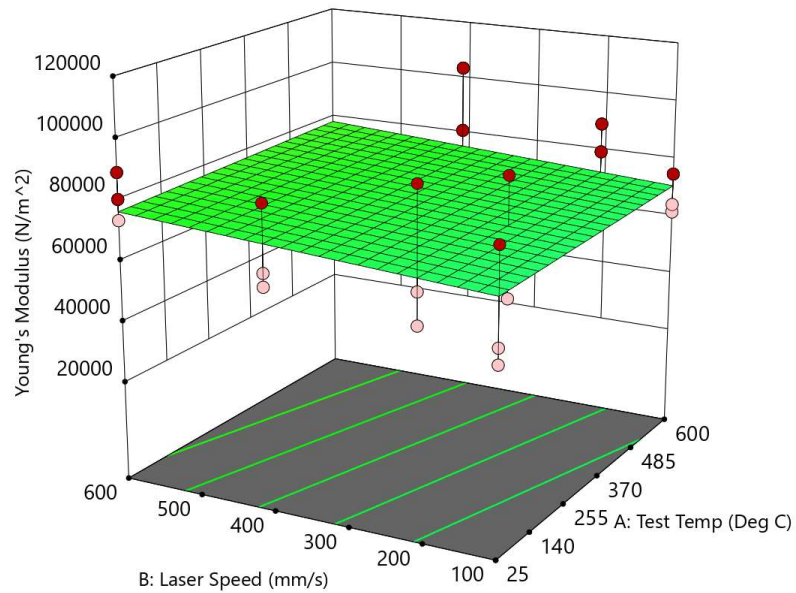


Figure 29 developed from the Stat-Ease software can also be used to predict the processing and testing parameters to maximize, or minimize future results. For instance, the Stat-Ease software uses the analyzed results and user desired optimization to predict the maximum the ultimate tensile stress within these test parameters would occur at 25°C, 315 mm/s laser speed, and an atmosphere with 3.34% H₂. The corresponding results are predicted to be 835 MPa ultimate tensile stress, 760 MPa yield stress, 0.017 mm/mm ultimate tensile strain, 0.01 mm/mm final strain, and 77,313 N/m² Young's modulus. While maximizing or minimizing any one factor closely follows the heat map of the same result, the software could also be used to optimize configuration when multiple targeted results are desired.

ANOVA Results by Atmosphere

The samples were sorted by atmosphere, removing that as a possible significant factor, and the same ANOVA tests conducted for yield stress, ultimate tensile stress, ultimate tensile strain, final strain, and Young's Modulus. The N₂ and 2.5 H₂ atmosphere tests were very similar in significant factors. The 2.5 H₂ tests had more significant factors and three of the significant tests were quadratic, refer to Table 2. Statistically significant ANOVA results by factor and analyzed sample groups. Neither atmosphere had significant results in Young's modulus. The 5 H₂ atmosphere only had significant results for the two strains.

Overall, not much new information is gleaned from separating the groups by atmosphere. For all three atmospheres, the ultimate tensile strain and final strain relationships look similar to Figure 27 and Figure 28, the strains of all samples. Even without temperature being a significant factor for ultimate tensile strain for N₂ samples, the interaction of temperature and speed remains significant. Also, nearly all the other significant factors remain the same across the atmospheres thus the similarities in all four figures.

The significant ANOVA results of the N₂ and 2.5 H₂ stresses differ compared to each other. The N₂ sample ANOVAs used a 2FI for yield stress and linear analysis for ultimate tensile stress rather than quadratic for all samples.

Figure 31 shows the graphical relationship of laser speed and test temperature to yield stress for N₂ where only temperature is a significant factor. This is the third of three tests where speed, the interaction of speed with another factor, or the square of speed, is not a significant factor.

For both atmospheres, the samples are brittle and have higher yield stresses at room temperature. The N₂ sample has the highest yield stresses at a speed of 100 mm/s,

Factor Coding: Actual

Yield Stress (MPa)

● Design Points

353.611 826.013

X1 = A

X2 = B

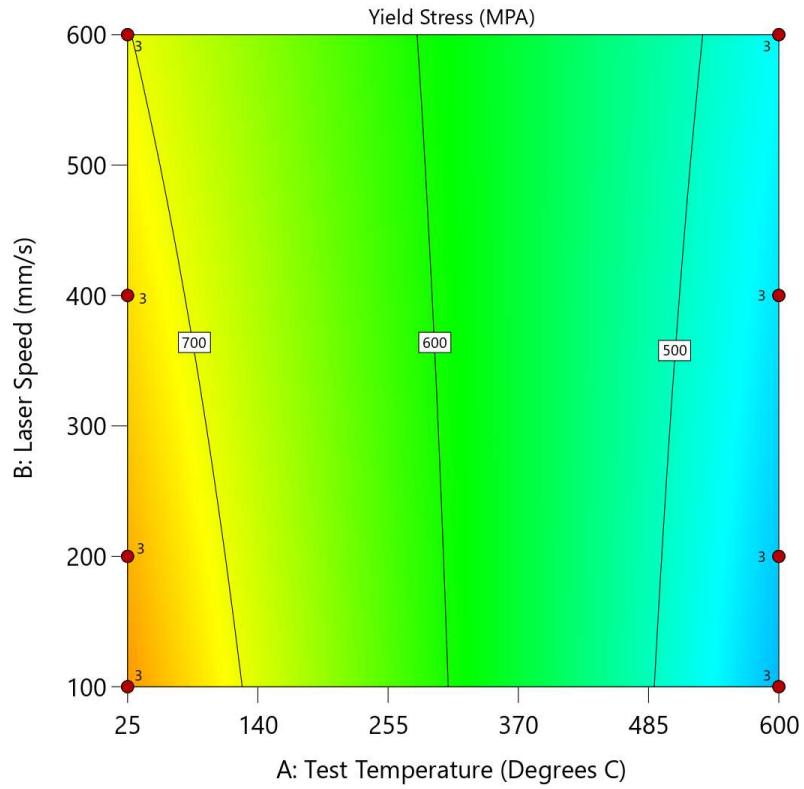


Figure 31. Yield Stress ANOVA model graph for N₂ samples

larger than the max stresses of the 2.5 H₂ samples. The 2.5 H₂ yield stress, Figure 32, mirrors the yield stress of all data points,

Factor Coding: Actual

Yield Stress (MPa)

● Design Points

246.202 834.346

X1 = A

X2 = B

Actual Factor

C = 2.5

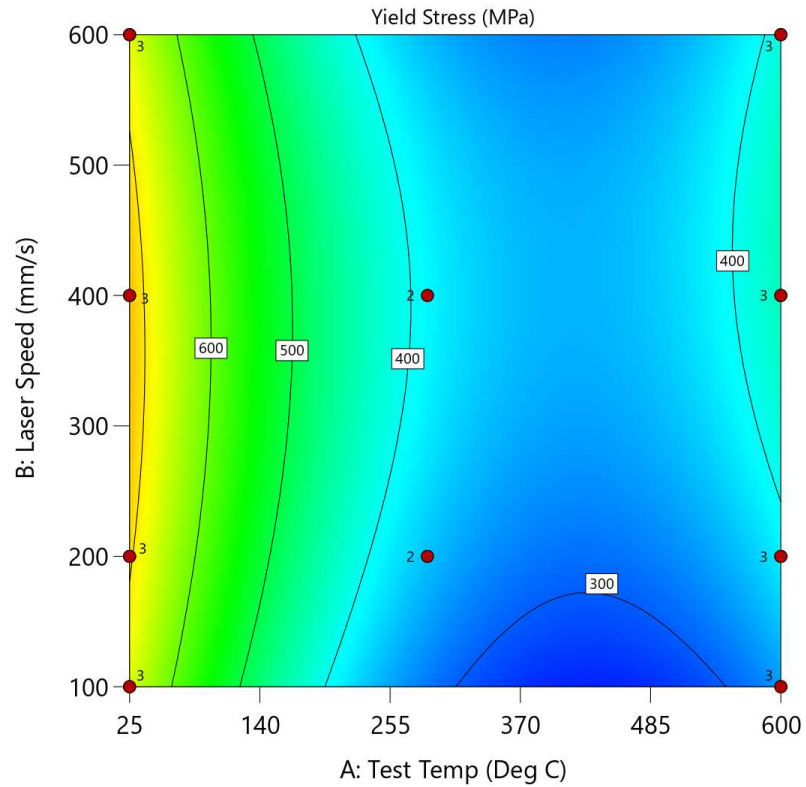


Figure 25. Since the data for the N₂ samples does not include any midpoints, there will not be a quadratic ANOVA and the yield stress results of the 2.5 H₂ and N₂ samples reflect this difference.

Factor Coding: Actual

Yield Stress (MPa)

● Design Points

308.63 794.266

X1 = A

X2 = B

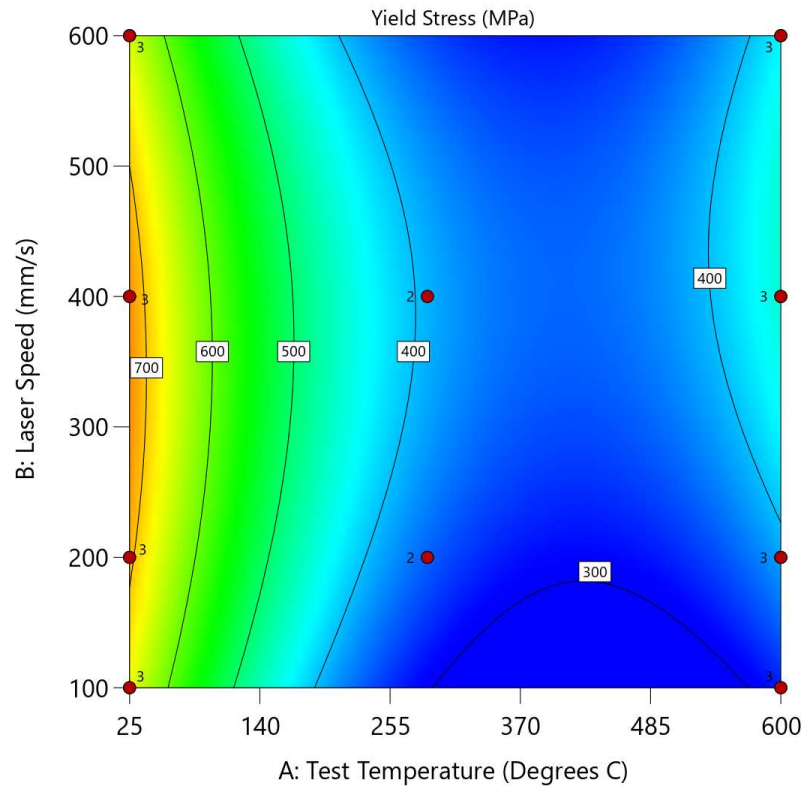


Figure 32. Yield Stress result of temperature and laser speed for 2.5% H₂ samples

For the ultimate tensile stress, Figure 33 and Figure 34, the differences in the linear versus quadratic relationship seen in the N₂ and 2.5 H₂ samples is evident again. Temperature is a significant factor of both, but the square of speed is significant in the 2.5 H₂ samples while just speed is a significant factor for the N₂ samples. Without the midpoints seen in the 2.5 H₂ samples, the N₂ and 5 H₂ results could never have a quadratic relationship and thus misleading in conclusions that could be drawn from those figures alone.

Factor Coding: Actual

Ultimate Tensile Stress (mm/mm)

● Design Points

452.483 861.743

X1 = A

X2 = B

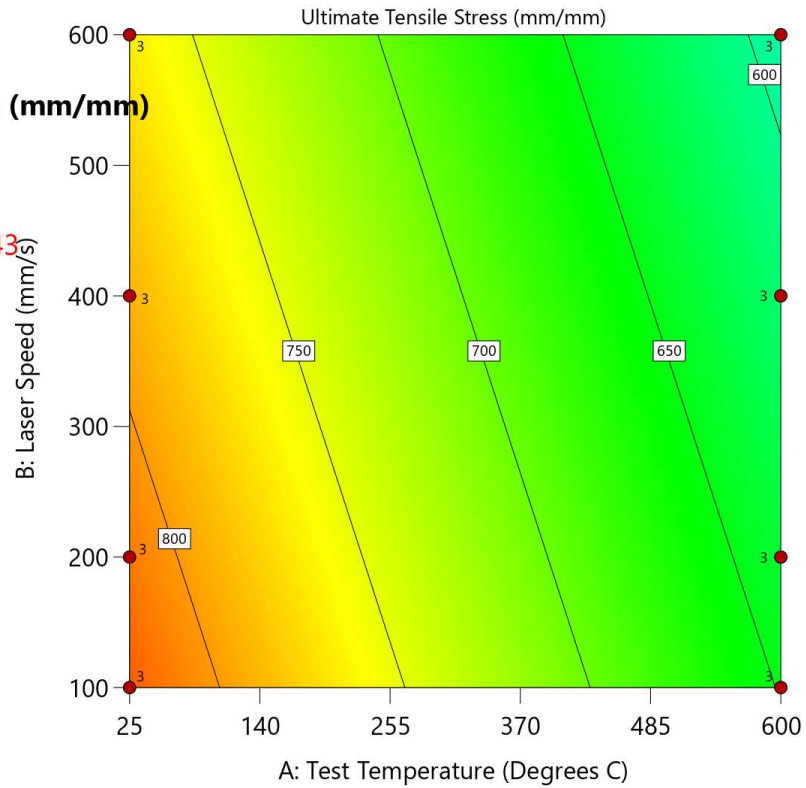


Figure 33. Ultimate Tensile Stress result of temperature and laser speed for N₂ samples

In both the ultimate and yield tensile strain results, atmosphere is not a significant factor. Temperature was moved as a factor by nature of the grouping, and without atmosphere as a significant factor, strain is only reliant on the laser speed and the square of the speed during the build. At lower laser speeds, higher VED, the samples are more ductile.

Factor Coding: Actual

Ultimate Tensile Stress (mm/mm)

● Design Points

512.882 512.882 883.868 883.868

X1 = A

X2 = B

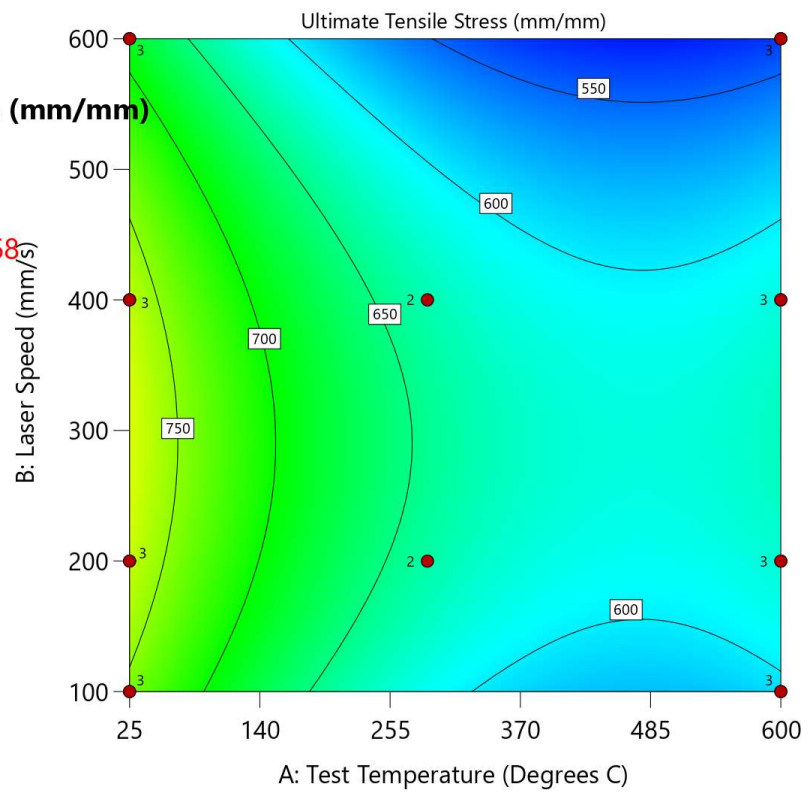


Figure 34. Ultimate Tensile Stress relationship between test temperature and laser speed for 2.5% H₂ samples.

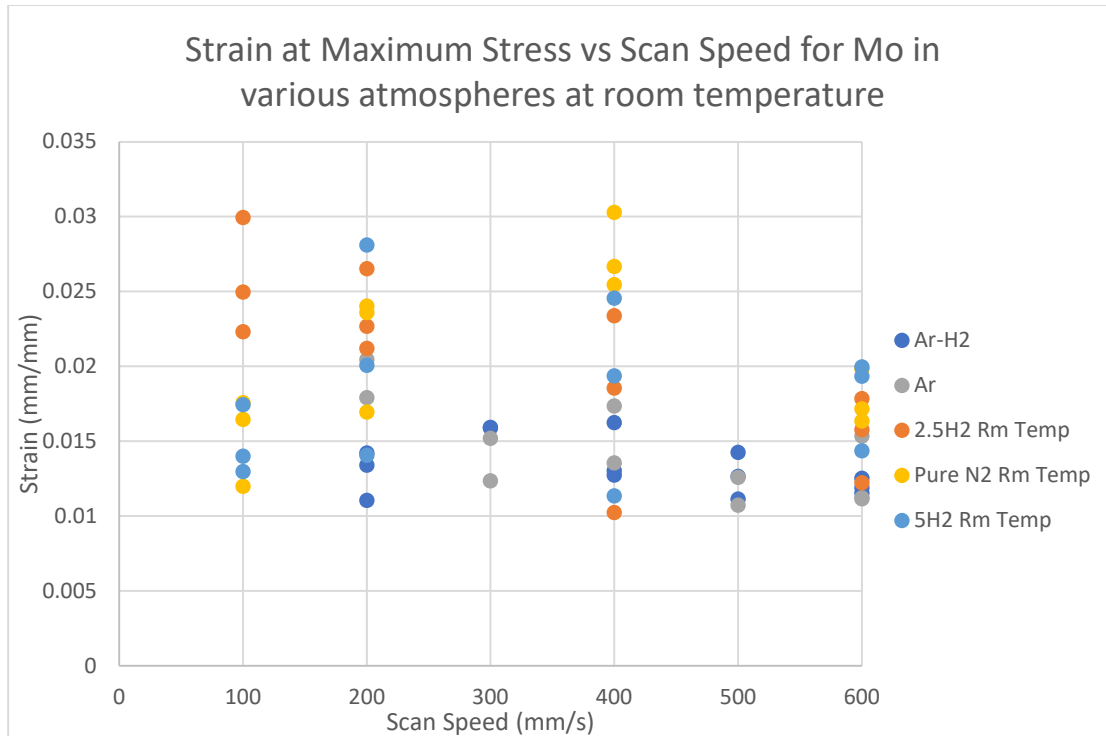


Figure 35. Strain at maximum stress data from unpublished Mo in Ar and Ar-3% H₂ and three N₂ and H₂ environments at room temperature

When considering the unpublished data from Kemnitz regarding Mo built in Ar and Ar-3% H₂ compared to the room temperature data from this study, there is no noticeable difference in strains (Figure 35). For comparison, Figure **Error! Reference source not found.** shows the data for higher scan speeds as well as the strains from the high temperature test data of Mo in the nitrogen atmospheres. As expected from previous results, the strains are noticeably larger for the high temperature, though there is no high temperature comparison data in an Ar environment. This does suggest that the less expensive nitrogen can be used for similar strain results in future experiments.

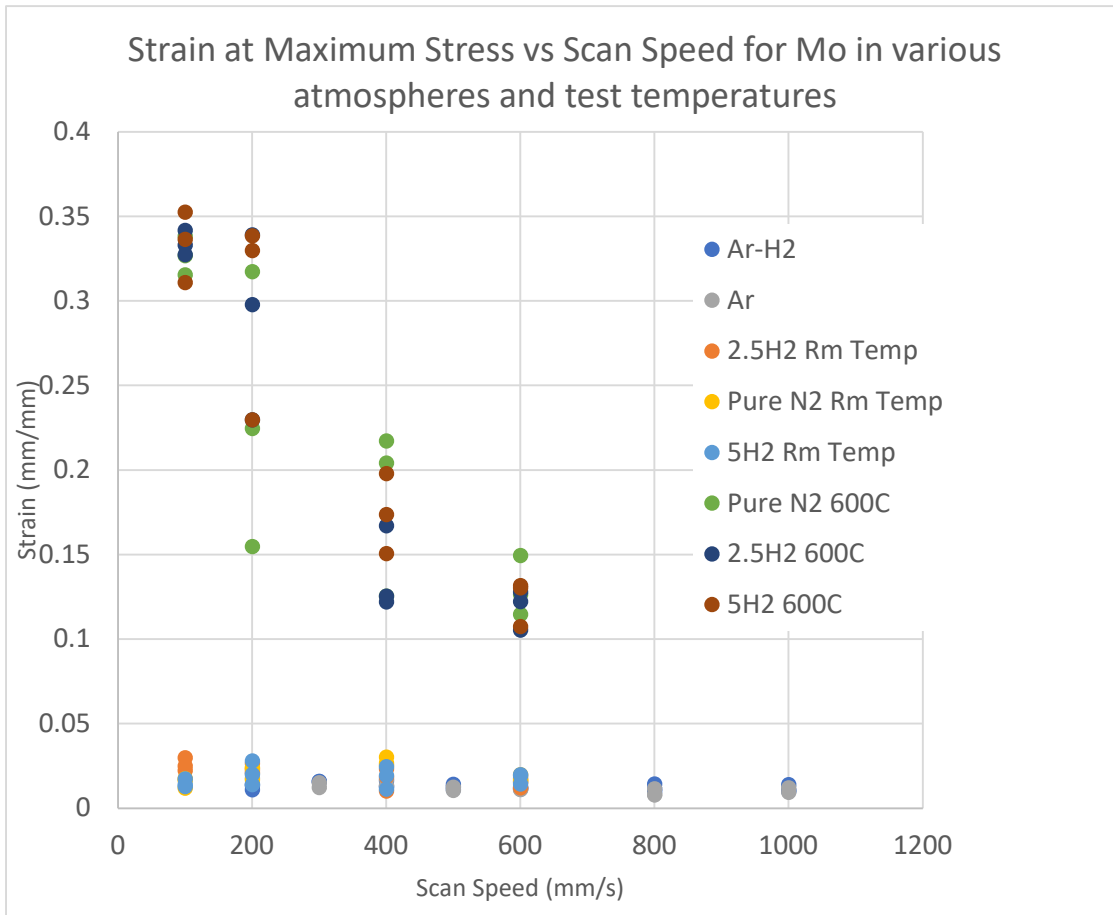


Figure 36. Strain at maximum stress data from unpublished Mo in Ar and Ar-3% H₂ and three N₂ and H₂ environments at room temperature and 600°C

Additionally, strain from the high temperature tests continually decrease as laser speed increases. Manufacturing speeds to achieve optimal strain should not involve scan speeds above 600 mm/s.

Stress data from the same experiments are plotted in Figure 36. Mo in pure Ar carried the lowest stress while the Ar and 3% H₂ atmosphere was the second lowest. The stresses at 600°C from the 5 H₂ and 2.5 H₂ followed by pure N₂ had the next highest stress values. Lastly, the least ductile specimens were the room temperature samples with the highest stress values. Comparing just room temperature samples, those build in

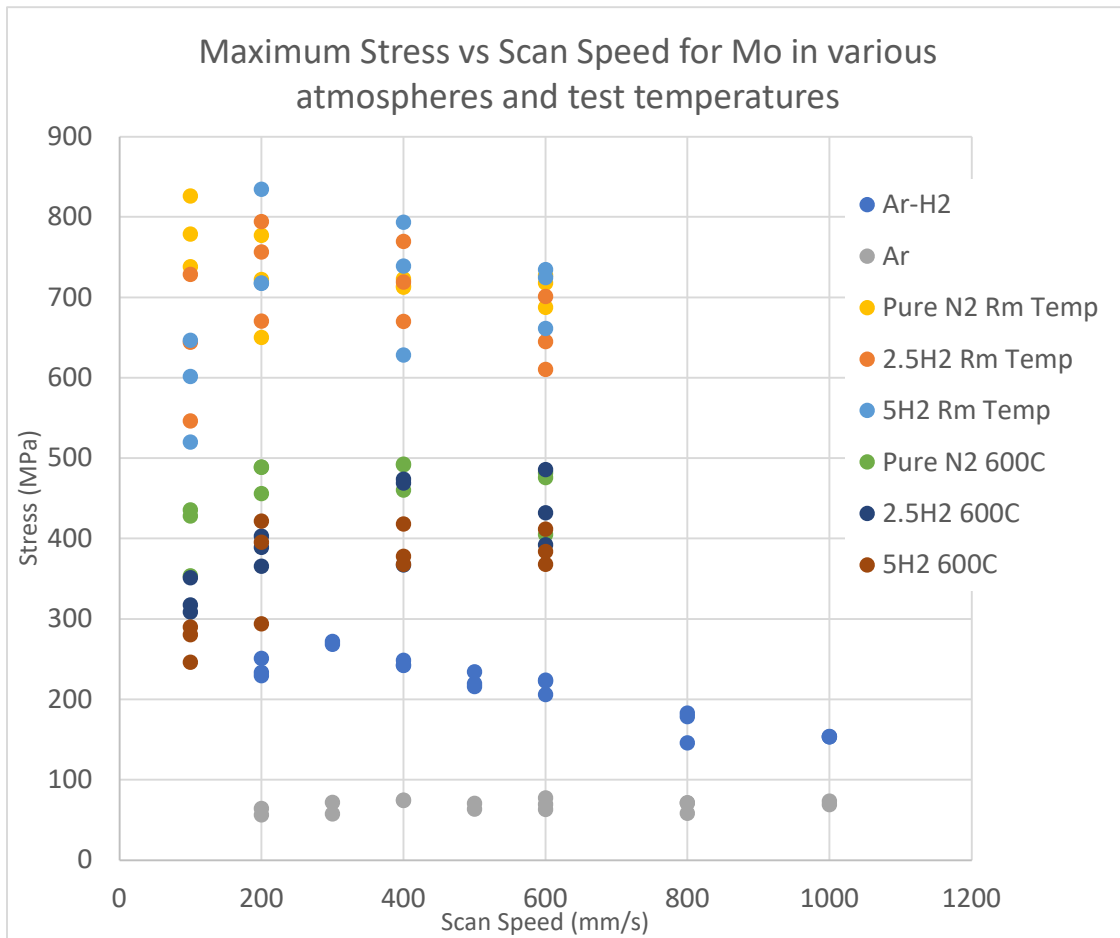


Figure 37. Maximum Stress data from unpublished Mo in Ar and Ar-3% H₂ and three N₂ and H₂ environments at room temperature and 600°C

the nitrogen or nitrogen-hydrogen atmosphere carried significantly more stress with comparable strain. Since Ar atmosphere does not improve maximum stress or strain at maximum stress under the same conditions compared to nitrogen, there is no need to continue using Ar instead of a nitrogen atmosphere.

ANOVA Results by Temperature

There are no significant ANOVA results for the room temperature test samples. In brittle materials, there can be more variability in mechanical behavior. This brittleness causes the standard deviation of samples to become larger. Picking any three samples at

random that are all brittle may get such a random distribution and large error bars that there is no statistical significance in the data. When conducting mechanical testing of a limited number of samples, you are pulling randomly from a statistical distribution. When the underlying distribution has a larger standard deviation, there is inherently more variability between the samples taken from that distribution. Therefore, so few samples are less characteristic of the underlying distribution and it becomes difficult to adequately compare different distributions of brittle materials.

In

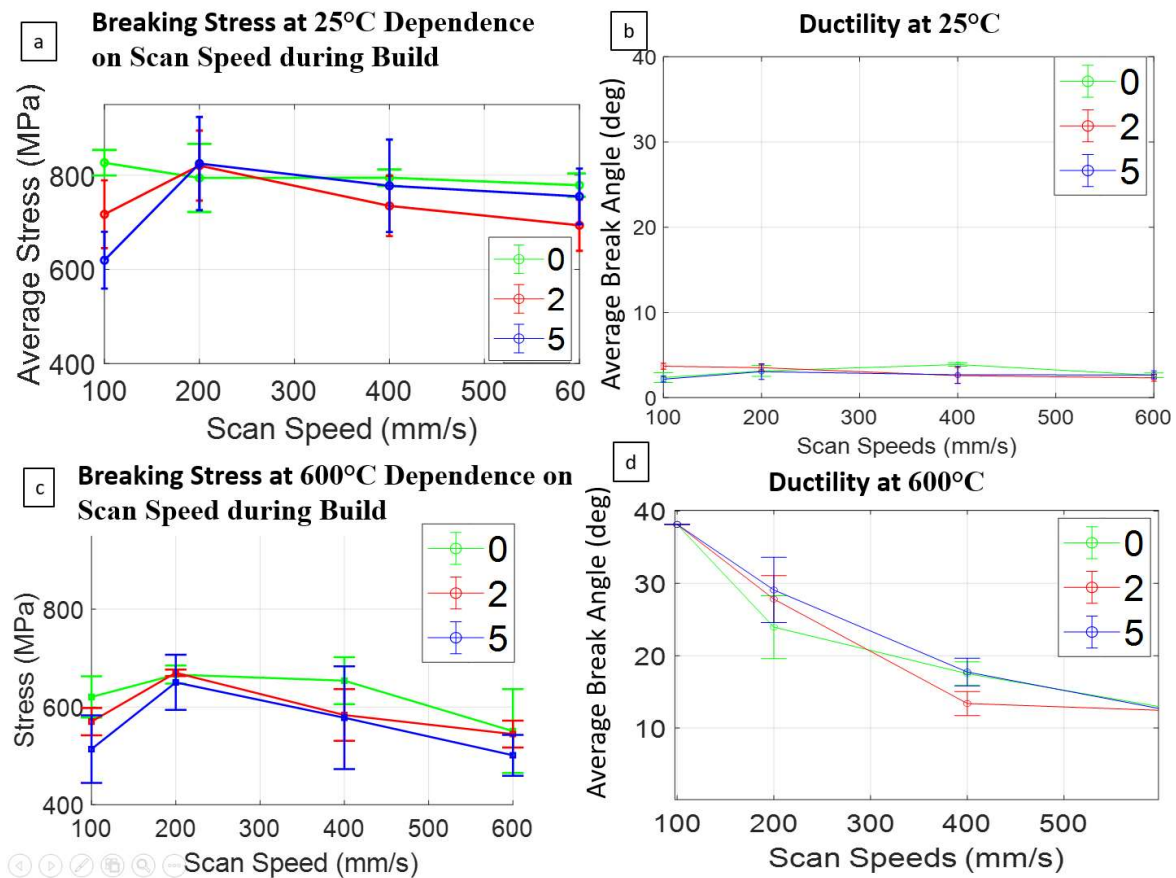


Figure 18b, the error bars in break angle are so large for the room temperature samples that no statistical significance can be noted. When looking at more ductile materials,

variability is reduced. The standard deviation of samples is much smaller, so the potential scatter of data points is much less. Small sample sizes with ductile materials generally produce statistically significant results. That case is what bears out in the room temperature three-point test of samples of various atmospheres and laser speeds. There is so much variation in the mechanical results in the room temperature testing of these brittle samples, that deducing effects of laser speed and atmosphere is impossible with the sample size used.

This difference in ductility is also the reason for using the high-temperature testing and grouping the samples for separate ANOVA tests. By making each sample more ductile than when at room temperature, scientists have the chance to observe or study the effects of other factors, such as the atmosphere and laser speed. That every ANOVA result of the high temperature test is significant shows that the difference in brittle and ductile materials as it relates to temperature and variability to be true. As shown in Table 2, all high temperature tests were quadratic, all had a significant factor in speed or the square of speed. The atmosphere was significant for the yield and ultimate tensile stresses and Young's modulus only.

The yield stress and ultimate tensile test results are similar to the results from the grouping of every sample, but with a much larger difference in response between samples due to the higher ductility. Rather than the room temperature samples showing high stress, the trend in laser speed is highlighted with the heat maps. The middle laser speeds show the highest stress over the other laser speeds in both yield stress and ultimate tensile stress, Figure 38 and Figure 39.

Factor Coding: Actual

Yield Stress (MPa)

● Design Points

246.202 492.56

X1 = A

X2 = B

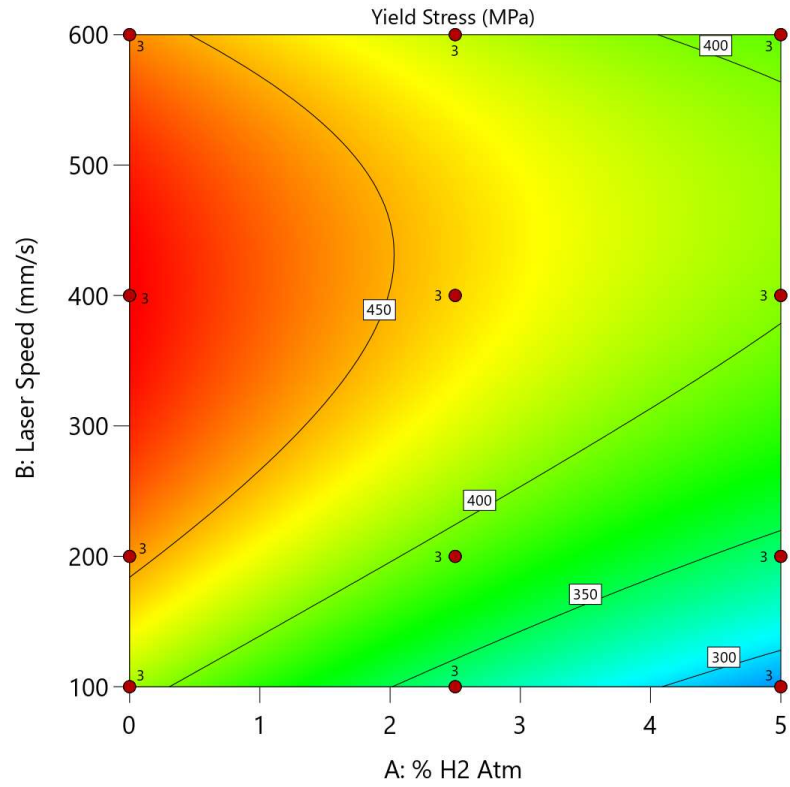


Figure 38. Yield Stress result for high temperature test samples.

Factor Coding: Actual

Ultimate Tensile Strength (mm/mm)

● Design Points

434.412 708.78

X1 = A

X2 = B

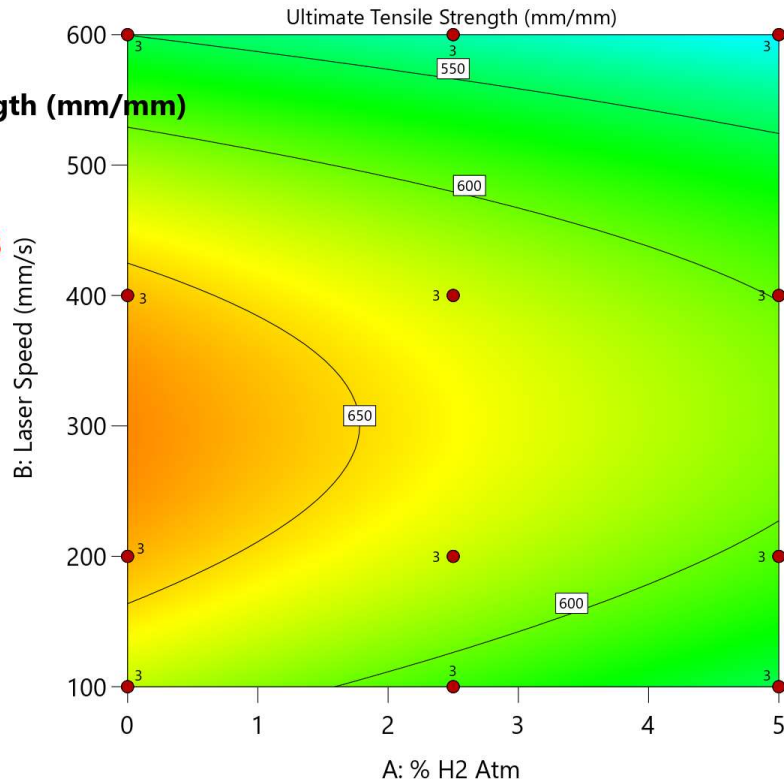


Figure 39. Ultimate Tensile Strength result for high temperature test samples.

The strain figures for the high temperature tests, Figure 43 – Figure 44, highlight another trend in the samples. The design space does not include the exact center points in laser speed but 200 and 400 mm/s as the middle speeds. The gradients between 600 and 400 mm/s are often more gradual than the gradients in the figures between 100 and 200 mm/s.

The underlying microstructure shows why the gradients vary as they do. Figure 40Error! Reference source not found. shows the fracture surfaces for representative samples tested at high temperature. Some characteristics are evident, such as relatively flat areas and those with un-sintered material. Yet every sample is covered in oxides,

making it difficult to distinguish characteristics like river patterns as easily as the room temperature fracture surfaces. The

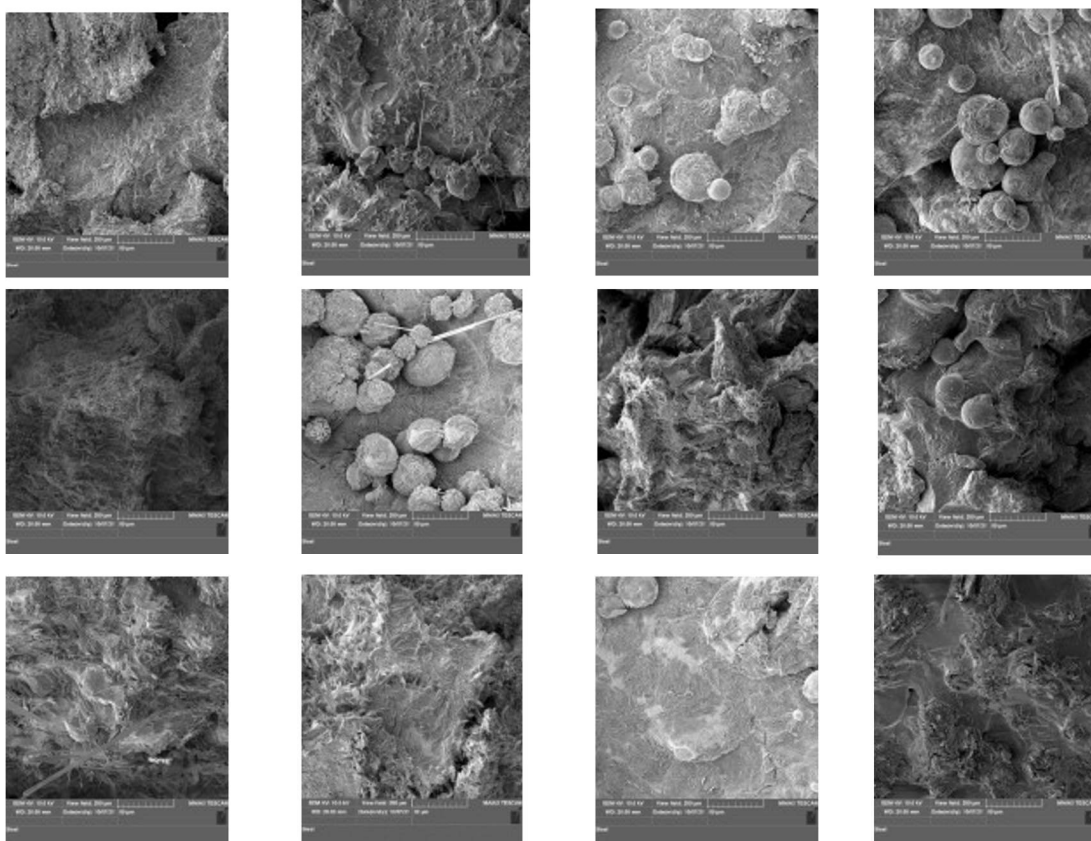


Figure 40 Fracture surfaces from high temperature three-point bending test. Top to bottom: 0% H₂, 2.5% H₂, 5% H₂. From left to right, 100, 200, 400, 600 mm/s laser speed.

600°C temperature was of relatively short duration and low enough that annealing did not occur. For those reasons, most of the analysis using SEM fractographs will continue with the room temperature figures.

Error! Reference source not found. Error! Reference source not found.

depicts a representative sample of the fracture surface of each of the build atmosphere and laser speed from the room temperature three-point bending tests. Both 100 and 200

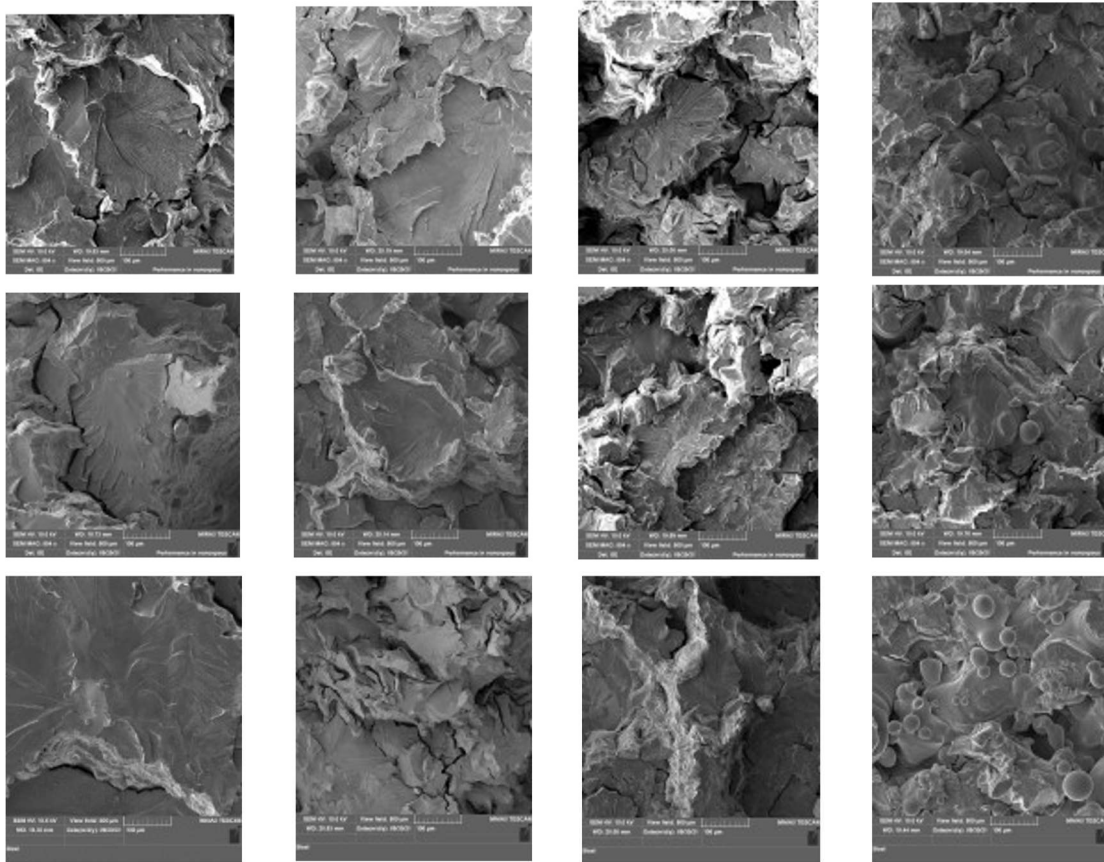


Figure 41. Fracture surface of representative samples from room temperature three-point bending test. Top to bottom: 0% H₂, 2.5% H₂, 5% H₂. From left to right, 100, 200, 400, 600 mm/s laser speed.

mm/s samples across atmospheres have larger flat areas, which are single grains. The size of the grains decreases with the increase in speed, and distinct variations in the microstructure are evident from one speed to the other. The differences in the 200 to 400 mm/s is also quite large. The 400 compared to the 600 mm/s microstructures look similar. Both have varied microstructures with very small areas of relatively flat surfaces. The relative change in microstructure as seen in the SEM fractographs mirrors the relative change in gradients between each change in laser speed as well.

Besides the size of grains being noticeably different with laser speed, un-sintered material is more common at higher scan speeds. The faster laser speeds means that a laser spends less time over any part of the melt during the manufacturing process, leading to a decreased temperature. The laser hatch spacing means that the laser does not cross over every part of the build, but relies on the laser heating up the surrounding area generating a melt pool of sufficient size to melt all the powder during the build. With too fast a laser speed, the melt pool is of insufficient size or of high enough temperature for a sufficient duration to melt all powder. The result is more powder, the spherical formations not fully melted in Figure 41, abundant at higher laser speeds across the atmospheres.

The etched samples also depict the changing grain size with laser speed, which is important to the fracture path. The etch in

Figure 42 has a notional fracture line around grain boundaries, with the 100 mm/s sample on the left and the 600 mm/s sample

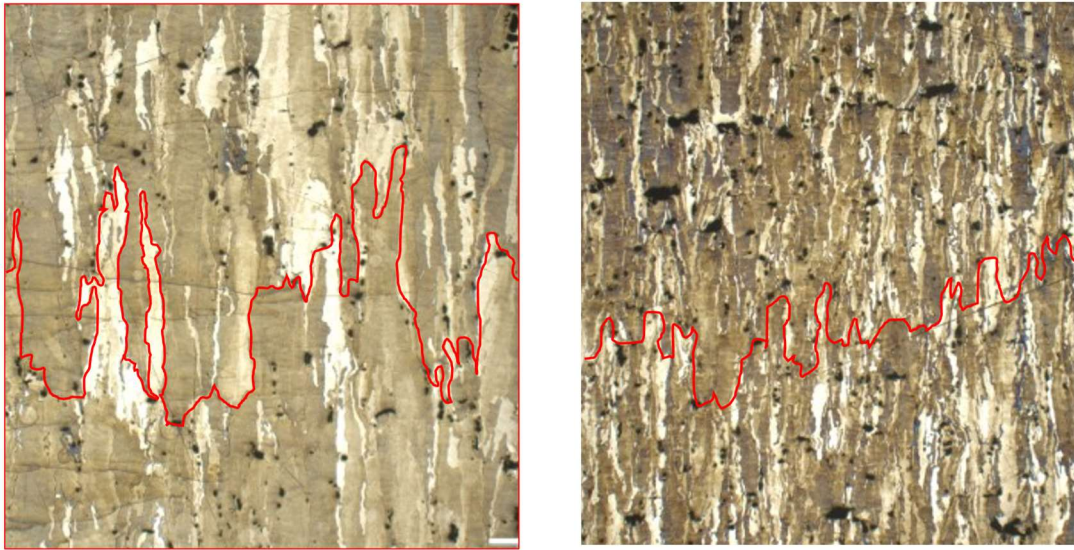


Figure 42. Notional fracture path around grain boundaries for 100 and 600 mm/s samples at 0% H₂

on the right. The 600 mm/s notional fracture path constantly changes direction around numerous grains while the 100 mm/s has much larger white sections of defined grains to avoid. The resulting fracture path, or variation in path, is noticeable in Figure 41 of SEM fractographs. Flatter sections are a single grain while the variation in fracture path is reflected in the variation in fractured angles and uneven surface in the 400 and 600 mm/s samples.

When force is applied to the samples during the three-point bending test to induce stress, dislocations of atoms build up at grain boundaries and require greater stress to cross the boundary. If the dislocations cannot move, plastic deformation occurs. Smaller

and more grains lead to a larger area of grain boundaries and less distance for the dislocations to travel before reaching a grain boundary. That decreased dislocation mobility leads to increased tensile stress. Since larger grains can accommodate more strain and deformation, the 100 mm/s sample is the most ductile and the higher laser speed samples with smaller grains are increasingly more brittle.

With weak grain boundaries, it takes more energy to go through a grain than around a grain. A fast break will have higher stress than a slower break, i.e., a slow strain rate, because the fracture path goes through the grains instead of having the time to find the path of least resistance around the grains. Increasing the temperature has the same effect of slowing the strain rate. Therefore, stress decreases with increased temperature and ductility increases, seen repeatedly in these reported results of tensile strain.

A brittle fracture that follows the path of least resistance along grain boundaries is called intergranular fracture, while a fracture through grains is called transgranular fracture. Mo suffers weak grain boundaries, so expected fracture is intergranular. As

Factor Coding: Actual

Ultimate Tensile Strain (mm/mm)

● Design Points

0.0106492 0.0464311

X1 = A

X2 = B

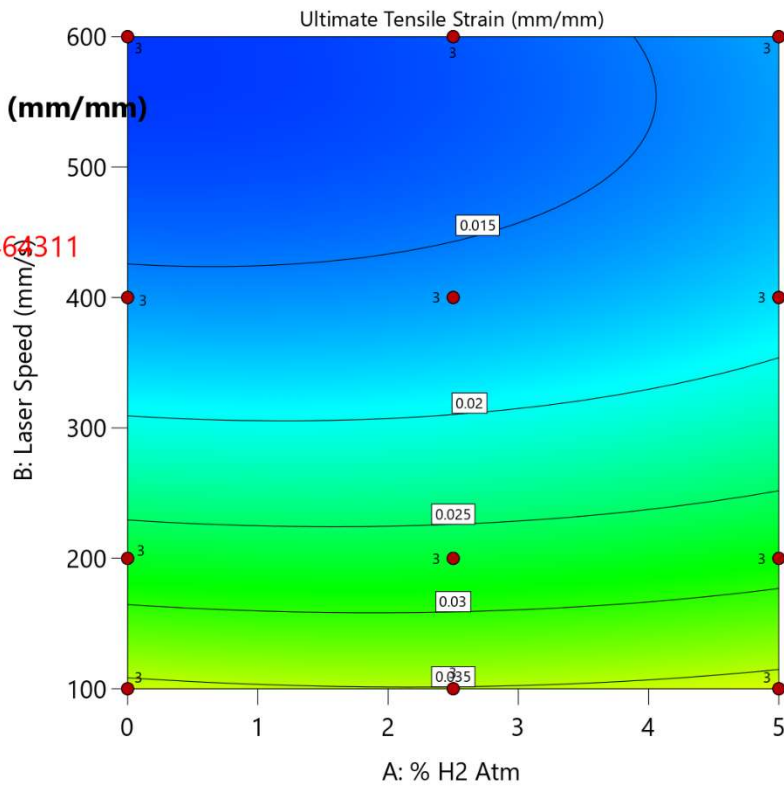


Figure 43. Ultimate Tensile Strain result for high temperature test samples.

grain boundaries become stronger, such as by reducing the amount of oxides at grain boundaries, or increasing temperature, more energy is required to break a sample (higher stress) and transgranular fracture is expected to be seen in SEM fractographs.

Factor Coding: Actual

Final Strain (mm/mm)

● Design Points

0.105486 0.352755

X1 = A

X2 = B

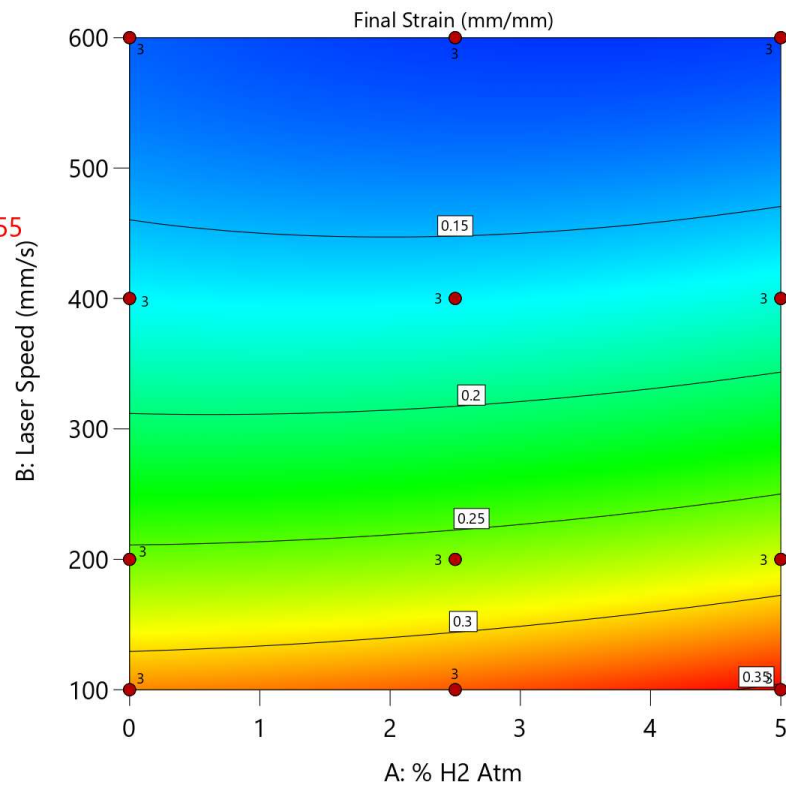


Figure 44. Final Strain result for high temperature test samples.

The purpose of breaking out the samples by temperature was to see if there are any significant factors that would otherwise be insignificant with all the data together. When looking at the Young's Modulus results, Figure 45, atmosphere and the square of laser speed are significant factors. That laser speed is significant is one of the only differences when just looking at the high temperature group compared to all data points. The figure for Young's Modulus is similar to that of stress of high temperature samples where the highest Young's Modulus occurs at the N₂ atmosphere and 400 mm/s

Factor Coding: Actual

Young's Modulus (N/m²)

● Design Points

43830.3 111280

X1 = A

X2 = B

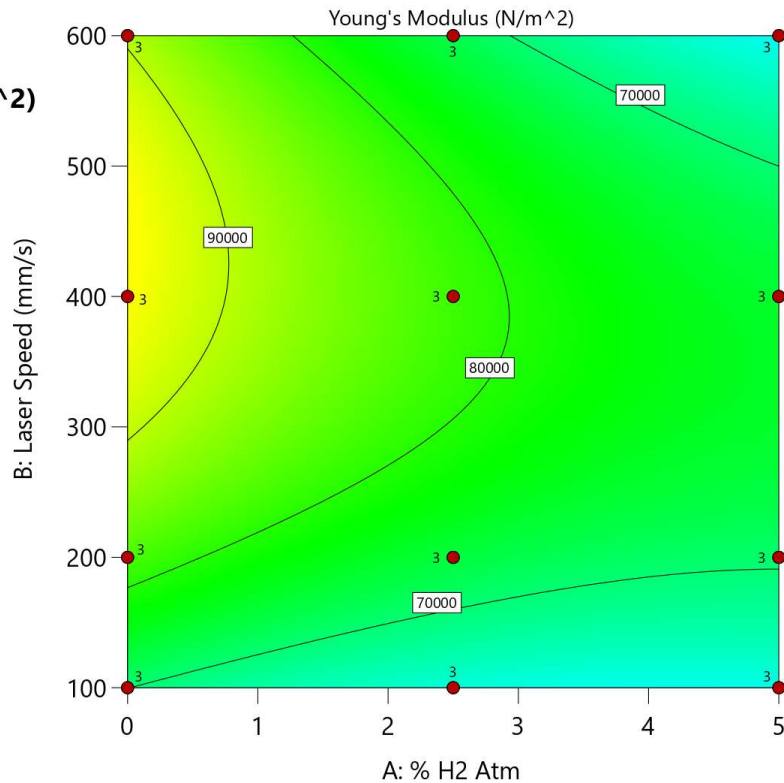


Figure 45. Young's Modulus result for high temperature test samples.

4.4 Investigative Questions Answered

The purpose of the present study was to investigate the effect of test temperature, build atmosphere or shield gas, and laser speed on mechanical properties of stress and strain or ductility on AM Mo. Chapter II of this thesis discussed the known effects of Ar as a shield gas on the properties of AM of W and Mo. This study concluded that it is beneficial to use nitrogen or a nitrogen-hydrogen mix as the build atmosphere or shield gas over Ar due to nitrogen being both less expensive to procure and the mechanical effects show the same if not an increase in both stress and strain under similar build and

testing conditions for Mo. The higher the percentage of H₂ in the shield gas, the less stress and more ductile the sample. However, the concentration of hydrogen had a much lower effect than the choice of nitrogen shield gas.

In most cases, larger effects in trends were seen from the change in test temperature or laser speed than the shield gas. There was no statistical significance of results amongst the room temperature tests. High temperature samples showed greater ductility than that of room temperature samples, with lower scan speeds having an increased ductility, larger grain sizes, and greater degree of transgranular fracture over the higher scan speeds.

4.5 Summary

Experimental data analysis showed trends in the stress and strain curves. The room temperature samples, below the DBTT, were brittle while the samples tested at the mid-point and 600°C still carried a load long after ultimate stress was reached. The elevated temperature samples exhibited greater plastic strain prior to reaching the ultimate stress and fracture than room temperature tested samples.

The ANOVA allowed for determination of statistical significance not possible with only graphing of the experimental results. Analysis with the DOE grouping did not fully identify trends and significant factors as it relates to stress, strains, and Young's Modulus. High density achieved by previous researchers, however, was not achieved here when looking at porosity. Decreasing grain sizes was easily discernable with increased laser speeds.

Analysis of all data highlighted the quadratic relationships not evident in the DOE grouping due to lack of sampling data. ANOVA by atmosphere matched similar results from the group of all data points. Since the N₂ and 5 H₂ atmospheres lacked middle points, linear relationships existed (if the ANOVA was significant) where the 2.5 H₂ atmosphere had quadratic relationships. Also, Mo in nitrogen versus an Ar environment with and without hydrogen showed an increase in stress with similar strains, making nitrogen the preferred shield gas for future work.

Analysis of data by temperature indicated the importance of testing above the DBTT. All room temperature samples were brittle, thus any data from samples held little variance if any statistical significance within the groupings. Above DBTT, every ANOVA for stresses, strains, and Young's Modulus was significant. As suggested in literature, and repeated in this study, increased ductility is related to decreased strength in Mo.

V. Conclusions and Recommendations

5.1 Conclusions of Research

AM Mo samples were varied in production by both the percentage of H₂ in the shield gas and laser speed, and during testing by varying the three-point bending test temperature. Results from the three-point bending test, SEM fractographs of the break surfaces, optical microscopy, and chemical analysis were used to analyze the variables and their effects on mechanical properties. Analysis of the microstructure helped explain the mechanical test results, and agreed with previous research of others.

Samples tested at room temperature were brittle with no statistically significant variation within sample groups. These samples carried higher stresses and exhibited less ductility than samples tested at higher temperatures. When tested at high temperatures, samples printed at low laser speeds (higher VED) exhibited higher ductility. High temperature groupings showed additional significant impact due to speed, or the square of speed in quadratic results, not seen when grouping all data together. The change in H₂ percentage in the build atmosphere was not a significant factor on strain, and elicited only small effects on the results compared to laser speed and test temperature. Atmosphere was the significant factor for Young's Modulus, though analysis showed the trends in both laser speed and atmosphere were not linear. Under the same test conditions at room temperature, samples with nitrogen reached larger ultimate tensile stresses but similar strains at ultimate tensile stress compared to Ar and Ar-H₂ mixtures. (Comparison of microstructure from the Ar samples in the earlier study could not be made).

Microstructure was analyzed with optical microscopes and SEM. Analysis of porosity revealed no discernible trends. The fracture surfaces readily showed the

increased quantity and decreased size of grains as laser speeds increased. The SEM images of fracture surfaces allowed for recognizing structural similarities and differences by laser speed, and to a much lesser degree atmosphere, that matched up with the quantifiable heat maps developed with the ANOVA analysis. There is an inverse relationship between VED and laser speed. Doubling the laser speed halved the VED, and large changes in final strain, or failure strain, for the high temperature samples especially were evident between the 100 and 200 mm/s laser speeds compared to the smaller spread of VED between 400 and 600 mm/s laser speeds. The chemical analysis highlighted the trend with oxygen content and ultimate tensile stresses across atmospheres, but not strain at ultimate tensile stress or final strain. This again fit the ANOVA results of atmosphere not being a significant factor in either the aforementioned strain results.

The trends and significant results can be explained by what was already known. The room temperature tested samples were below the DBTT, therefore brittle, and provided no statistically significant data but yielded trends. Yield stress trends fit keyhole porosity expectations when looking at a single atmosphere. Inverse relationship of ductility or strain and stress follow knowledge of grain sizes. Smaller sizes and larger quantities of grains lead to less ductile materials with higher stresses, which was found with increased laser speeds without regard to atmosphere. There is a tradeoff in ductility and stress within any given sample. SEM analysis supported the decision to choose data points at 100 mm/s and 200 mm/s laser speed, the former doubling the VED, followed by 400 mm/s and 600 mm/s laser speed instead of just the 100 mm/s, 350 mm/s, and 600 mm/s laser speeds in order to see greater changes at the lower speeds otherwise missed.

It was notable to see the significance, trends, or lack thereof as it relates to atmospheric composition in comparison to the laser speed and test temperature. Atmospheric composition had no significant bearing on grain size, thus ductility and strain. Atmospheric composition did not change the porosity. Atmospheric composition had some influence on the chemical makeup, but there were not the expected linear relationships in the atmosphere and chemical impurities. Trends in fracture surfaces followed VED but not atmospheric changes. The use of nitrogen over argon did make a difference as to both increased stresses and strains in samples and would be the preferred gas for future studies. There is no reason to continue with H₂ added to the shield gas.

Based on the present study, one looking to optimize the ultimate strength of Mo should use the following parameters: 25°C test temperature, 314 mm/s laser speed, and 3.3% H₂ /96.6% N₂ build atmosphere. The corresponding results are predicted to be 835 MPa ultimate tensile stress, 760 MPa yield stress, 0.017 mm/mm ultimate tensile strain, 0.01 mm/mm final strain, and 77,313 N/m² Young's modulus.

5.2 Recommendations for Future Work

Chapter 2.3 discussed methods to produce AM crack-free, pure Mo to include: heating the substrate plate [3], using shield gas [3], rotating 67° between layers [3,4], using skinny supports [4], and using a higher laser power to increase VED [4,25,36]. This study changed the shield gas and found an effect, but the samples contained visible porosity, cracks, and impurities, limiting the usefulness of samples in real-world applications. One recommendation is to utilize proven methods for producing crack-free AM Mo with the changing of the shield gas to determine effects on mechanical

properties. It may not be possible to assure the powdered Mo remains free from oxygen contamination during handling, and impurities in the powder may occur. In that situation, the shield gas may play a factor in readily manufacturing crack-free, fully dense Mo.

The difference in using nitrogen instead of Ar made a significant difference in the stress and strain of the samples. The amount of hydrogen in the shield gas made very little difference, but more H₂ led to samples with a lower max stress. Future work should just use nitrogen instead of a mixed nitrogen-hydrogen atmosphere. Also, there were no trends in porosity, no indications of which parameters were favorable to any mechanical properties. Future study of the effects of these variables on porosity can be neglected, while changes in how similar VEDs were reached, or changing other variables, may support studies on porosity.

A second recommendation is to include heat treatments. Mechanical processing of Mo after AM changes the grain structure of Mo to achieve desired mechanical properties or shape and size [10]. Heat treatments also change grain structure by eliminating residual stresses in the material, making samples more ductile. The duration and temperature of heat treatments would need to be investigated for these AM samples. The cost in strength for this increased ductility post heat treatment would need to be assessed to ascertain the usefulness of any such end product.

A third recommendation is to utilize sufficiently high VED to fully melt the material and reduce porosity. The ductility measured by ultimate strain continually decreased as laser speed increased, which resulted in lower VED. The Mo is not properly welding during the AM process, likely causing the generation of increased porosity

which impacted ductility. The trend would only continue at higher laser speeds. If the goal is to optimize ductility, and ductile materials are preferred to brittle in mechanical applications, higher laser speeds will not achieve desired results.

5.3 Summary

The effect of atmosphere and percentage of atmosphere was an unknown variable in this study. The effects from laser speed, VED, temperature, and DBTT of Mo were expected. Microstructural changes under each condition and the trends seen amongst the samples were readily explained from previous studies. The new data collected related to atmosphere was interesting. Both stress and strain in samples improved when the shield gas changed from Ar to nitrogen. The amount of H_2 in the shield gas made very little difference despite an initial hypothesis to the contrary. Future work in this field should include changes to the shield gas when using additional methods to manufacture crack-free Mo samples, continue to use hydrogen free nitrogen vice Ar, and not increase the laser speed over 600 mm/s to maximize ductility.

Bibliography

- [1] Toensing, C. H. Molybdenum Metal Powder. In *The Metal Molybdenum* (J. J. Harwood, ed.), American Society for Metals, Cleveland, 1958, pp. 31–50.
- [2] Freeman, R. R. Properties and Applications of Commercial Molybdenum and Molybdenum Alloys. In *The Metal Molybdenum* (J. J. Harwood, ed.), American Society for Metals, Cleveland, 1958.
- [3] Kaserer, L., Braun, J., Stajkovic, J., Leitz, K. H., Tabernig, B., Singer, P., Letofsky-Papst, I., Kestler, H., and Leichtfried, G. “Fully Dense and Crack Free Molybdenum Manufactured by Selective Laser Melting through Alloying with Carbon.” *International Journal of Refractory Metals and Hard Materials*, Vol. 84, 2019. <https://doi.org/10.1016/j.ijrmhm.2019.105000>.
- [4] Wang, D., Yu, C., Ma, J., Liu, W., and Shen, Z. “Densification and Crack Suppression in Selective Laser Melting of Pure Molybdenum.” *Materials and Design*, Vol. 129, 2017, pp. 44–52. <https://doi.org/10.1016/j.matdes.2017.04.094>.
- [5] Lai, G. Y. *High-Temperature Corrosion and Materials Applications*. ASM International, Materials Park, 2007.
- [6] Thornley, J. C., and Wronski, A. S. “The Relation Between the Ductile-Brittle Transition Temperature and Grain Size in Polycrystalline Molybdenum.” *Scripta METALLURGICA*, Vol. 3, 1969, pp. 935–938.
- [7] Campbell, J. E., Goodwin, H. B., Wagner, H. J., Douglass, R. W., and Allen, B. C. *Introduction to Metals for Elevated-Temperature Use*. Columbus, 1961.
- [8] Zelikman, A. N., Krein, O. E., and Samsonov, G. v. *Metallurgy of Rare Metals*. Nova Science Publishers, Inc., New York, 2018.

- [9] Klopp, W. D. "A REVIEW OF CHROMIUM, MOLYBDENUM, AND TUNGSTEN ALLOYS." *Journal of the Less-Common Met&*, 1975, p. 261.
- [10] Gupta, C. K. *Extractive Metallurgy of Molybdenum*. CRC Press, Boca Raton, 1992.
- [11] Perepezko, J. H. "The Hotter the Engine, the Better." *Science*, Vol. 326, No. 5956, 2009, pp. 1068–1069. <https://doi.org/10.1126/science.1179117>.
- [12] Murty, K. L., and Charit, I. "Structural Materials for Gen-IV Nuclear Reactors: Challenges and Opportunities." *Journal of Nuclear Materials*, Vol. 383, Nos. 1–2, 2008, pp. 189–195. <https://doi.org/10.1016/j.jnucmat.2008.08.044>.
- [13] Gilbert, M. R., Packer, L. W., and Stainer, T. Experimental Validation of Nuclear Reaction Data for Inventory Simulations on Molybdenum. No. 2020-March, 2020, pp. 1820–1828.
- [14] Northcott, L. *Metallurgy of the Rarer Metals*. Academic Press, Inc., New York, 1956.
- [15] Agnew, S. R., and Leonhardt, T. *The Low-Temperature Mechanical Behavior of Molybdenum-Rhenium*. 2003.
- [16] Schneibel, J. H., Felderman, E. J., and Ohriner, E. K. "Mechanical Properties of Ternary Molybdenum-Rhenium Alloys at Room Temperature and 1700 K." *Scripta Materialia*, Vol. 59, No. 2, 2008, pp. 131–134. <https://doi.org/10.1016/j.scriptamat.2008.02.057>.
- [17] Knapton, A. G. "The Molybdenum-Rhenium System." *J. Inst. Metals*, Vol. 87, 1958.
- [18] Devan, J. H. *Catastrophic Oxidation of High-Temperature Alloys*. 1961.

- [19] Tripathy, P. K., and Rakhasia, R. H. “Chemical Processing of a Low Grade Molybdenite Concentrate to Recover Molybdenum.” *Transactions of the Institutions of Mining and Metallurgy, Section C: Mineral Processing and Extractive Metallurgy*, Vol. 115, No. 1, 2006, pp. 8–14.
<https://doi.org/10.1179/174328506X91329>.
- [20] Hot Isostatic Pressing. *European Powder Metallurgy Association (EPMA)*.
- [21] Scott, H., Taebel, W. A., and Lawthers, D. D. Consolidation of Molybdenum by Powder Metallurgy Practice. In *The Metal Molybdenum* (J. J. Harwood, ed.), American Society for Metals, Cleveland, 1958, pp. 51–75.
- [22] Sun, J., Pantoya, M. L., and Simon, S. L. “Dependence of Size and Size Distribution on Reactivity of Aluminum Nanoparticles in Reactions with Oxygen and MoO₃.” *Thermochimica Acta*, Vol. 444, No. 2, 2006, pp. 117–127.
<https://doi.org/10.1016/j.tca.2006.03.001>.
- [23] Bruckart, W. L. The Working of Molybdenum and Its Alloys. In *The Metal Molybdenum* (J. J. Harwood, ed.), American Society for Metals, Cleveland, 1958, pp. 109–127.
- [24] Saleh Alghamdi, S., John, S., Roy Choudhury, N., and Dutta, N. K. “Additive Manufacturing of Polymer Materials: Progress, Promise and Challenges.” 2021.
<https://doi.org/10.3390/polym13>.
- [25] Faidel, D., Jonas, D., Natour, G., and Behr, W. “Investigation of the Selective Laser Melting Process with Molybdenum Powder.” *Additive Manufacturing*, Vol. 8, 2015, pp. 88–94. <https://doi.org/10.1016/j.addma.2015.09.002>.

- [26] Körner, C., Attar, E., and Heinl, P. “Mesoscopic Simulation of Selective Beam Melting Processes.” *Journal of Materials Processing Technology*, Vol. 211, No. 6, 2011, pp. 978–987.
- [27] Anderson, T. L. *Fracture Mechanics, Fundamentals and Applications*. CRC Press, Boca Raton, 2005.
- [28] Stephens, J. R. *EFFECT OF OXYGEN ON MECHANICAL PROPERTIES OF TUNGSTEN*. Cleveland, 1963.
- [29] Xing, H., Hu, P., Han, J., Li, S., Ge, S., Hu, B., Yang, F., Wang, K., and Feng, P. “Effects of Oxygen on Microstructure and Evolution Mechanism of Body-Centred-Cubic Molybdenum.” *International Journal of Refractory Metals & Hard Materials*, Vol. 103, 2022.
- [30] Braun, J., Kaserer, L., Stajkovic, J., Leitz, K. H., Tabernig, B., Singer, P., Leibenguth, P., Gspan, C., Kestler, H., and Leichtfried, G. “Molybdenum and Tungsten Manufactured by Selective Laser Melting: Analysis of Defect Structure and Solidification Mechanisms.” *International Journal of Refractory Metals and Hard Materials*, Vol. 84, 2019. <https://doi.org/10.1016/j.ijrmhm.2019.104999>.
- [31] Leitner, K., Scheiber, D., Jakob, S., Primig, S., Clemens, H., Povoden-Karadeniz, E., and Romaner, L. “How Grain Boundary Chemistry Controls the Fracture Mode of Molybdenum.” *Materials and Design*, Vol. 142, 2018, pp. 36–43. <https://doi.org/10.1016/j.matdes.2018.01.012>.
- [32] Braun, J., Kaserer, L., Letofsky-Papst, I., Leitz, K. H., Kestler, H., and Leichtfried, G. “On the Role of Carbon in Molybdenum Manufactured by Laser Powder Bed

- Fusion.” *International Journal of Refractory Metals and Hard Materials*, Vol. 92, 2020. <https://doi.org/10.1016/j.ijrmhm.2020.105283>.
- [33] Pöhl, C., Schatte, J., and Leitner, H. “Solid Solution Hardening of Molybdenum-Hafnium Alloys: Experiments and Modeling.” *Materials Science and Engineering A*, Vol. 559, 2013, pp. 643–650. <https://doi.org/10.1016/j.msea.2012.09.004>.
- [34] Zhou, X., Liu, X., Zhang, D., Shen, Z., and Liu, W. “Balling Phenomena in Selective Laser Melted Tungsten.” *Journal of Materials Processing Technology*, Vol. 222, 2015, pp. 33–42. <https://doi.org/10.1016/j.jmatprotec.2015.02.032>.
- [35] Liu, X. ping, Wang, K. she, Hu, P., Chen, Q., and Volinsky, A. A. “Spheroidization of Molybdenum Powder by Radio Frequency Thermal Plasma.” *International Journal of Minerals, Metallurgy and Materials*, Vol. 22, No. 11, 2015, pp. 1212–1218. <https://doi.org/10.1007/s12613-015-1187-7>.
- [36] Higashi, M., and Ozaki, T. “Selective Laser Melting of Pure Molybdenum: Evolution of Defect and Crystallographic Texture with Process Parameters.” *Materials and Design*, Vol. 191, 2020. <https://doi.org/10.1016/j.matdes.2020.108588>.
- [37] Kinkade, R. X. *THE EFFECT OF PROCESS PARAMETERS ON THE ADDITIVE MANUFACTURING OF MOLYBDENUM AND MOLYBDENUM RHENIUM ALLOYS* AIR FORCE INSTITUTE OF TECHNOLOGY. Wright-Patterson Air Force Base, 2021.
- [38] Dong, J., Liu, S., Chen, H., Li, D., Zhang, T., Chen, C., and Zhou, K. “Effect of Atmosphere on the Microstructure and Properties of Additively Manufactured Tungsten.” *Materials Science and Technology*, Vol. 36, No. 18, 2020.

- [39] Antony, J. *Design of Experiments for Engineers and Scientists*. Elsevier, Oxford, 2003.

REPORT DOCUMENTATION PAGE				Form Approved OMB No. 074-0188	
<p>The public reporting burden for this collection of information is estimated to average 1 hour per response, including the time for reviewing instructions, searching existing data sources, gathering and maintaining the data needed, and completing and reviewing the collection of information. Send comments regarding this burden estimate or any other aspect of the collection of information, including suggestions for reducing this burden to Department of Defense, Washington Headquarters Services, Directorate for Information Operations and Reports (0704-0188), 1215 Jefferson Davis Highway, Suite 1204, Arlington, VA 22202-4302. Respondents should be aware that notwithstanding any other provision of law, no person shall be subject to a penalty for failing to comply with a collection of information if it does not display a currently valid OMB control number.</p> <p>PLEASE DO NOT RETURN YOUR FORM TO THE ABOVE ADDRESS.</p>					
1. REPORT DATE (DD-MM-YYYY) 06-09-2022		2. REPORT TYPE Master's Thesis		3. DATES COVERED (From – To) March 2021 – July 2022	
TITLE AND SUBTITLE Additive Manufacturing of Molybdenum for High Temperature Structural Applications				5a. CONTRACT NUMBER	
				5b. GRANT NUMBER	
				5c. PROGRAM ELEMENT NUMBER	
6. AUTHOR(S) Bustin, Megan L., Major, USMC				5d. PROJECT NUMBER	
				5e. TASK NUMBER	
				5f. WORK UNIT NUMBER	
7. PERFORMING ORGANIZATION NAMES(S) AND ADDRESS(S) Air Force Institute of Technology Graduate School of Engineering and Management (AFIT/EN) 2950 Hobson Way, Building 640 WPAFB OH 45433-7765				8. PERFORMING ORGANIZATION REPORT NUMBER AFIT-ENY-MS-22-S-111	
9. SPONSORING/MONITORING AGENCY NAME(S) AND ADDRESS(ES) Intentionally left blank				10. SPONSOR/MONITOR'S ACRONYM(S)	
				11. SPONSOR/MONITOR'S REPORT NUMBER(S)	
12. DISTRIBUTION/AVAILABILITY STATEMENT DISTRIBUTION STATEMENT A. APPROVED FOR PUBLIC RELEASE; DISTRIBUTION UNLIMITED.					
13. SUPPLEMENTARY NOTES This material is declared a work of the U.S. Government and is not subject to copyright protection in the United States.					
14. ABSTRACT This research considered additive manufactured (AM) molybdenum (Mo) and the effect of three variables on microstructure, mechanical properties, and the relationship between the two. Test temperature, laser speed, and shield gas or build atmosphere were varied, and samples tested and analyzed using a three-point bending test, chemical composition, and optical and scanning electron microscopy. The relationship among variables and results using a Design of Experiments was limited compared to the inclusion of every tested sample. Most effects were expected: samples tested at room temperature were brittle without statistical significance; increasing laser speed resulted in decreased ductility and strain, smaller grain sizes, and increased quantity of grains; and percentage of hydrogen in the shield gas had very little effect compared to the other variables. Nitrogen was preferable to an argon shield gas, results showing both higher stresses and strains under the same conditions. Stress followed expectations given oxygen content, keyhole porosity, and un-sintered materials. Maximum stress occurred at an intermediate laser speed and volumetric energy density (VED). Despite resulting porosity, nitrogen as a shield gas shows promise in AM fully dense Mo. Heat treatments and adjusting VED contribute to producing fully dense Mo and should be considered in future work.					
15. SUBJECT TERMS Additive manufacturing, molybdenum, high temperature application, shield gas					
16. SECURITY CLASSIFICATION OF:			17. LIMITATION OF ABSTRACT UU	18. NUMBER OF PAGES 135	19a. NAME OF RESPONSIBLE PERSON Ryan Kemnitz, AFIT/ENY
a. REPORT U	b. ABSTRACT U	c. THIS PAGE U			19b. TELEPHONE NUMBER (Include area code) (937) 255-3636, ext 4775 (ryan.kemnitz@afit.edu)